Spring 5-2022

Design of Path Correction for Improved Gait Rehabilitation

Zvonimir Pusnik
University of Nebraska-Lincoln, zpusnik@huskers.unl.edu

DESIGN OF PATH CORRECTION FOR IMPROVED GAIT REHABILITATION

by

Zvonimir Pusnik

A THESIS

Presented to the Faculty of

The Graduate College at the University of Nebraska

In Partial Fulfillment of Requirements

For the Degree of Master of Science

Major: Mechanical Engineering and Applied Mechanics

Under the Supervision of Professor Carl A. Nelson

Lincoln, Nebraska

May, 2022

DESIGN OF PATH CORRECTION FOR IMPROVED GAIT REHABILITATION

Zvonimir Pusnik, M.S.

University of Nebraska, 2022

Advisor: Carl A. Nelson

Following a serious neurological injury or disease, such as a spinal cord injury or multiple sclerosis, many patients develop impaired gait (the ability to walk). There are many different pieces of equipment to help rehabilitate people with impaired gait, ranging from over ground walking with exoskeletons to treadmills with partial bodyweight support. Since the 1990s and 2000s, elliptical trainers have entered the rehabilitative field as a machine with low impact forces and gait-like motion. This led researchers at Madonna Rehabilitation Hospitals to collaborate with the University of Nebraska-Lincoln to create the Intelligently Controlled Assistive Rehabilitation Elliptical (ICARE).

While the ICARE is currently used in rehabilitating patients, its motion patterns tend to deviate from normal gait at more distal joints. In order to correct these deviations and further improve the ICARE's performance, a four-bar mechanism was created to attach to the ICARE while assisting a patient in rehabilitative exercise. The kinematic synthesis input for this problem specifically focused on the gait of the right foot centroid. Both traditional kinematic synthesis techniques and modern synthesis software were utilized in the process of creating a solution to this synthesis problem.

It was observed that the designed mechanism greatly improved the horizontal and vertical displacements of the foot centroid with milder improvements for the angular displacement.

Acknowledgements

This thesis would not have been possible without the contributions of Dr. Judith M. Burnfield. Dr. Burnfield not only served on my committee, but she provided her kinesiology expertise and clinic experience to help understand the problem and design a solution. Additionally, Dr. Burnfield provided access to equipment and other professionals at Madonna Rehabilitation Hospitals, both of which proved vital for my thesis project. I am indebted to the mentorship she provided me for both this project and my time with Madonna as an intern during my undergrad.

Table of Contents

Chapter 1 Introduction

This chapter outlines the necessary clinical background and history on what is the ICARE, how it performs for gait rehabilitation, and how it may be improved. In order to improve it, a mechanism was created and tested using several of the kinematic synthesis techniques outlined in this chapter. These techniques are organized in this chapter, starting from traditional graphical to analytical and lastly, to modern synthesis techniques.

1.1 Clinical Background

After a serious neurological injury or illness, such as a spinal cord or brain injury, most individuals will go through rehabilitation to recover lost walking function. Rehabilitation in the past was performed with over-ground walking, walking on a treadmill that has a partial-bodyweight-support system (PBWS), or robotic systems such as exoskeletons [1-4]. Treadmills with PBWS have been used with patients who do not have the strength and/or coordination to walk on their own; where a physical therapist may have to manually move their legs in a gait-like pattern for the rehabilitation session [3]. Similarly, robotic systems require the assistance of skilled professionals during rehabilitation and can be expensive for clinics and hospitals to purchase (>$100,000) [5]. Then during the 1990s and 2000s, elliptical trainers, or ellipticals, gained popularity in gyms and homes. The limitations in existing technology and the rise of ellipticals led researchers at Madonna Rehabilitation Hospitals in collaboration with the University of Nebraska-Lincoln to investigate the potential usage of ellipticals in gait rehabilitation [2-5].

In a previous study [4], Madonna researchers compared four different ellipticals with walking to test how feasible they are for rehabilitation. The four ellipticals were the SportsArt Fitness E870, Life Fitness X7, Octane Fitness Pro4500, and True Fitness Technology TSXa [4]. Using the Qualisys Motion Analysis System and Qualisys Track Manager software to track the motion of the trunk, pelvis, and lower limbs, the testing showed that ellipticals have similar motion patterns to gait [4]. From this study, it was observed that all of the ellipticals were within gait range for the first half of the gait cycle for thigh extension/flexion, hip extension/flexion, and ankle plantar flexion/dorsiflexion [4]. The ellipticals had higher angular values than gait for trunk flexion, pelvic anterior tilt, and knee extension/flexion, with the exception of the SportsArts elliptical being in range for trunk flexion [4].

All of the ellipticals were better at mimicking gait's motion patterns at the proximal joints compared to the distal joints, and the SportsArt elliptical performed the best at mimicking gait kinematics as a whole for all of the joints [4]. Electromyography (EMG) was also tracked in this study, specifically for the gluteus maximus, gluteus medius, lateral hamstring, medial hamstring, vastus lateralis, gastrocnemius, soleus, and tibialis anterior [4]. In comparison to over-ground walking, all of the ellipticals increased activation in the gluteus maximus and vastus lateralis [4]. The ellipticals had lower activation for the medial hamstring, gastrocnemius, soleus, and tibialis anterior [4]. All of the ellipticals had comparable muscle activation to walking for the gluteus medius and lateral hamstring, except for True, which had slightly lower activation in the peak

and mean EMG amplitude for the lateral hamstring. These EMG results do not favor any particular elliptical over another. Therefore, since they all had comparable EMG results, but the SportsArt elliptical had more gait-like kinematics than the other three, it was selected as the elliptical to be modified.

Next, safety and assistive features (body weight support system, safety sensors, electronically adjustable seat height, modified handles for users with weakness, sensory loss, and cardiorespiratory deficits) were added on to the SportsArt elliptical to create the Intelligently Controlled Assistive Rehabilitation Elliptical (ICARE) [3, 5-8]. While sagittal-plane motion patterns are emulated fairly well for the trunk, pelvis, and thighs on the ICARE, its ability to mimic the distal leg joints' motions needs improvement [9]. The ICARE has an ovaloid foot path that lacks a proper heel lift in the late stance of gait [6]. This ovaloid foot path leads to discrepancies with gait, as shown in Figures 1.1 and 1.2, comparing the foot centroid's position and angle between the ICARE and healthy adult gait modeled in OpenSim (OpenSim, California, USA), a popular biomechanics simulation software [9-10].

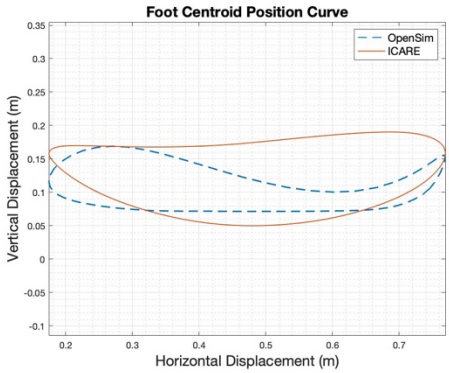

Figure 1.1. Comparison of ICARE's foot centroid trajectory with normal gait from OpenSim [9-10].

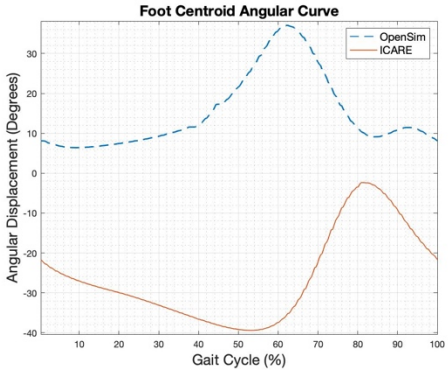

Figure 1.2. Comparison of ICARE's foot centroid angle with normal gait from OpenSim [9-10].

Despite these discrepancies, the ICARE is similar enough to normal gait that it is an effective tool for rehabilitating patients and is currently being used by clinicians and

patients. But given that it does not perfectly mimic gait, there is the potential that the device could produce even better rehabilitation results for patients with improvements to the ICARE's gait pattern. In order to improve the ICARE, a mechanism could be made to attach to the ICARE to correct its gait pattern. This was the underlying goal and mission of the work presented in this thesis. In order to create a mechanism to attach onto the ICARE, kinematic synthesis was utilized. Kinematic synthesis has a rich history spanning over two centuries with contributions from mathematical giants, like Leonhard Euler and Pierre-Simon Laplace. Synthesis was traditionally done with both graphical and analytical methods [11].

1.2 Traditional Graphical Synthesis Methods

1.2.1 The Two Prescribed Positions Problem for Graphical Synthesis

Graphical synthesis can be done for motion (e.g., two and three prescribed positions), path (e.g., three prescribed points) and function generation (e.g., Freudenstein's equation) [12]. In the graphical synthesis of the two prescribed positions problem, two positions are given for the coupler as it rotates with the mechanism's motion. The corresponding edges of the two positions will be drawn by lines A_1A_2 and B_1B_2, as seen in Figure 1.3 [12]. Perpendicular lines a_{12} and b_{12} are drawn at the midpoint of lines A_1A_2 and B_1B_2, respectively. The intersection of these points is the pole P_{12}.

P_{12} represents the pivot point for which the linkage can rotate from position 1 to position 2. The ground pivot points A_0 and B_0 will lie on lines a_{12} and b_{12}, respectively. When designing a mechanism with this method, P_{12} may fall out of the workable frame, meaning the ground link's endpoints may not be in a feasible location for the machine. In the situation where the mid-normal of A_1A_2 does not have a desirable location for A_0, then different points in the moving body C_1 and C_2 can be selected to create C_1C_2. From the mid-normal of C_1C_2, the ground pivot point C_0 can be found. The ground pivot points, along with one of the prescribed positions, will create a four-bar mechanism.

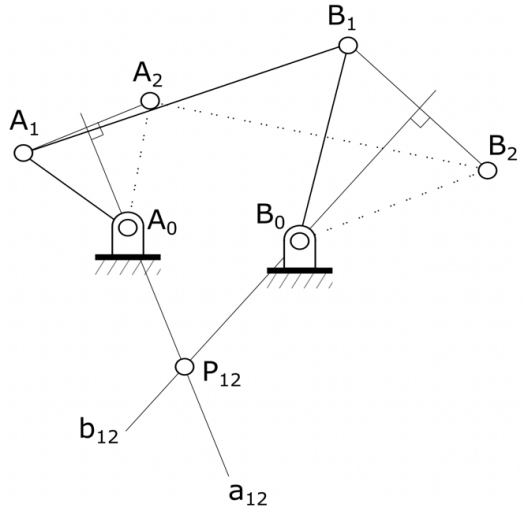

Figure 1.3. Schematic of the two prescribed positions problem for motion generation [12].

1.2.2 The Three Prescribed Positions Problem for Graphical Synthesis

Next in complexity for motion generation with graphical synthesis is the three prescribed positions problem. In Figure 1.4, lines a_{12}, a_{13}, b_{12}, and b_{13} can be found in the same way as in the two prescribed positions problem [13]. The difference now is that A_0 and B_0 can be found via the intersection of a_{12} and a_{13} and b_{12} and b_{13}, respectively. With A_0 and B_0 found, a four-bar mechanism solution has been generated by using one of the three coupler positions. Note that for both the two and three prescribed positions problems, the discovered solution is an exact solution, meaning they will hit all of the coupler positions used to synthesize the mechanism. If one had more than three positions to choose from, then the designed mechanism will be an approximate solution and match several, but not all, of the desired positions.

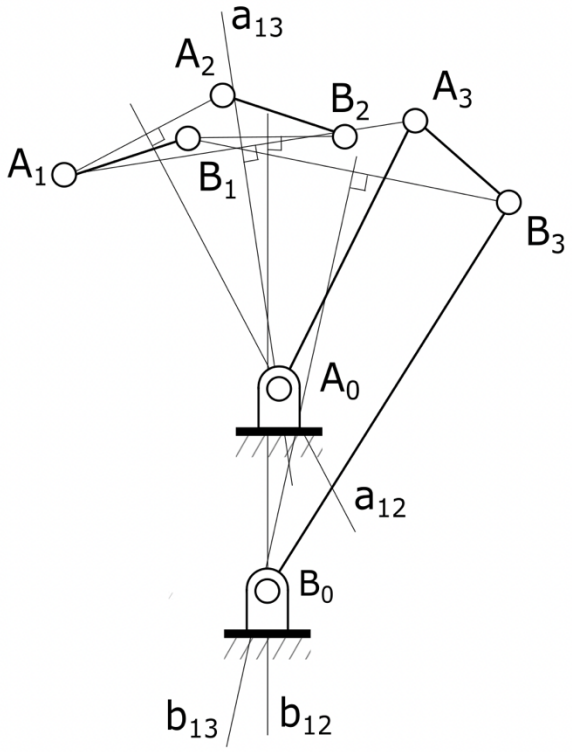

Figure 1.4. Schematic of the three prescribed positions problem for motion generation [13].

1.2.3 The Three Prescribed Points Problem for Graphical Synthesis

The three prescribed positions problem has a path generation variation called the three prescribed points problem. Rather than having three positions of a linkage that the designed mechanism must pass through, the end effector P of the coupler triangle will pass through the three points P_1, P_2, and P_3 [12]. The designer then selects the positions for A_0 and B_0 and chooses a length for the crank. Using the crank length, they will draw a circle centered around A_0 and then select position A_1 to find the length of AP using P_1. With the length of AP known, P_2 and P_3 are used to find A_2 and A_3,

respectively. Angles $ß_1$, $ß_2$, and $ß_3$ represent the angle between A_0A_1 and A_1P_1, A_0A_2 and A_2P_2, and A_0A_3 and A_3P_3, respectively. This completes the graphical setup of the three prescribed points problem for path generation, as showcased in Figure 1.5 [12].

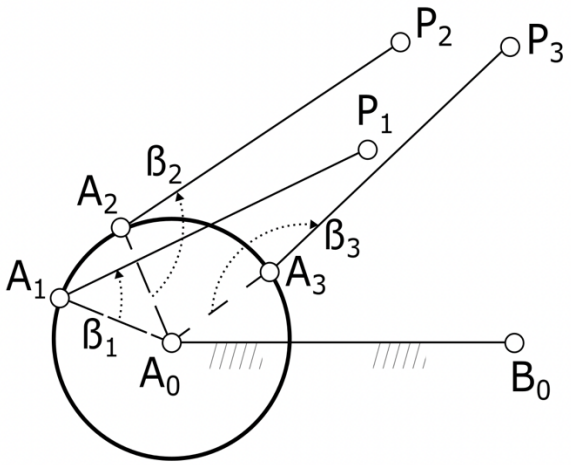

Figure 1.5. Schematic of the three prescribed points problem setup for path generation [12].

B will be found by using kinematic inversion [12] and the schematic can be referenced in Figure 1.6. First A_0' will be found by rotating A_0 about A_1 by an angle of the difference between $ß_2$ and $ß_1$. Then an arc will be drawn centered at A_0' with a radius of A_0B_0. Another arc will be drawn centered at P_1 with a radius of P_2B_0 and the intersection of these two arcs is B_0'. A_0" can be discovered in a similar way as A_0', but with the rotation of A_0 about A_1 being the difference between angles $ß_3$ and $ß_1$. Using an arc centered at P_1 with a radius of P_3B_0, B_0" can be found by intersecting this arc with the arc drawn from A_0" with a radius of A_0B_0. B_1 is then drawn as the intersection of the mid-normal lines to B_0B_0' and B_0'B_0". The lengths of B_0B_1 and B_1P_1 are now known and the location needs to be verified with P_2 and P_3. If the verification fails, new assumptions must be considered for the positions of A_0, B_0, and A_1.

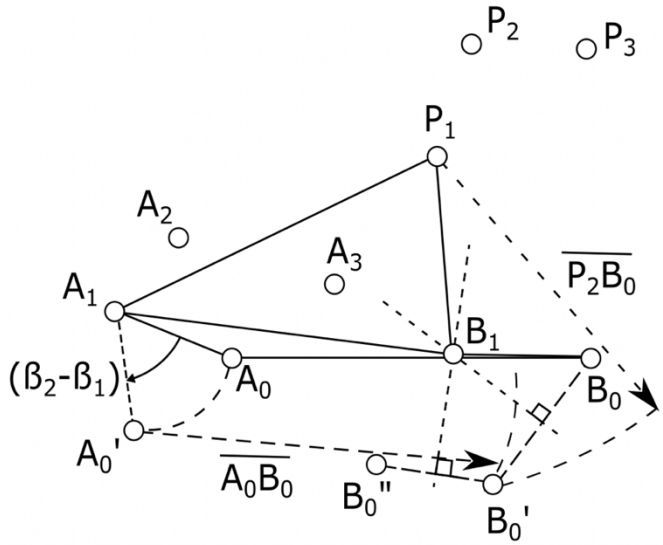

Figure 1.6. Schematic of the solution to the three prescribed points problem for path generation [12].

All of these methods have their own advantages and disadvantages. The graphical methods generally are more intuitive for an engineer than analytical methods, but are limited to the precision of the drafting tools available. Graphical methods are also susceptible to human error as the drafter must be cautious with drawing linkages to scale. The two prescribed positions problem is the simplest method presented here, but is very limited as many problems will require hitting more than two positions. Additionally, points A_0 and B_0 will lie on lines a_{12} and b_{12}, respectively, but additional information will be needed to find their exact locations on those lines.

The three prescribed positions problem is more commonly seen, but it presents its own difficulties. The three prescribed positions problem is fairly straight-forward with similar limitation as the two prescribed positions problem in terms of human error and drawing tools. Graphical synthesis of the three prescribed positions problem has an advantage over the two prescribed positions problem as the third coupler position allows the engineer to find the exact location of A_0 and B_0. As stated before, these two and three prescribed positions problems will only give an exact solution for two or three coupler positions. If more than three are provided, then an approximate solution will be created.

Contracting these methods with the three prescribed points problem for path generation, the three prescribed points problem is more cumbersome. This is because the engineer has to make assumptions for the location and size of the ground and crank links. They will also have to perform kinematic inversion with this method and may iterate through this process several times before finding a mechanism that follows the given path.

1.3 Analytical Synthesis Methods

1.3.1 The Three Prescribed Points Problem for Analytical Synthesis

Many of the graphical techniques have an analytical counterpart. For example, the three prescribed points problem has an analytical synthesis method for path generation. For the analytical synthesis version of the three prescribed points problem, a designer has to use vector space with dyads, geometry, and trigonometry (Figure 1.7) [12]. Here, rather than drawing a mechanism, its links will be treated as lines to be calculated as a form of vector-loop closure equations to find intersection points of significance. This method may involve knowing several constraints, or assumptions may have to be made for such things as the location and orientation of the ground link. This analytical method contains many limitations, for example, the orientation and location of several links may need to be assumed.

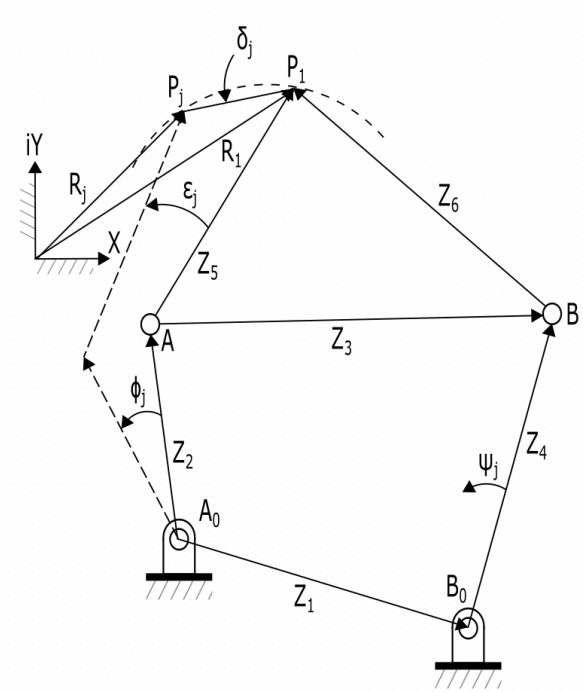

Figure 1.7. Schematic of a four-bar motion and path generator mechanism for analytical synthesis [12].

1.3.2 The Freudenstein's Equation for Analytical Synthesis

Another problem type in kinematic synthesis is function generation [12]. Function generation is a problem type where the angles of the input and output links must be mathematically related [12]. An analytical technique for this problem type is Freudenstein's equation, which is used to determine the link lengths of a four-bar mechanism [12]. The diagram referenced for Freudenstein's equation is shown in Figure 1.8 [12]. The basic premise is that given the desired angles of the input and output links, the link lengths can be calculated by equating their vector sums to zero [12] (i.e., a loop closure approach). For Freundenstein's equation, the engineer is presented with a series of equations that are intuitive once they have analyzed the geometry of a four-bar mechanism. But this method is limited to primarily one problem type, whereas graphical

and other analytical synthesis methods can solve both motion and path generation problems.

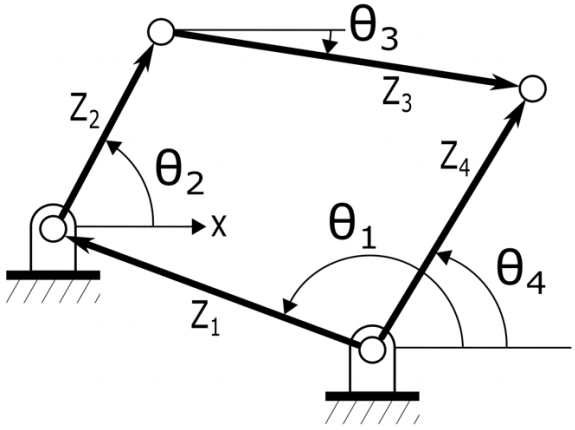

Figure 1.8. Schematic of a four-bar mechanism for Freudenstein's equation [12].

1.4 Modern Analytical and Graphical Synthesis Methods

1.4.1 Clifford Algebra

More modern analytical techniques utilize more complicated vector spaces. By using Clifford algebra, one can derive an eight-dimensional vector with dual quaternion units [14]. This equation can be broken into its segments that involve lines and screws. By performing the product of exponentials of the line and screw components, the engineer can then have the kinematic equations for tracking a body from its initial to final position via rotating and sliding along an axis [14]. Essentially the equations are expanded from trigonometric functions to higher order polynomials via change of variables and solved using root finding techniques [14]. These equations are then paired with nR planar serial chains, where there are n revolute joints connected by a cable drive with one degree of freedom, to create planar mechanisms [14-15]. These equations are fairly complex and not as intuitive as the more historical analytical methods. Additionally, there are a large number of equations to solve, for example a 5R chain can have 130 total equations to solve [14]. But given the advancements in computing technology, Clifford Algebra methods can provide engineers solutions to difficult kinematic problems that would have been computationally too heavy to solve in the past.

1.4.2 Poles and Rotation Angles in CAD

With improved computers, graphical methods have also benefited via Computer Aided Design (CAD) software. CAD software is traditionally used to design parts and assemblies to then manufacture into physical components. But researchers have created graphical methods using the constraints on target positions via the poles and rotation angles (PRC) in CAD [16], effectively leveraging the numerical solvers which allow animation of mechanisms in CAD software. In this method, one can use the number of motion, path, and function constraints to create a four-bar mechanism with prismatic and revolute joints; meaning the PRC method is a mixed synthesis method

[16]. The general procedure for the PRC method involves applying the motion, function, and path constraints, then constraining the fixed and moving pivots of the input and output links [16]. In the PRC method, the problems are written as M-P-F; where M, P, and F are the numbers of motion, path, and function constraints, respectively. For example, consider the 2-1-1 mixed synthesis problem (two target poses, one target point, and 1 specified input angle) in Figure 1.9 [16].

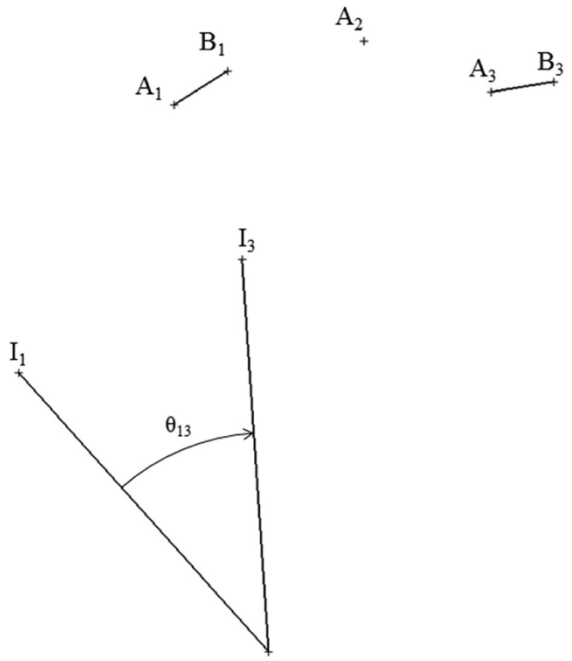

Figure 1.9. The set up to a 2-1-1 mixed synthesis problem for the PRC method [16].

The motion constraints will create a set of moving and fixed pivot lines from the P_{13} pole, one for the input link and the other for the output link [16]. Applying the function constraint involves rotating the input link by angle ϕ_{13}, which causes the coupler to move from positions 1 to 3 [16]. The angle between the fixed pivot line and the input link in position 1 is now half of ϕ_{13} [16]. The path constraint involves finding P_{12} and ϕ_{12}, then drawing two sets of fixed and moving pivot lines from P_{12} to the input and output links [16]. Lastly, the fixed and moving pivots of the input and output links are constrained by finding the intersection of their fixed and moving pivot lines, respectively [16]. The 2-1-1 problem with its drawn constraints and designed mechanism is shown in Figure 1.10 [16].

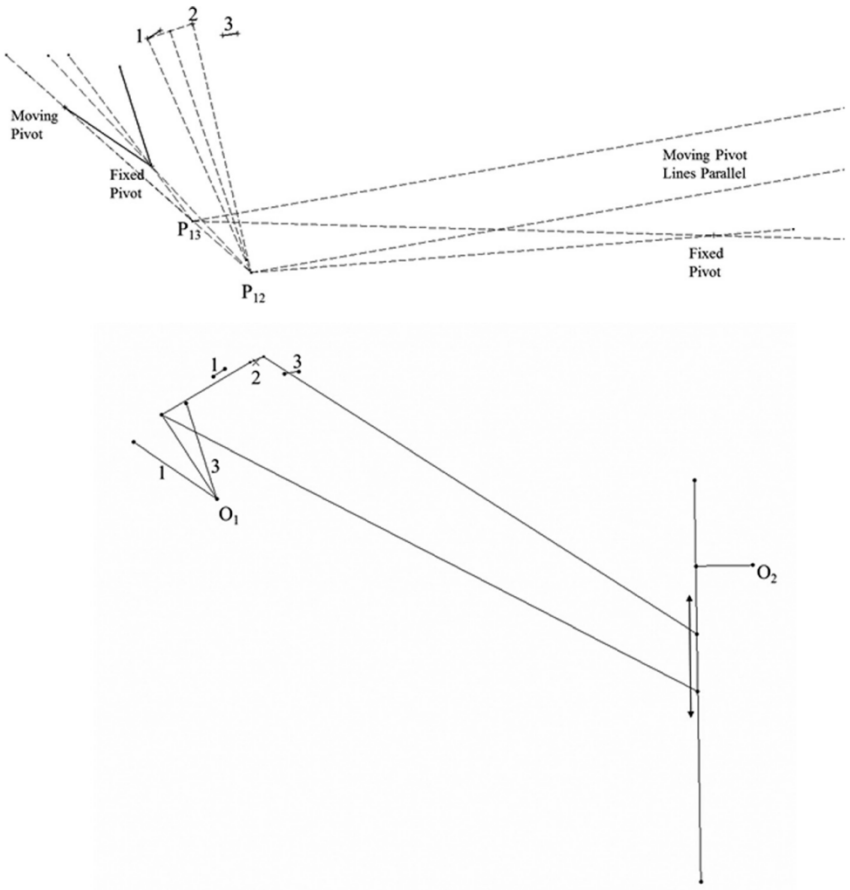

Figure 1.10. The 2-1-1 synthesis problem with its drawn constraints and solution [16].

Since the PRC method creates mechanisms for mixed synthesis problems, it is a more applicable method in real world situations as synthesis problems rarely have one type of constraint. But in order to use the PRC method, one must not only identify their constraints, but make sure that the summation of the function, path, and two times the motion constraints is not greater than 10 [16]. Otherwise, the problem is over-constrained and a new set of constraints will have to be created.

1.4.3 Six-bar Mechanisms in CAD

Another CAD based method is the Geometric Constraint Programming (GCP) for six-bar mechanisms. This method is applicable to Stephenson I-III and Watt I six-bar mechanisms [17]. In general, GCP method involves creating three overlaying sketches in CAD; the first layer will contain the target positions, the second will have a mechanism drawn with the geometric constraints of the problem, and the final sketch has a mechanism drawn with the second layer's mechanism as it moves between the different target positions [17]. The described method slightly varies depending on the type of six-bar mechanism, with there being two main groups; the Stephenson I, Stephenson III, and Watt I grouped together and the Stephenson II grouped by itself [17].

For the former group, this family of mechanisms consist of having a four-bar mechanism within the larger six-bar mechanism, where the four-bar mechanism is

attached to the ground [17]. First, a dyad or triad will be synthesized between a ground pivot point and a point P on one of the target positions [17]. Another dyad/triad will be drawn from the second pivot point to create a four-bar mechanism [17]. Lastly, another dyad/triad is added to complete the six-bar mechanism [17]. At each of these three steps, equality constraints are applied to ensure the integrity and motion of the mechanism [17]. An example of the synthesis of a Stephenson I six-bar mechanism is shown in Figure 1.11 [17].

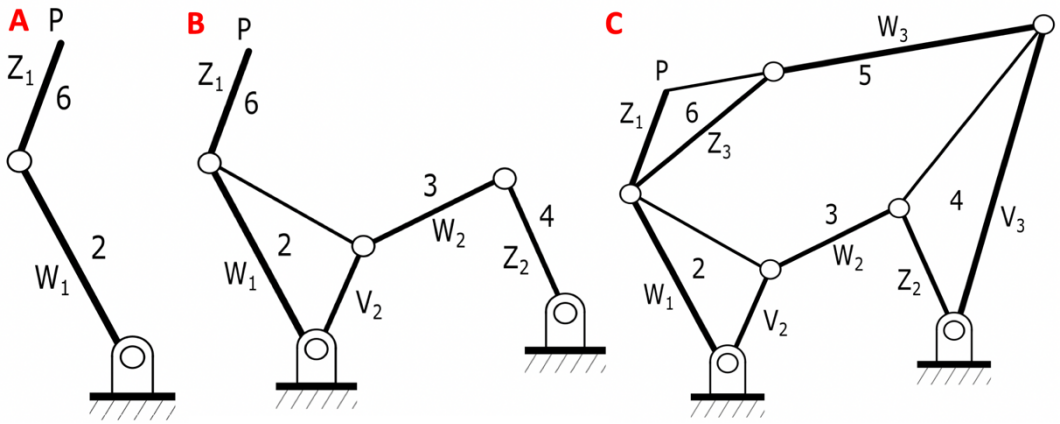

Figure 1.11. Synthesizing a Stephenson I six-bar mechanism with the GCP method via A) the first dyad/triad, B) the second dyad/triad, and C) the third dyad/triad [17].

For the Stephenson II mechanism, a dyad is drawn between a ground pivot point and point P on a target position [17]. Then, a triad is drawn to create a five-bar mechanism before a second triad is drawn to complete the six-bar mechanism [17]. Similarly, with the other six-bar mechanisms, equality constraints have to be applied at each step of synthesizing a Stephenson II mechanism [17]. These steps are illustrated in the synthesis of a Stephenson II mechanism in Figure 1.12 [17].

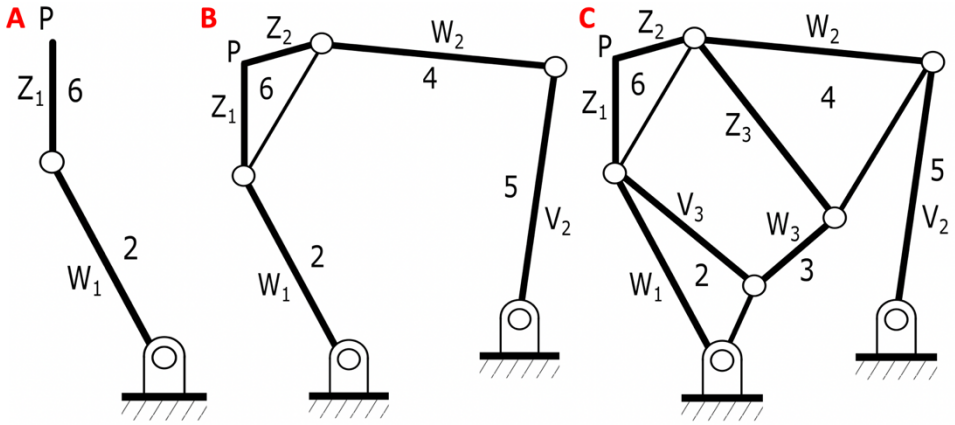

Figure 1.12. Synthesizing a Stephenson II six-bar mechanism with the GCP method via A) the first dyad, B) the first triad, and C) the second triad [17].

Six-bar mechanisms are capable of tracing more complex paths than four-bar mechanisms, but have several issues to consider [17]. They are more prone to synthesis complications such as circuit defects and crank rotatability [17]. Also, by having more links, they can be more difficult to fit in the geometric constraints of the design problem.

1.4.4 MotionGen

Along with computer based analytical and CAD software based graphical methods, other software is being developed to visually create a kinematic solution for the user, with the ability to change constraints on the fly and see resulting solutions in real time. An example of such a software is the four-bar mechanism generator, MotionGen [18]. MotionGen accomplishes this by using a 3x3 homogeneous transformation matrix and then creating different algebraic manifolds for revolute-revolute, revolute-prismatic, prismatic-revolute, and prismatic-prismatic dyads [19-20]. These manifolds are intersected in the image space with constraints, known as algebraic fitting of a pencil of quadratics [19-20]. From this intersection, represented as a matrix, singular value decomposition is performed to find the eigenvectors [19-20]. The software will use quadratic relations to add the last constraints to the mechanism or it will use least squares fit to finish the last constraints and provide a mechanism [19-20]. Using this matrix-based approach, MotionGen is able to produce coupler curves and mechanism faster than more complicated analytical methods.

In summary, when synthesizing a mechanism, there is a large range of possible techniques that an engineer can use. Adding more constraints and/or links may yield a mechanism that more accurately accomplishes the design criteria, but computing and analyzing such solutions is computationally taxing and may be more prone to complications. Resulting from the desire to simplify the calculations, one of the most common mechanisms used in synthesis is the four-bar mechanism, usually incorporating revolute and/or prismatic joints. Therefore, this thesis outlines the usage of both traditional and modern synthesis techniques to create a gait correcting four-bar mechanism to attach to the ICARE.

Chapter 2 Methods

This section lays out how the kinematic synthesis input was created, several kinematic synthesis methods that were utilized to make the mechanism, the optimization function of the theoretical design, the fabrication process of the physical prototype, and device testing. The different methods are laid out in chronological order of their implementation. Each successive iteration focused on addressing one or more weaknesses identified in the previous synthesis method, as explained in each synthesis section. Much of this chapter's work may also be found in a conference article [9].

2.1 Kinematic Synthesis Problem Definition

To begin, kinematic data were collected by placing reflective markers on the pelvis and legs of a young adult (age = 34 years, height = 1.8 m, weight = 93.2 kg) and having them use the ICARE at a self-selected motor-assisted pace [6]. The data were collected with the Qualisys Motion Analysis System and Track Manager software (Qualisys, Gothenburg, Sweden) [6]. This data series was then imported into MATLAB (MathWorks, Natick, Massachusetts, USA), where it was divided into individual movement cycles using the reference limb's toe marker data. These motion cycles were then averaged together to create a single representative ICARE movement cycle for each respective kinematic variable.

Model 2354 from OpenSim was used as the standard for normal gait. The model is based on a person with a height and weight of 1.8 m and 75.16 kg, respectively [10]. The kinematic data for model 2354 were transferred to MATLAB and then segmented using successive initial contacts of the heel. This produced two OpenSim gait cycles which were then averaged together to create an ensemble average profile.

Next, foot centroids were created for both the ICARE and OpenSim datasets. This was done by averaging the ankle and toe data for each set. Then linear interpolation (resampling) was utilized to ensure that both vectors were of the same length in MATLAB. The OpenSim data were scaled so that the horizontal range matched that of the ICARE data to compensate for any stride length differences. The two position curves were overlaid with their center points aligning, and the starting points of the two data sets were aligned.

The ICARE position curve was then subtracted from the OpenSim position curve to create the kinematic synthesis position input curve (Figure 2.1) [9]. The horizontal and vertical displacement data for both the ICARE and OpenSim were used to find their respective angles at each data point. The ICARE's angular data was subtracted from the OpenSim angular data to create the kinematic synthesis angular input curve (Figure 2.2) [9].

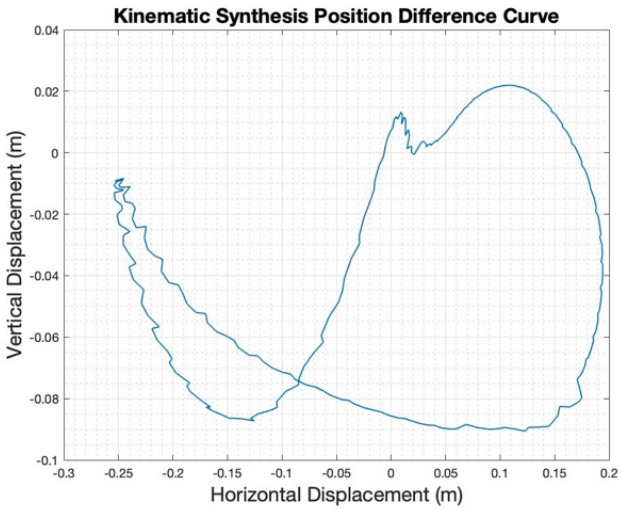

Figure 2.1. The position difference curve used in kinematic synthesis [9].

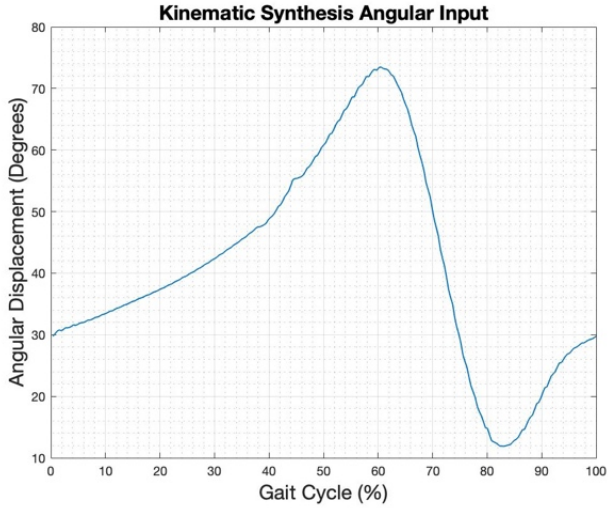

Figure 2.2. The angular difference curve used in kinematic synthesis [9].

2.2 Kinematic Synthesis Methods

2.2.1 Three Prescribed Positions Problem Graphical Synthesis

The first method used was the three prescribed positions graphical synthesis, as referenced in Figure 2.3 below, and was performed in MATLAB to bypass the human error and drafting tool limitations described earlier in this thesis for this technique [12].

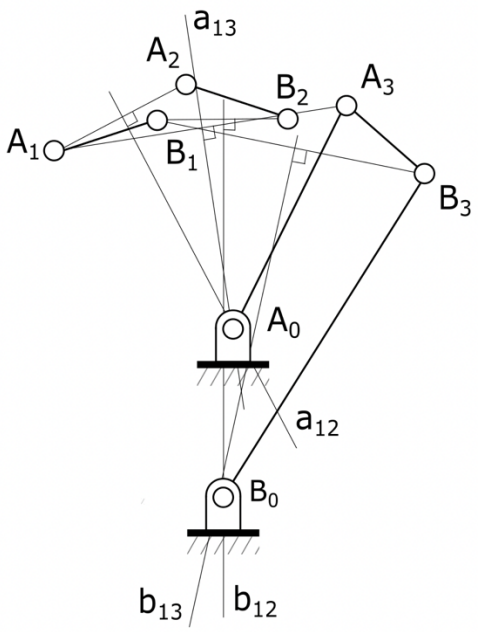

Figure 2.3. Schematic of the three prescribed positions graphical synthesis [12].

A length was chosen for the coupler, as well as the coordinates for the center point of the coupler and the angle of the coupler for three positions from the synthesis input curves. By using the coupler angle, length, and coordinates of its center point, the two potential x-coordinates of the rocker-coupler endpoint were found using Equation 2.1:

$$B_{nx} = C_{nx} \pm \sqrt{\frac{L^2}{1+(tan(\varphi_n))^2}} \tag{2.1}$$

where n = 1 to 3, B_{nx} is the x-coordinate of the rocker-coupler endpoint for the n^{th} position, C_{nx} is the x-coordinate of the center point for the n^{th} position, L is half of the coupler length, and φ_n is the coupler's angle for the n^{th} position. Next the angle of the coupler was used to check which quadrant the rocker-coupler endpoint should be in, giving the correct x-coordinate. The y-coordinate of the rocker-coupler endpoint was calculated with Equation 2.2:

$$B_{ny} = C_{ny} + tan(\varphi_n) * (B_{nx} - C_{nx}) \tag{2.2}$$

Here B_{ny} and C_{ny} are the y-coordinates for the rocker-coupler endpoint and coupler center point, respectively, for the n^{th} position. The coordinates of the crank-coupler endpoint (A_{nx} and A_{ny}) were then found by finding the differences in the x and y coordinates from the rocker-coupler endpoint to the coupler center point, then subtracting these distances from the coupler center point. With the endpoints of the coupler positions now known, the slopes of the lines connecting A_1 to A_2 (A_1A_2), A_1 to A_3 (A_1A_3), B_1 to B_2 (B_1B_2), and B_1 to B_3 (B_1B_3) were found by dividing the change in the y-

coordinates by the change in the x-coordinates. The midpoints for these four lines were calculated by averaging the x- and y-coordinates, respectively, for their endpoints.

Next, the perpendicular lines a_{12}, a_{13}, b_{12}, and b_{13} were drawn. In order to do this, first the slope needed to be found, which was the negative inverse of the previous lines. For example, the slope of a_{12} is the negative inverse of the slope for A_1A_2. These lines can be drawn with equations in point-slope form with their slopes and the midpoints from lines A_1A_2, A_1A_3, B_1B_2, and B_1B_3, respectively. Then lines a_{12} and a_{13} were equated to each other to find the coordinates of A_0. The coordinates of B_0 were found using the same process with lines b_{12} and b_{13}, completing a four-bar mechanism. This method provided limited success as the size of the coupler link had to be assumed. Therefore, to bypass this restriction, the three prescribed points analytical synthesis method was examined next.

2.2.2 Three Prescribed Points Problem Analytical Synthesis

The three prescribed points problem differs from the previous one as it does not require a coupler angle to synthesize a mechanism. For this design problem, several assumptions needed to be made from Figure 2.4 [12]. First, it was assumed that the coordinates for A_0, B_0, P_1, P_2, and P_3, as well as the values for ϕ_j, ε_j, and ψ_j were known. ϕ_j, ε_j, and ψ_j are the changes in the input, coupler, and output links' angles, respectively, from point P_1 to point P_j [12]. The R_j vector represents the position vector of P_j in the coordinate frame.

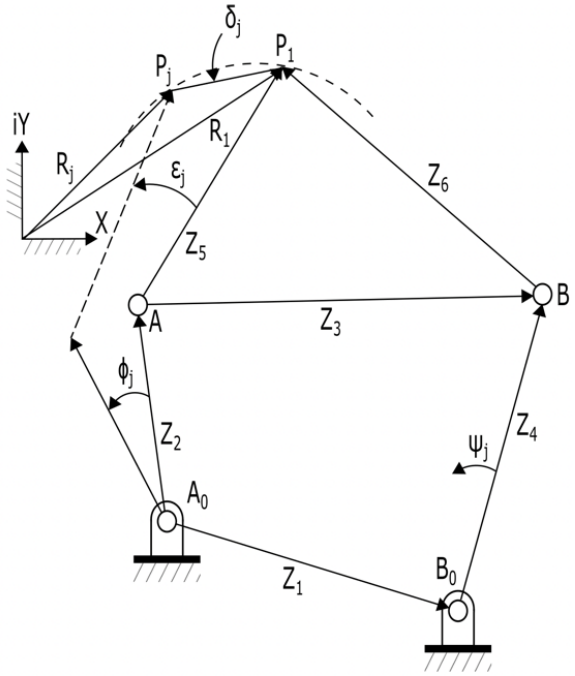

Figure 2.4. Schematic of the three prescribed points analytical synthesis [12].

As seen in Figure 2.4, the links are represented by vector equations Z_1 through Z_6 for the ground link, crank, bottom of the coupler triangle, rocker, left and right sides of

the coupler triangle, respectively. These vector equations are represented by Equations 2.3-2.6 [12], where δ_j is the displacement from P_1 to P_j:

$$\delta_j = Z_2\left(e^{i\varphi j} - 1\right) + Z_5\left(e^{i\varepsilon j} - 1\right);\ j = 2,3 \tag{2.3}$$

$$\delta_j = Z_4\left(e^{i\psi j} - 1\right) + Z_6\left(e^{i\varepsilon j} - 1\right);\ j = 2,3 \tag{2.4}$$

$$Z_3 = Z_5 + Z_6 \tag{2.5}$$

$$Z_1 = Z_2 + Z_3 - Z_4 \tag{2.6}$$

Rearranging these equations gave Equations 2.7 and 2.8 [12]:

$$\begin{bmatrix} \delta_2^x \\ \delta_2^y i \\ \delta_3^x \\ \delta_3^y i \end{bmatrix} = \begin{bmatrix} a * cos\left(\theta_{Z_2}\right) - b * sin\left(\theta_{Z_2}\right) & c * cos\left(\theta_{Z_5}\right) - d * sin\left(\theta_{Z_5}\right) \\ i[b * cos\left(\theta_{Z_2}\right) + a * sin\left(\theta_{Z_2}\right)] & i[d * cos\left(\theta_{Z_5}\right) + c * sin\left(\theta_{Z_5}\right)] \\ e * cos\left(\theta_{Z_2}\right) - f * sin\left(\theta_{Z_2}\right) & g * cos\left(\theta_{Z_5}\right) - h * sin\left(\theta_{Z_5}\right) \\ i[f * cos\left(\theta_{Z_2}\right) + e * sin\left(\theta_{Z_2}\right)] & i[h * cos\left(\theta_{Z_5}\right) + g * sin\left(\theta_{Z_5}\right)] \end{bmatrix} \begin{bmatrix} Z_2 \\ Z_5 \end{bmatrix} \tag{2.7}$$

$$\begin{bmatrix} \delta_2^x \\ \delta_2^y i \\ \delta_3^x \\ \delta_3^y i \end{bmatrix} = \begin{bmatrix} k * cos\left(\theta_{Z_4}\right) - l * sin\left(\theta_{Z_4}\right) & c * cos\left(\theta_{Z_6}\right) - d * sin\left(\theta_{Z_6}\right) \\ i[l * cos\left(\theta_{Z_4}\right) + k * sin\left(\theta_{Z_4}\right)] & i[d * cos\left(\theta_{Z_6}\right) + c * sin\left(\theta_{Z_6}\right)] \\ m * cos\left(\theta_{Z_4}\right) - n * sin\left(\theta_{Z_4}\right) & g * cos\left(\theta_{Z_6}\right) - h * sin\left(\theta_{Z_6}\right) \\ i[n * cos\left(\theta_{Z_4}\right) + m * sin\left(\theta_{Z_4}\right)] & i[h * cos\left(\theta_{Z_6}\right) + g * sin\left(\theta_{Z_6}\right)] \end{bmatrix} \begin{bmatrix} Z_4 \\ Z_6 \end{bmatrix} \tag{2.8}$$

$$a = cos(\varphi_2) - 1$$

$$b = sin(\varphi_2)$$

$$c = cos(\varepsilon_2) - 1$$

$$d = sin(\varepsilon_2)$$

$$e = cos(\varphi_3) - 1$$

$$f = sin(\varphi_3)$$

$$g = cos(\varepsilon_3) - 1$$

$$h = sin(\varepsilon_3)$$

$$k = cos(\psi_2) - 1$$

$$l = sin(\psi_2)$$

$$m = cos(\psi_3) - 1$$

$$n = sin(\psi_3)$$

where θ_Z represents the angle of its respective Z vector, as defined in Figure 2.5 [12].

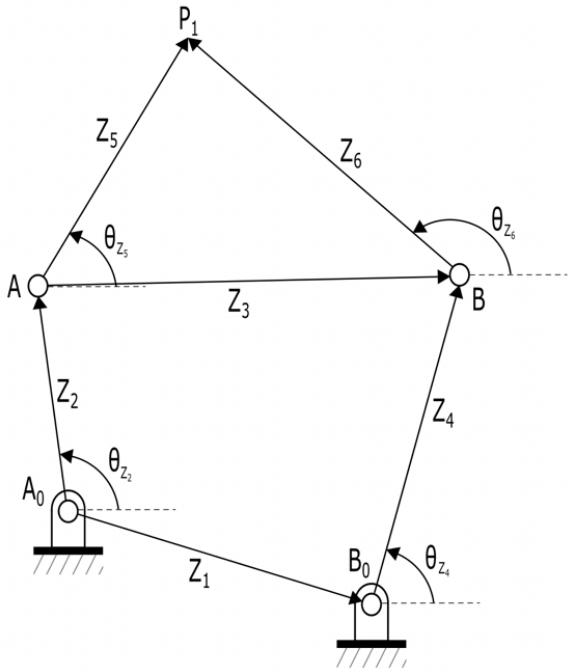

Figure 2.5. Angular definitions of the Z vectors [12].

While the three prescribed points method was an improvement given the size of the coupler was not assumed, it was still insufficient for this design problem as it made many design assumptions, such as the location and orientation of the ground link and the change in the angle of the links. The next method intended to remedy these issues as it used the MotionGen software. MotionGen can produce a coupler curve in real-time as the engineer changes the location of the endpoints of links and key poses in the desired coupler curve. Therefore, MotionGen allowed more design freedom and quicker analysis of how the coupler curve changes with different design constraints.

2.2.3 MotionGen Kinematic Synthesis

Following the three prescribed positions analytical synthesis technique, the five-point synthesis tool was used in MotionGen as the problem lacked strict design constraints for the position and orientation of the ground link. Since the software approximates a solution, 11 different rigid body guidance problems were tested using different sets of poses. In test sets 1-6, the vector length of the synthesis input curves was divided into five to ten sections, respectively, with each section having the same number of data points as the others.

In test sets 7-11, the data were again divided into five sections of equal vector length. Then left and right markers were placed at +/- 10 data points from these points to create the colored regions seen in Figure 2.6 [9]. During these synthesis experiments, four of the five poses were placed on the center point of the colored regions, while the fifth point was allowed to float between the left and right markers of the last region. Test sets 7-11 varied the dark blue, red, green, yellow, and light blue regions, respectively.

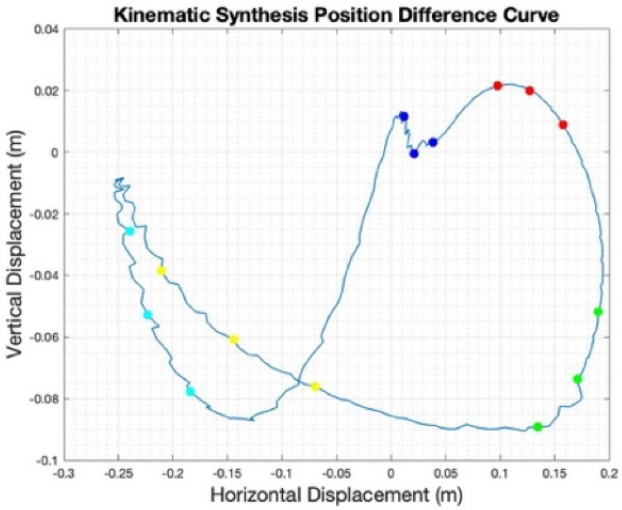

Figure 2.6. The position difference curve with the five colored regions, including the center point with the +/- 10 data points markers [9].

While MotionGen gave more freedom to the designers, the number of possible mechanisms that could be built is infinite. The three prescribed positions and points methods mentioned earlier drastically narrowed down the number of possible mechanisms, but the assumed positioning of the ground link could have been ill placed. The next section describes a method that arose from the need to have design constraints to limit the number of possible mechanisms, but the design constraints are already known to produce a potentially viable solution.

2.2.4 Atlas Search Kinematic Synthesis

From the MotionGen method, nine of the 11 problem sets did not produce closed loop cycles and were too large to fit onto the ICARE. The other two solutions did not fit the position synthesis curve well. Therefore, an alternative design method, referred to as the atlas search method, was utilized for creating a four-bar mechanism to approximately fit the position synthesis curve [9, 21]. This method involved searching through an atlas of coupler curves to find a four-bar mechanism to approximate the solution [9, 21]. With a mechanism selected, it was then drawn in MotionGen to capture the coordinates of the endpoints of each link.

Then the mechanism was created and scaled in MATLAB using the coordinates from MotionGen. The MATLAB function creates the diagonal z that connects points A

and O_4, as shown in Figure 2.7 [9, 11]. Using the law of cosines, a relationship was derived between the angles of the crank and rocker. With the scaling in MATLAB, the crank and rocker link lengths were known, which now given the angles, produced the crank and rocker curves. From MotionGen, the angles in the coupler triangle were calculated using the law of cosines. Now with crank, rocker, and coupler triangles lengths and angles known, the end effector's position was calculated at each stage of motion. The pose was then completed by using the inverse tangent function with the horizontal and vertical displacements to create the end effector's angle.

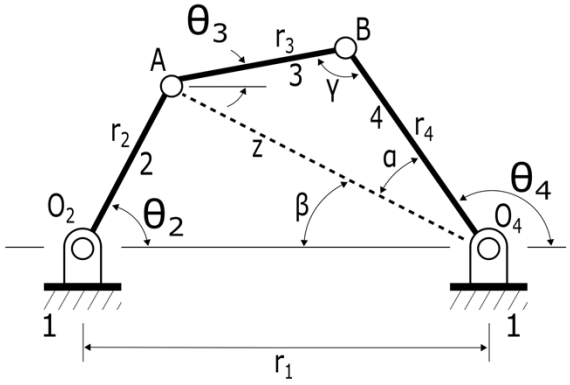

Figure 2.7. Schematic of a four-bar mechanism to derive the relationship of the crank and rocker angles with the law of cosines [9, 11].

2.3 Optimization

With a mechanism selected from the atlas and modeled in MATLAB, it was further optimized using *fmincon()*. In order to accomplish this, the starting point of the mechanism's coupler curve was aligned with the starting point of the synthesis input. The variables for optimization were the link lengths and the location of the ground link. The links were allowed to lengthen or shorten by +/- 10% of the original longest and shortest link lengths. Additionally, the ground link was allowed to move and re-orient itself within a 2 m by 2 m area centered at the origin.

The goal function that was minimized is:

$$f = \sum_{i=1}^{n}[(1-W) * \sqrt{A(i)} + W * B(i)] \tag{2.9}$$

$$A(i) = \left(KI_x(i) - P_x(i)\right)^2 + \left(KI_y(i) - P_y(i)\right)^2$$

$$B(i) = \left|P_\theta(i) + \delta - KI_\theta(i)\right|$$

where n is the total number of data points, KI is the kinematic synthesis input, P is the coupler curve, W is the weight of the angular component of the equation, and δ is the angular offset between the original solution and the kinematic synthesis input. The horizontal, vertical, and angular displacement components are notated by x, y, and θ subscripts, respectively.

The weight values (n=101) ranged from 0 to 1 and were incremented by 0.01. W=0 is a solution solely based on the position component of Equation 2.9, while W=1 is a solution solely based on the angular component of the equation. In addition to the weight extremes, three other solutions were subjectively selected for further comparison based on their merits as design solutions. The final comparison between the five candidates consisted of computing the value of Equation 2.9 for a given solution with the other four weight values, and the average lowest value should be the best candidate.

2.4 Fabrication Process

2.4.1 CAD Design/Physical Parts

The parts were drawn and assembled in SolidWorks (Dassault Systèmes SE, France), then simulated with the static finite element analysis (FEA) study in SolidWorks using a force ranging from 200 to 300 lbf on the pedal in order to identify possible stress concentrations and redesign them. While SolidWorks FEA can identify locations of concern, the accuracy of the stress values that it calculates may not be as high for more complicated structures. Therefore, hand calculations were performed to find the bending stress in the crank, rocker, and rectangular tube making up the vertical support of the mechanism, as well as the shear stress on the bolts and crank shaft. The bending and shear stress equations are displayed in Equations 2.10 and 2.11.

$$\sigma = \frac{M*y}{I} \tag{2.10}$$

$$\tau = \frac{F}{A} \tag{2.11}$$

where σ is the bending stress, M is the moment from the applied force, y is the distance from the neutral axis, I is the area moment of inertia, τ is the shear stress, F is the applied force, and A is the area of shear.

These locations were chosen as their distance from the force application and material thickness of the part made these locations vulnerable to failing. The chosen material for both CAD and fabrication was an aluminum 6061 alloy. Additionally, it was assumed that the entire force went through the crank and rocker, solely, when their respective bending stresses were calculated. After verifying these calculations, the components were then fabricated by the UNL machine shop and fitted to the ICARE to ensure a proper fit.

2.4.2 Electronics

While the components were being fabricated, the electrical circuit was also being designed. The electronics consist of a 36 V 14 Ah Ebike battery, Flipsky 1150 W brushless DC motor (Flipsky, Dongguan City, China), Nema23 planetary gearbox with a 100:1 gear ratio, Flipsky VESC 4.12 speed controller, Flipsky VX1 Bluetooth remote controller, 40 A circuit breaker, 36 V 40 A relay switch, and 660 V 10 A emergency stop bottom. The circuit diagram is shown in Figure 2.8 below. MISUMI High Torque S5M

Timing Pulleys (MISUMI USA, Illinois, USA) were placed on the crank shaft and gearbox with a MISUMI S5M Series High Torque Timing Belt connecting them. The assembled mechanism with electronics was then tested in the lab.

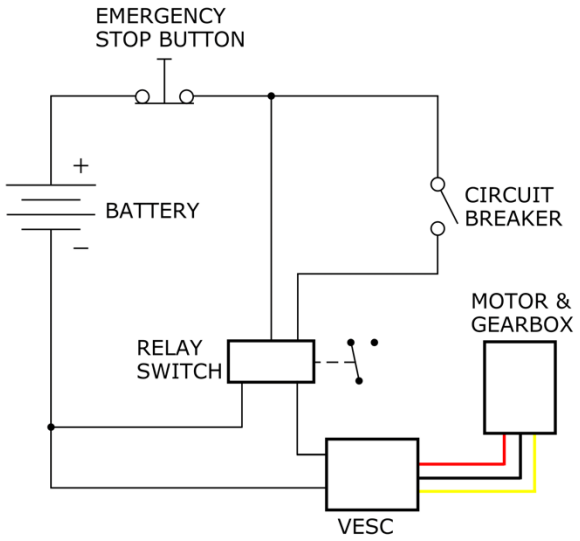

Figure 2.8. Circuit diagram of the electronics.

2.5 Device Testing

Only the right foot's mechanism was created to gather pilot data. The reason for only fabricating one mechanism was to have a relatively low-cost pilot comparison between a foot equipped with the mechanism and one without it. The mechanism was bolted onto a table in the lab and the motor was tested to see if the crank could fully rotate. The crank was not able to fully rotate and a grinding noise was heard, so the mechanism was troubleshot to determine what the issues were. A plan was laid out for how to solve these issues in future work; more details on the mechanism's performance and this plan can be found in the Results and Discussion section.

Chapter 3 Results & Discussion

This section presents the results of the various kinematic synthesis techniques outlined in the Methods sections, as well as an analysis of the results. Much of the content of this chapter can be found in [9].

3.1 Three Prescribed Positions Problem - Graphical Synthesis

Three coupler positions (Table 3.1) were chosen to have two positions in the larger right-hand side of the curve and one on the left-hand side (Figure 3.1). The coupler length was chosen to be 0.2 m as the pedal of the ICARE will be attached to the coupler. Therefore, it needed to be large enough to support the pedal.

Table 3.1. The center points' coordinates and angles of the assumed positions in the three prescribed positions problem set up.

Prescribed Position	x-coordinate (m)	y-coordinate (m)	Angle (°)
1	0.02	0	29.76
2	0.17	-0.08	48.11
3	-0.24	-0.04	36.04

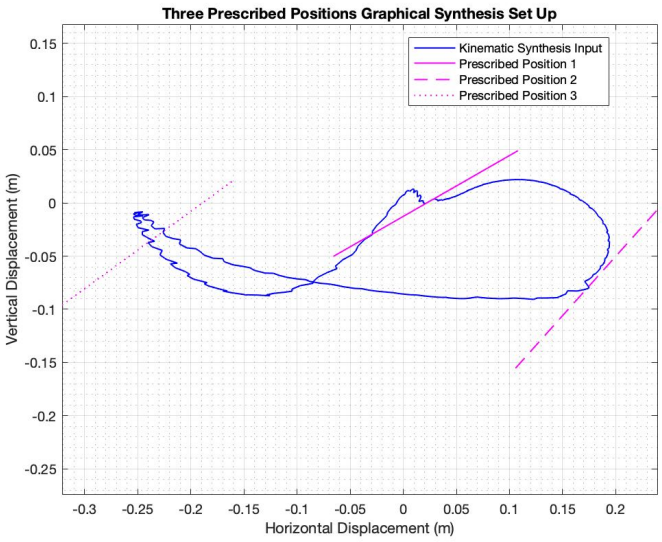

Figure 3.1. The three prescribed coupler positions used in the graphical synthesis method.

By using the three prescribed positions graphical synthesis method, a rocker-rocker mechanism was produced (Figure 3.2). Since none of the links fully rotate, the coupler curve will not be a cycle, unlike the synthesis input. Synthesis with this method proved undesirable as there were many variables to manipulate (size of the coupler as well as the location and orientation of each coupler position) and can result in fairly large mechanism.

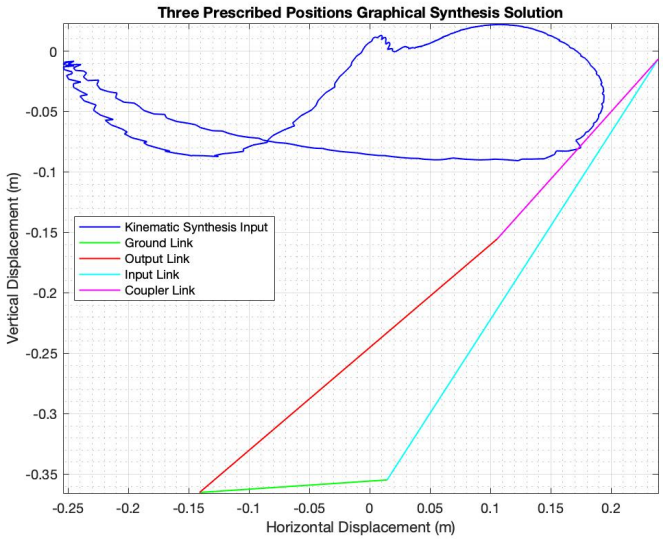

Figure 3.2. Resulting mechanism from the three prescribed positions graphical method.

3.2 Three Prescribed Points Path Generation Problem - Analytical Synthesis

Where the three prescribed positions graphical synthesis method had many assumptions, so too does the three prescribed points problem for analytical synthesis. But the key benefits to attempting this method were that the coupler's size and orientation did not have to be assumed. This prevented the engineer from creating a mechanism like in Figure 3.2, where the mechanism dipped well outside of the feasible workspace. Additionally, the coupler positions avoided limiting the coupler to a certain size and freed the engineer from having to assume the coupler's angle at those positions.

Similar to the previous method, two coupler points were on the right-hand side of the curve, while the third point was on the left-hand side. The produced mechanism was once again a rocker-rocker mechanism. The pitfalls of this method were similar to the ones in the graphical three-positions synthesis method, relying too heavily on the assumptions made. For both methods, there is an infinite number of problem setups based on the assumptions.

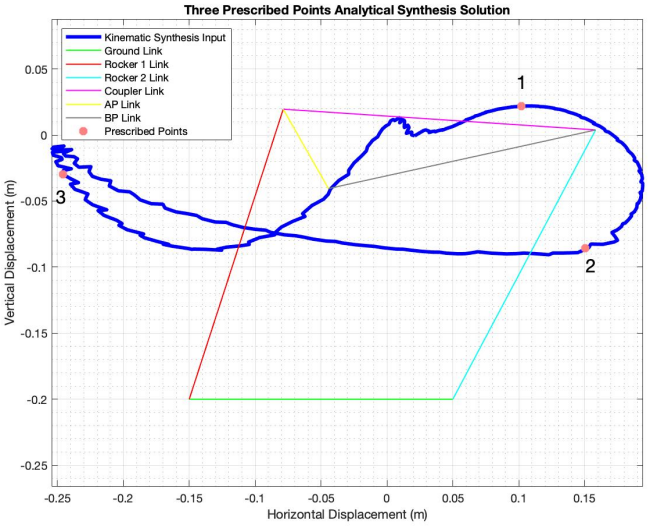

Figure 3.3. Resulting mechanism from the three prescribed points analytical method with the three prescribed points highlighted as orange dots.

3.3 MotionGen Kinematic Synthesis

With the previous two methods, another limitation they had was that they do not provide live feedback on how the coupler curve changes with the mechanism. MotionGen provided a solution to this by updating the coupler curve in real time as the endpoints of the links are moved, allowing trends to be observed more easily. For each solution in MotionGen, the mechanism had two different coupler curves that it could follow (shown as red and blue lines in Figures 3.4 and 3.5). Of the eleven test sets, only test sets 2 and 9 produced coupler curves that were closed loop cycles. For test set 2, the blue coupler curve follows the top of the right-hand side of the synthesis input curve, but then deviates greatly for the rest of the cycle. The red coupler curve hovers above the left-hand side of the synthesis input curve, but then deviates for the rest of the cycle. Additionally, the mechanism is far too large to be feasible with the design space allotted around the ICARE. Test set 9 had similar issues, but it overall had a better fit than test set 2 as its coupler curves were horizontally oriented, matching up more with the synthesis input curve. But like test set 2, test set 9 produced a mechanism that was not feasible. The other test sets can be seen in Appendix A1.

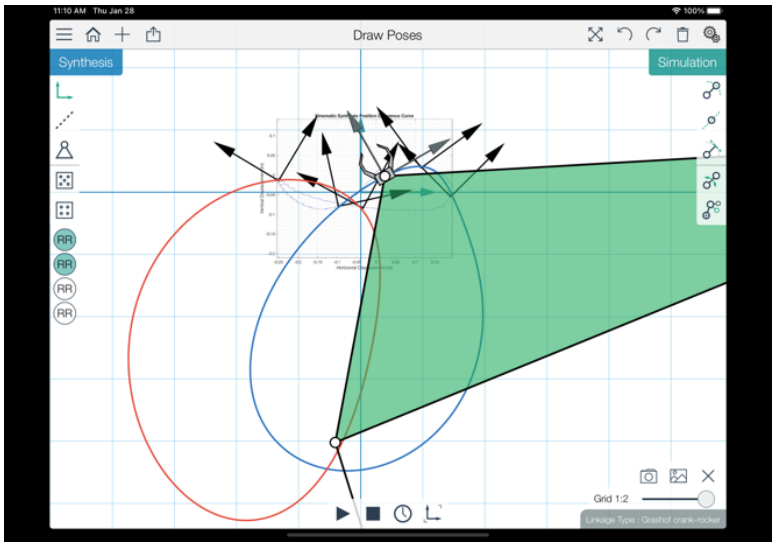

Figure 3.4. The mechanism coupler curves from test set 2.

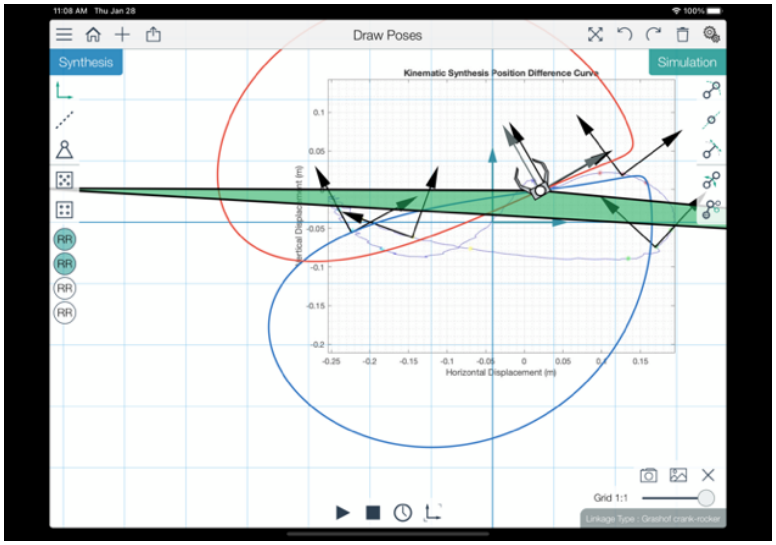

Figure 3.5. The mechanism coupler curves from test set 9.

MotionGen allowed the research team to test different poses in real time, changing the coupler curves as the mechanism was modified. This level of freedom turned into a drawback, similar to the previous synthesis methods, as this creates a near infinite number of potential test sets. Also, the software allowed fairly large mechanisms to be constructed to fit as many of the poses as possible. This led to mechanisms that were too large given the real-world design space.

3.4 Atlas Search Kinematic Synthesis

The previous methods were different from each other, but had the common challenge of having too many possible mechanisms. Rather than try an endless number of test conditions to find a reasonably sized mechanism that fits the synthesis input position curve, an atlas of coupler curves was searched through for an approximate

solution. An approximate solution (Figure 3.6) [21] was selected from the atlas and then recreated in MATLAB (Figures 3.7 and 3.8).

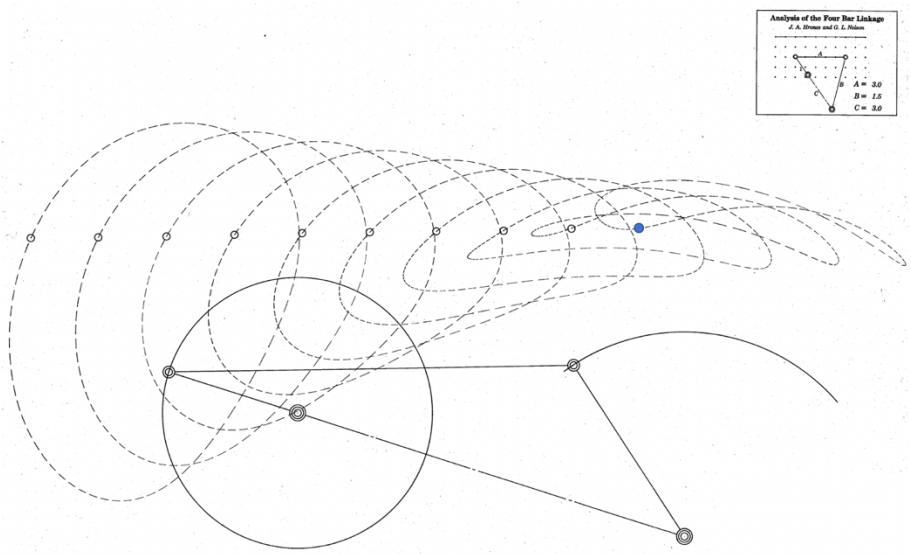

Figure 3.6. The coupler curves of the selected mechanism with the end effector of the selected coupler curve highlighted in blue [21].

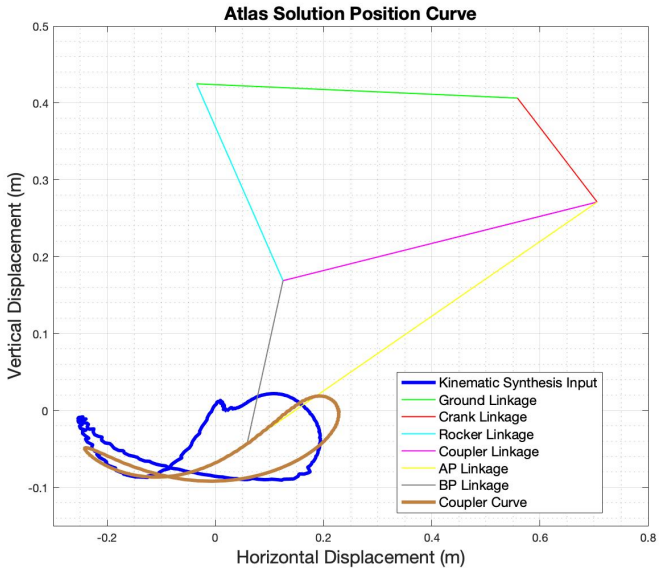

Figure 3.7. The coupler curve of the approximate mechanism.

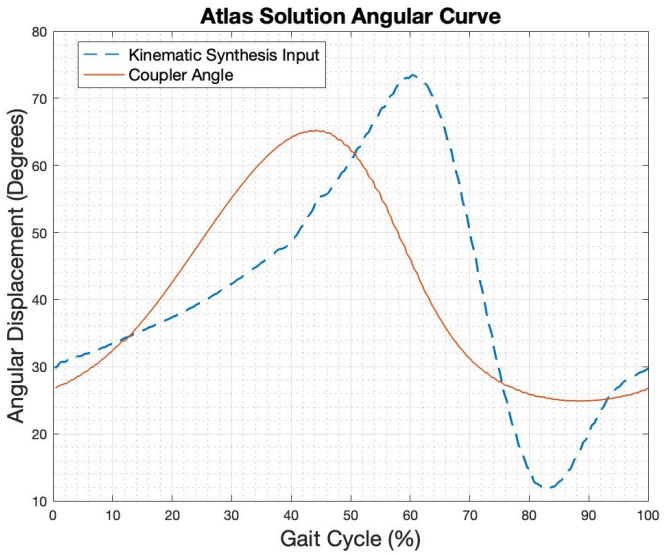

Figure 3.8. The angular curve of the approximate mechanism.

This design had a horizontal figure-eight coupler curve with the right-hand side being larger than the left-hand side. The right-hand side of the curve was slimmer than in the synthesis input and the left-hand side of the curve was shorter than in the synthesis input. The cross-over point in the figure-eight lined up fairly close to where it is in the synthesis input, deviating by ~3 cm. For the angular curve, the maximum angle occurred ~16% earlier in the gait cycle. The angular range was 40.4°, compared to 61.6° in the synthesis input.

3.5 Optimization

Compared with the previous methods, a feasible and acceptable design was produced using the atlas search method without testing a large number of ideas or assumptions. But given the shortcomings of the atlas mechanism, it was ideal to further optimize it before making a prototype. For the W=1 mechanism (shown in Figures 3.9 and 3.10), the coupler curve transformed from a figure-eight to a comma-like shape and shifted away to the right of the workspace. Therefore, the data was rotated and re-shifted so that the coupler curve lies on top of the kinematic synthesis input curve. With this rotation shifting, the angular range for this mechanism decreased to 34.2° and the peak angle occurred ~1% earlier in the gait cycle than in the atlas mechanism. Additionally, the peak angle was ~17° higher than the kinematic synthesis input.

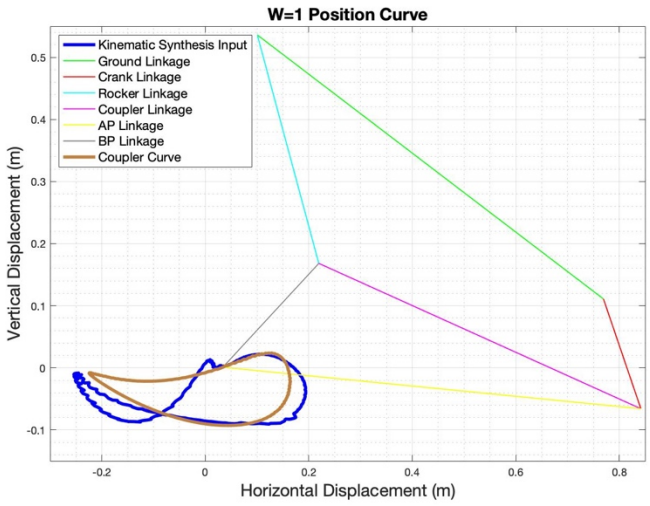

Figure 3.9. The coupler curve of the W=1 mechanism.

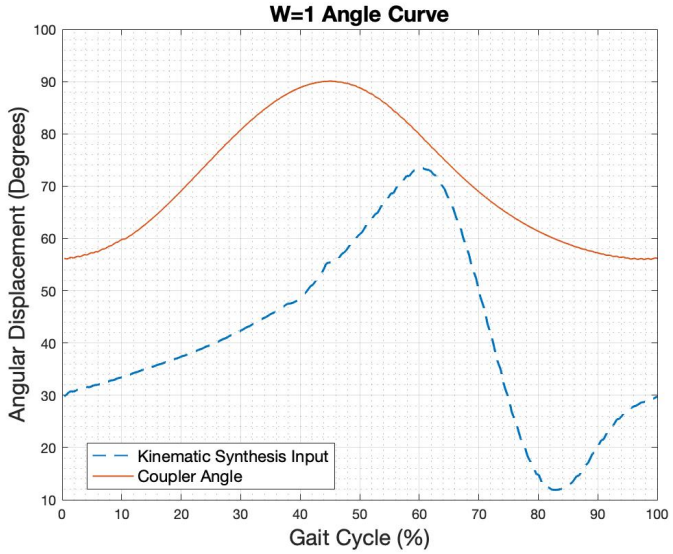

Figure 3.10. The angular curve of the W=1 mechanism.

With the W=1 mechanism representing an angular optimal solution, W=0 (Figures 3.11 and 3.12) represented a solution optimized purely for the position curve. The position curve did not change greatly from the atlas mechanism. The right-hand of the coupler curve is closer to the data points of the right-hand side of the synthesis input and the cross-over point of the figure-eight is closer to the synthesis input as well. The angular curve saw a drop in its range to 27.8° and the curve shifted downwards by 4°.

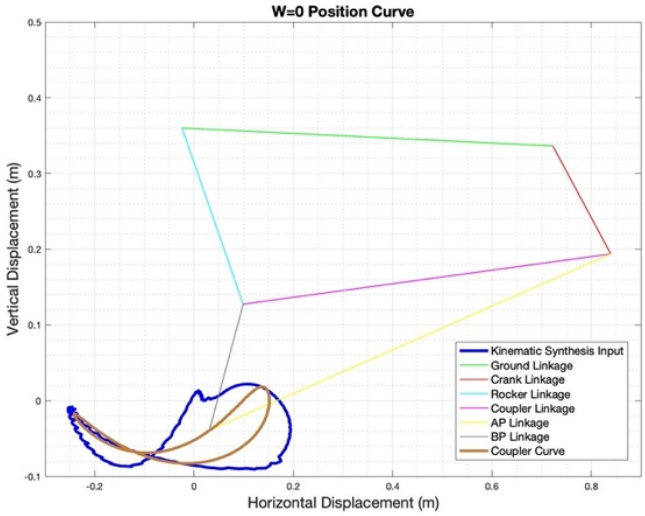

Figure 3.11. The coupler curve of the W=0 mechanism.

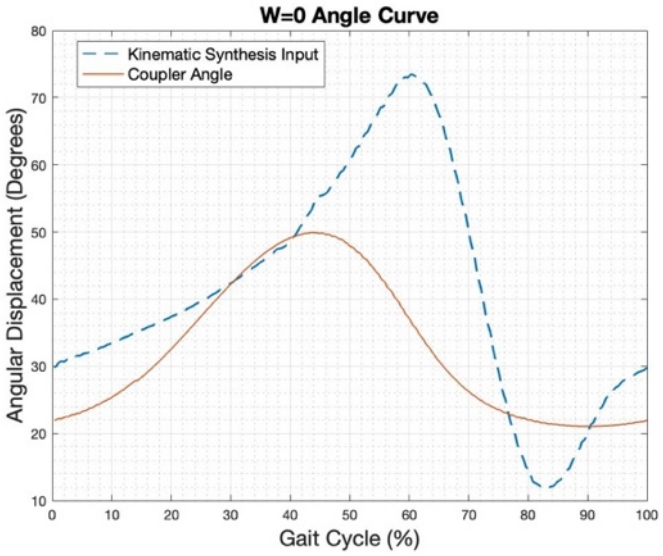

Figure 3.12. The angular curve of the W=0 mechanism.

Next, three mechanisms were selected that visually fit the position and angular curves better than the two extremes. The three selected weights were W=0.06, 0.08, and 0.16. For the W=0.06 mechanism (Figures 3.13 and 3.14), the right-hand side of the position curve expanded from the atlas mechanism while maintaining its figure-eight shape and its orientation relative to the synthesis input curve. Additionally, its angular range decreased to 28.2°.

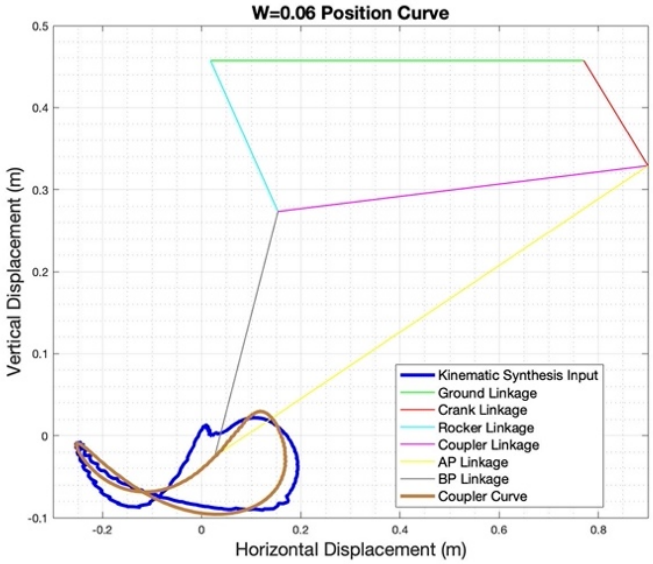

Figure 3.13. The coupler curve of the W=0.06 mechanism.

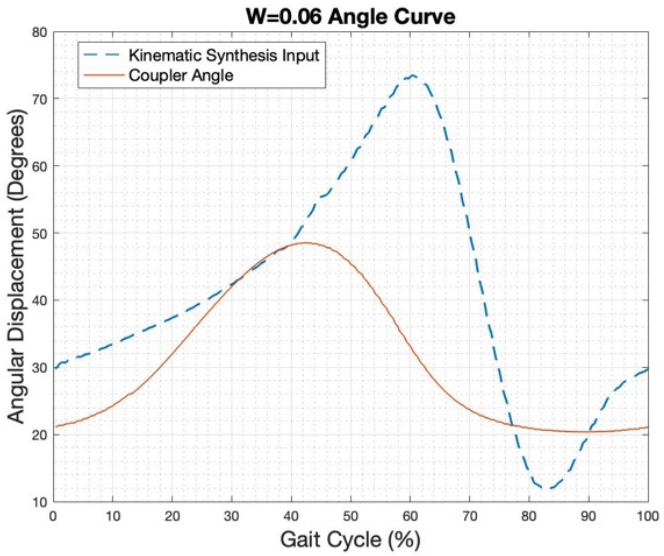

Figure 3.14. The angular curve of the W=0.06 mechanism.

Compared to W=0.06, the W=0.08 (Figures 3.15 and 3.16) mechanism was almost identical. The major difference in the position curves was that the W=0.08 mechanism's coupler curve was closer to the synthesis input curve in the portions that were outside of the synthesis input curve. The shape of their angular curves was identical, though the W=0.08 mechanism had a larger angular range at 28.6°.

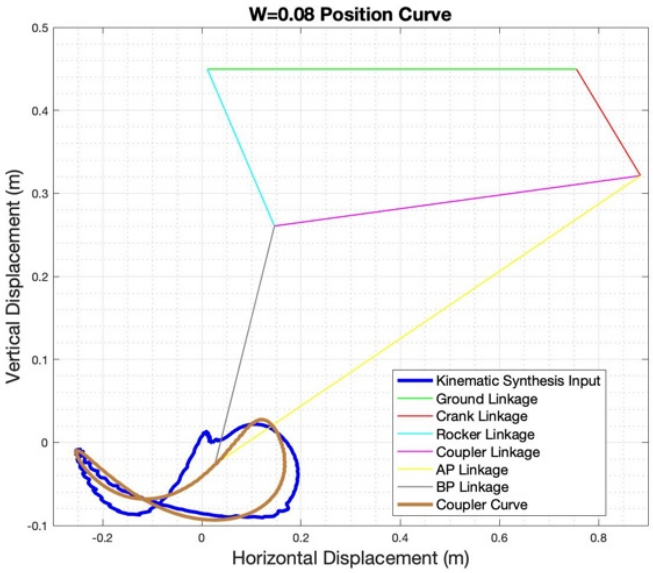

Figure 3.15. The coupler curve of the W=0.08 mechanism.

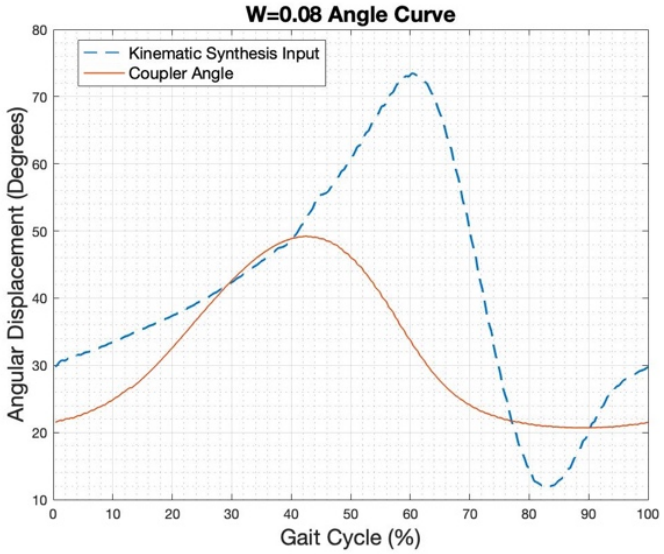

Figure 3.16. The angular curve of the W=0.08 mechanism.

Lastly, the W=0.16 (Figures 3.17 and 3.18) mechanism created a coupler curve that was smaller than W=0.06 and W=0.08. The angular range increased for this mechanism to 29.4° compared to 28.2° and 28.6° for W=0.06 and W=0.08, respectively. From this study, it was observed that the coupler's angle did not vary as significantly as the coupler curve did. The coupler's angular range was higher for higher values of W as well has having the maximum angle occur later in the gait cycle and an upward shift in angular values. The coupler curve would transition from a horizontal figure-eight to a comma-like shape between W=0.5 and W=0.75. The coupler curve would also rotate and move below and to the right of the synthesis input curve. This is due to *fmincon()*

finding a four-bar mechanism with the given link sizes and locations for a given weight, allowing the coupler curve to shift its relative placement to the synthesis input curve. The shifting coupler curve could be accommodated by shifting the location relative location of a physical prototype in reference to the ICARE.

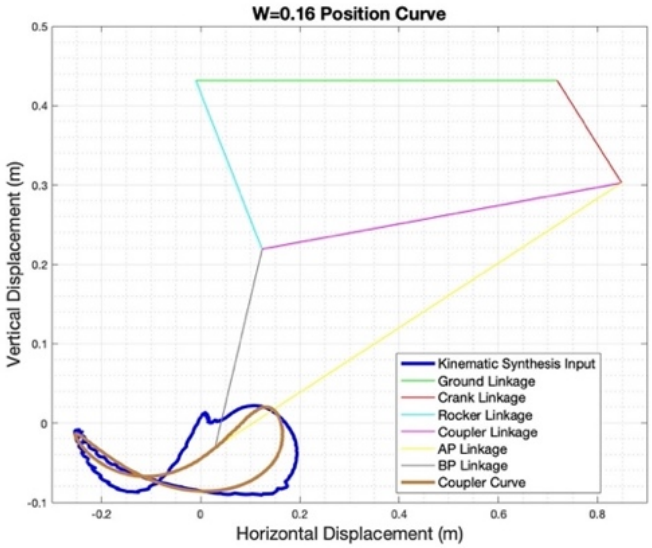

Figure 3.17. The coupler curve of the W=0.16 mechanism.

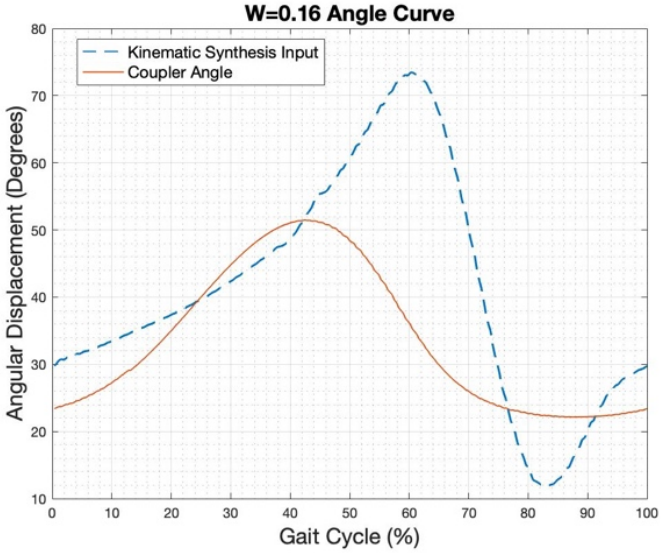

Figure 3.18. The angular curve of the W=0.16 mechanism.

How well these mechanisms fit the synthesis input curves was only one factor to consider; another was their size. Table 3.2 displays the link lengths for each mechanism. The atlas solution had the shortest link length for two of the six links, W=0.06 had the shortest link length for three of the six links (tied for the shortest crank, O2A, with W=0.08), and W=0 had the shortest length for the short side of the coupler triangle.

Table 3.2. The link lengths (cm) of the different designs.

		Weight Value				
	Atlas	1	0	0.06	0.08	0.16
O4O2	59.4	79.3	74.7	75.3	74.4	72.9
O4B	30.2	38.7	26.3	22.9	23.2	25.1
O2A	20.0	19.1	18.4	18.2	18.2	18.3
AB	59.1	66.4	74.5	75.0	74.2	73.1
AP	72.1	70.4	69.3	61.7	63.0	63.7
BP	22.2	25.0	18.0	32.5	31.1	26.8

Looking at a bounding-box to fit the mechanisms and allow them to move in their full range of motion (Table 3.3), none of the solutions produced a smaller mechanism than the atlas solution. Despite W=0.06 having shorter link lengths for half of the links, its assembly created a larger workspace than all of the other mechanisms. All of the mechanisms were under 1 m^2 for their bounding box, not automatically disqualifying any particular mechanism.

Table 3.3. The horizontal and vertical ranges and rectangular area of each solution.

		Weight Value				
	Atlas	1	0	0.06	0.08	0.16
Horizontal Range (m)	1.000	0.992	1.185	1.206	1.191	1.155
Vertical Range (m)	0.698	0.793	0.629	0.735	0.725	0.701
Area (m^2)	0.699	0.787	0.745	0.886	0.864	0.810

Therefore, a final comparison had to be made to choose an optimal design. An assessment between W=0.06, 0.08, and 0.16 (as stated before, W=0 and W=1 did not fit the curves as well since they were the extremes and therefore were not considered as final candidates) showed that 0.08 had the smallest goal function value in the optimization (Table 3.4). W=0.08 was then selected as the mechanism with which to conduct a further investigation.

Table 3.4. The goal function value assessment data of the three selected weights.

Weight Tested	Weight Used To Optimize		
	0.06	0.08	0.16
0.06	10.28	10.31	10.66
0.08	11.36	11.35	11.61
0.16	15.63	15.50	15.38
Average Value	12.42	12.39	12.55

After applying the W=0.08 mechanism's curves to the ICARE's curves in MATLAB (Figures 3.19 and 3.20), it can be seen that the position curve improved greatly. The overall shape of the position curve is closer to normal gait with only the right tip of the curve deviating significantly from normal gait. The angular curve did not improve as greatly, having an 8-10° offset and being out of phase with the maximum angle by ~20% in the gait cycle.

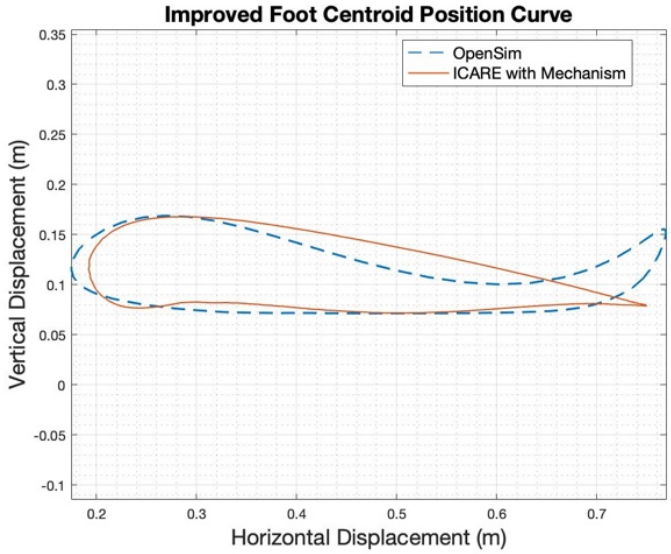

Figure 3.19. The coupler curve of the ICARE with the W=0.08 mechanism compared to OpenSim.

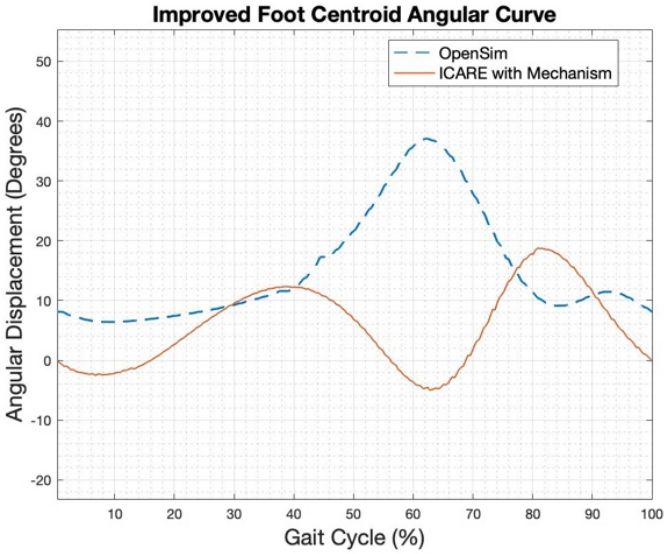

Figure 3.20. The angular curve of the ICARE with the W=0.08 mechanism compared to OpenSim.

3.6 Fabrication of the Physical Prototype

3.6.1 CAD Design

In this section, drawing files for all of the finalized parts of the mechanism can be viewed in Appendix A2. The first FEA was performed with plain carbon steel with an applied force of 300 pounds to see if the design would not fail with a commonly found, strong material with a high force (relative to the participant's weight used in testing). Later FEA runs used a force of 200 pounds due to the software crashing with higher force values. After several successful FEA runs, all of the part materials were switched to aluminum 6061 alloy to make the mechanism lighter while still having the proper strength. The ICARE's bodyweight support system was going to be used in human testing to add another layer of safety to prevent the mechanism from breaking and endangering the participant.

Also, for the SolidWorks FEA simulations, nuts and bolts were often removed and substituted with pegs extending out of the links. This was done due to the software crashing from the complicated geometries that accompanied imported CAD files of nuts and bolts. While using pegs instead of connective hardware did take a degree of accuracy away from the FEA, the impact was not significant enough to prevent the identification of areas of stress concentration in the mechanism. The purpose of the FEA was to identify potential areas of failure that will need modification rather than as a perfectly accurate mathematical mapping of the stresses in the mechanism.

Additionally, the crank-coupler, rocker-ground link, and rocker-coupler joints used the same connective hardware. Each joint used a ½" diameter 3/8"-16 shoulder bolt, custom washer, flanged ½" shaft diameter oil-embedded sleeve bearing, ½" screw size washer, and 3/8"-16 grade 5 nut; all from McMaster-Carr (McMaster-Carr, United States) except for the custom washer. The connective hardware used at the crank-ground link joint is described in section 3.6.1.3. The following subsections outline the transformation of the different mechanism components to achieve a working prototype with minimal weight and machining complexity.

3.6.1.1 Ground Link and Backbone

The ground link was originally a long rectangular link with two cylinders on the sides. An FEA analysis in SolidWorks was performed with plain carbon steel to see if the geometry of the parts would cause failure. After performing the initial FEA analysis with plain carbon steel (Figure 3.21), it was observed that the maximum stress in the link was ~15 MPa, while plain carbon steel's yield stress ranges from 200 MPa to 900 MPa [22], meaning that the ground link could be thinned, as well as switched to aluminum (yield stress of 169-542 MPa [22]), to save weight and potential material costs. The next iteration was a half inch piece of material with bent edges that had machined L-brackets to add additional support (Figure 3.22). The L-brackets were originally meant to be welded onto the ground link, but the physical prototype had the ground link machined out of a block of material with the L-brackets. This new design was 1455 cm^3 smaller in volume, while still being able to withstand the stresses seen in the FEA.

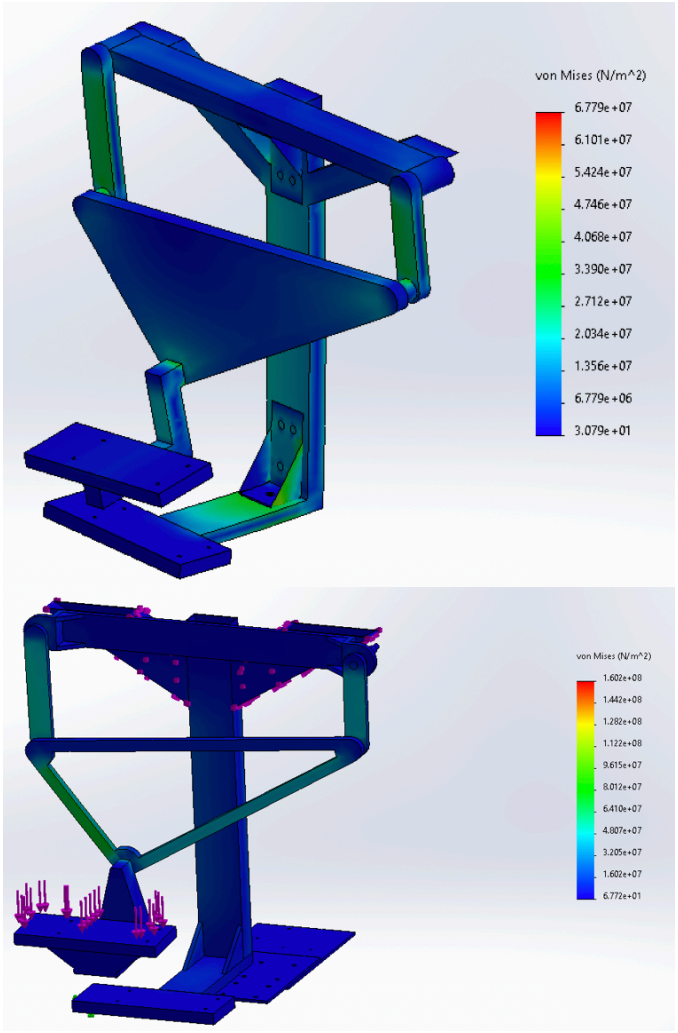

Figure 3.21. FEA analysis of the first (top image with plane carbon steel) and final (bottom image with aluminum 6061 alloy) ground link designs.

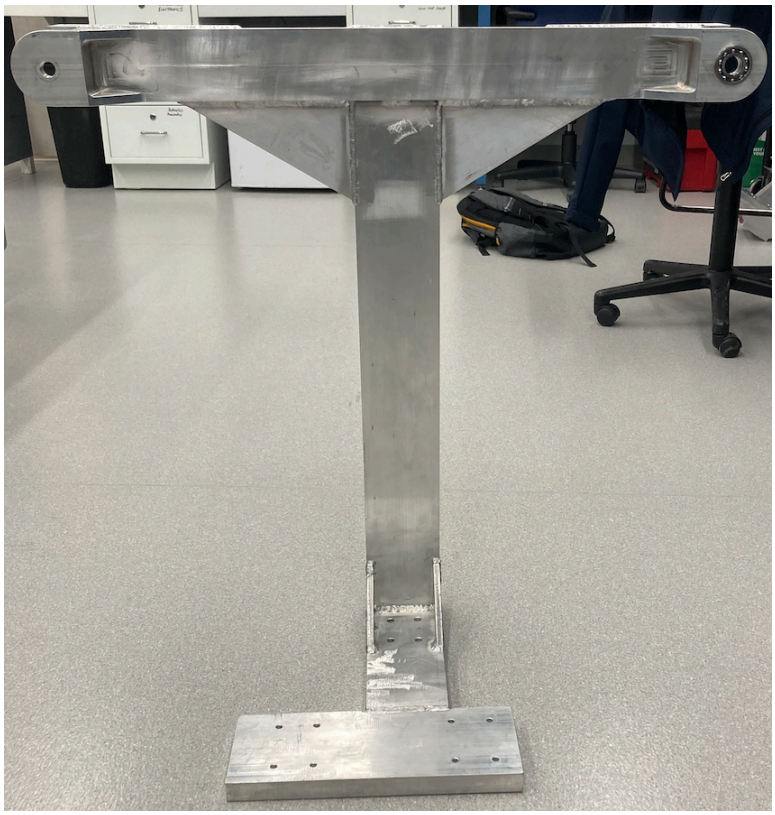

Figure 3.22. The ground link welded onto the backbone.

Additionally, the mechanism had to attach to the ICARE while still having enough space for a person to get on, off, and use the ICARE and for the mechanism to iterate through its full range of motion. Being that the designed mechanism is too large to fit between a person's legs, the ground link was attached to a large L-shaped structure that connects the ICARE with the mechanism. This structure was named the backbone and it consisted of a vertical stand made out of 4 in. x 2 in. x 1/8 in. wall rectangular tubing and a 1 in. thick slab of aluminum as the base that connects to a foot plate. The foot plate was also a 1 in. thick slab of aluminum that had holes drilled into it so that it could be bolted onto the ICARE.

The backbone was also drawn with L-brackets at the base and at the connection with the ground link. But the L-brackets at the ground link connection were later replaced with welds because the L-brackets were very small at this location. The backbone brought the weight of the mechanism more to the outside of the ICARE. While the FEA suggested that the backbone would not fail, its bending stress was hand calculated for assurance. Using a force of 200 pounds applied at a distance of 14.75 in., the second moment of inertia and bending stress values were 0.992 $in.^4$ and 2974 psi (~20.5 MPa), respectively, well below the yield stress.

3.6.1.2 Rocker

In comparison to the ground link, the rocker was more simplistic in its design and did not have any major design changes (Figure 3.23). The final SolidWorks FEA with

aluminum 6061 alloy showed a maximum von Mises stress value of ~30 MPa. While this value is within a safe range, hand calculations were performed to ensure that the rocker does not fail. With an approximation as a rectangular prism with a half circle at each end, a thickness of 0.5 in., and an applied force of 200 lbf at a distance of 10.125 in., the second moment of inertia and bending stress were 0.0208 $in.^4$ and 24300 psi (~168 MPa), respectively. This bending stress is close to the yield stress of weaker 6061 alloys, but the bodyweight support that would be used in human testing would lower the experienced bending stress on the rocker. For the shear stress of the rocker where it interfaces with the bolt that connects it to the coupler triangle, the shear stress fluctuated between 200 and 246 psi (~1.38-1.70 MPa), which is lower than the yield stress.

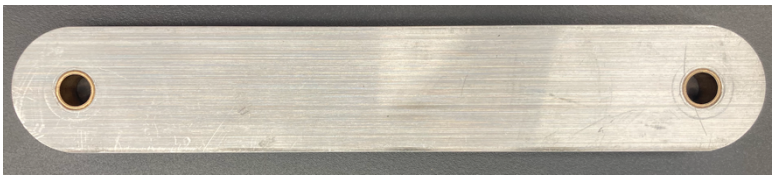

Figure 3.23. The final design of the rocker.

3.6.1.3 Crank and Crank Shaft

The crank was almost identical to the rocker except it had a shorter length. In the sagittal plane, the crank experienced the same bending and shear stress at the bolt as the rocker. The shear stress for the crank shaft varied between 200 and 320 psi (~1.38-2.21 MPa). Therefore, it did not undergo many design iterations. However, the crank had an additional complexity as it interfaced with the crank shaft, which interfaced with the motor via a belt and gearbox. This meant that larger bearings had to be used at the crank-ground link joint, while still maintaining the same distance between the crank and ground link as the rocker and ground link. Therefore, an indentation was originally created in the crank to accommodate a bearing and the crank shaft was going to be press-fit into the bearing. The design was then modified by finding smaller, yet still structurally sound bearings for the application. This enabled the crank to have the same design as the rocker (i.e., no indentation) and the crank shaft went through a hole and was welded on one side rather than being press-fit in. The final crank design can be seen in Figure 3.24.

Figure 3.24. The crank shaft welded to the crank.

For the crank shaft, it was originally two different rods with one of them having a threaded end and the other having a threaded hole. One rod would press fit into the bearing at the crank-ground link joint while the other rod had indented grooves to interface with a belt. This design then transformed into a single rod with indented grooves, before lastly changing into a cylinder with one end being machined down to a smaller diameter. The grooves were removed and instead a timing pulley was placed on the end with the smaller diameter to interface with the belt. This progression occurred to minimize the number of parts that needed to be machined and the difficulty of machining the parts.

For the crank-ground joint, there were three bearings and a clamp holding the joint together, all from McMaster-Carr. There was an indentation in the ground link to house a ¾" shaft diameter open ball bearing. Between the crank and the ground link was a ¾" shaft diameter thrust ball bearing, with another one behind the ground link. Lastly, a ¾" shaft diameter shaft collar was placed behind the second thrust ball bearing to press it against the ground link.

3.6.1.4 Coupler and Foot Plate Adapter

The coupler originally started as a solid slab of half inch-thick aluminum in a triangular shape. After the original plain carbon steel alloy FEA analysis, the it was observed that the maximum stress value was ~30 MPa, concentrated at the joints. Therefore, the majority of the center of the coupler triangle was carved out, leaving only the edges to save weight (Figure 3.25).

Figure 3.25. The coupler and adapter assembled.

While the coupler triangle did not change any further, the location of the end effector with respect to the foot still needed to be addressed. The end effector represents the foot centroid; therefore, the pedal of the ICARE has to be placed lower than the end effector. This connective piece was called the adapter and it went through many evolutions to its final form. The adapter first began as a hook-like piece of material before transitioning to a thicker adapter with added-in triangles for support and material removed in lower areas of stress concentration. The triangular supports and thickness of the different areas continued to change until a design was finalized, and then it was broken up into four different pieces for machining. The four different adapter designs can be seen in Figure 3.26.

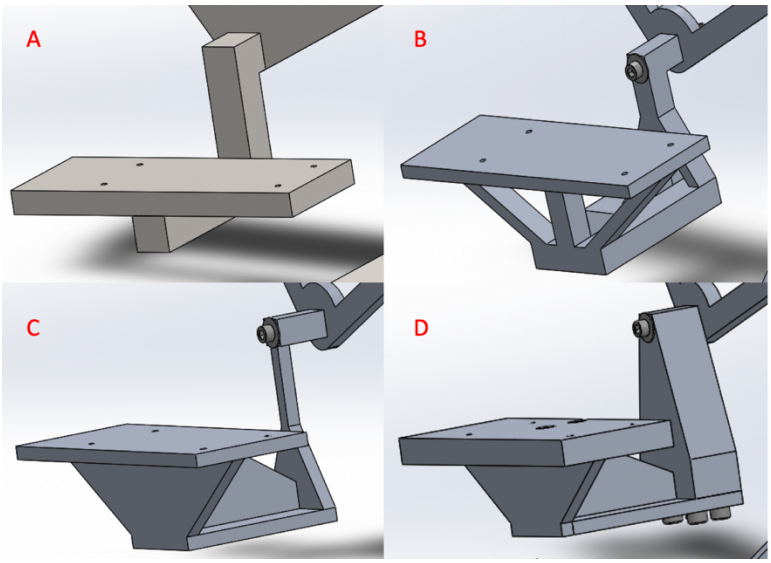

Figure 3.26. Images of the A) first adapter, B) second adapter, C) third adapter, and D) final adapter designs.

3.6.1.5 Motor Mount and Electronics Platform

The motor mount was the name of the subassembly connecting the gearbox and motor together, and its design did not change since it was first created, as shown in Figure 3.27. The motor and gearbox were bolted onto L-shaped slabs of aluminum and then they were mated together via an adapter. Additionally, there are two spacer blocks between the motor and gearbox. One side of the subassembly was machined down by 7/32 in. to accommodate the weld thickness on the side of the backbone. The motor mount subassembly had holes in the bottom for it to be bolted onto the main electronics platform.

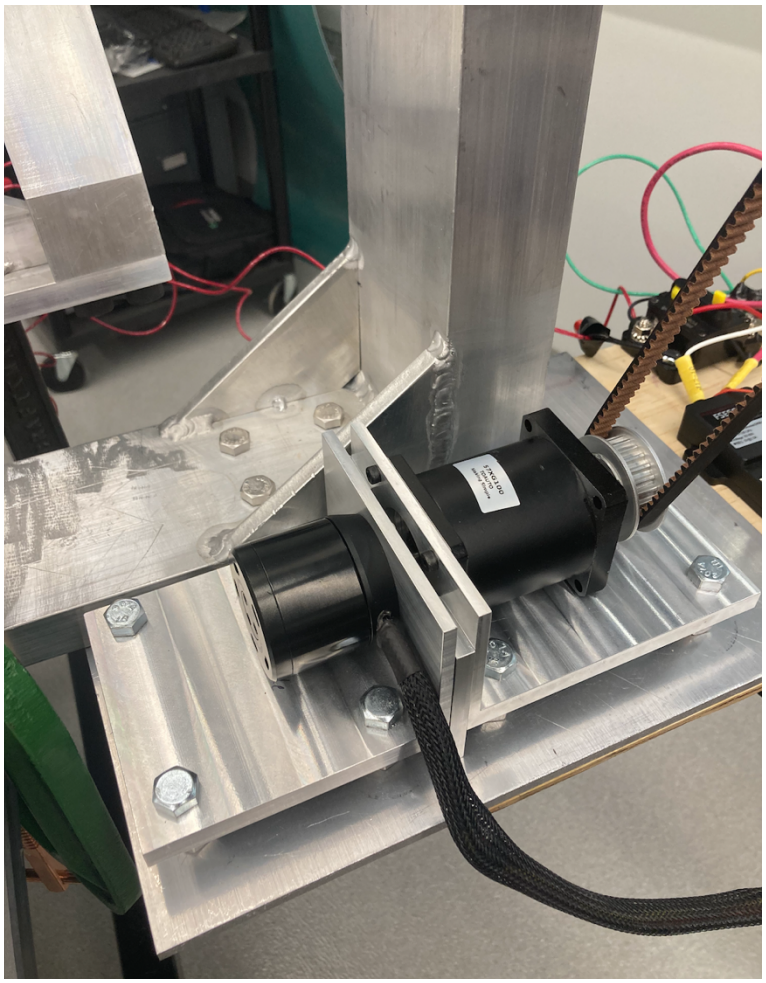

Figure 3.27. The motor mount subassembly.

Since the gearbox connects to the crank shaft via a belt, there needed to be some method of adjusting the tension in the belt. Therefore, two nuts were placed between the motor mount and the platform to allow the motor mount to raise or lower vertically, as seen in Figure 3.28. This solution was simpler and lighter than adding a jack or another height adjusting mechanism, but it did add complexity as eight bolts had to be adjusted to the same height.

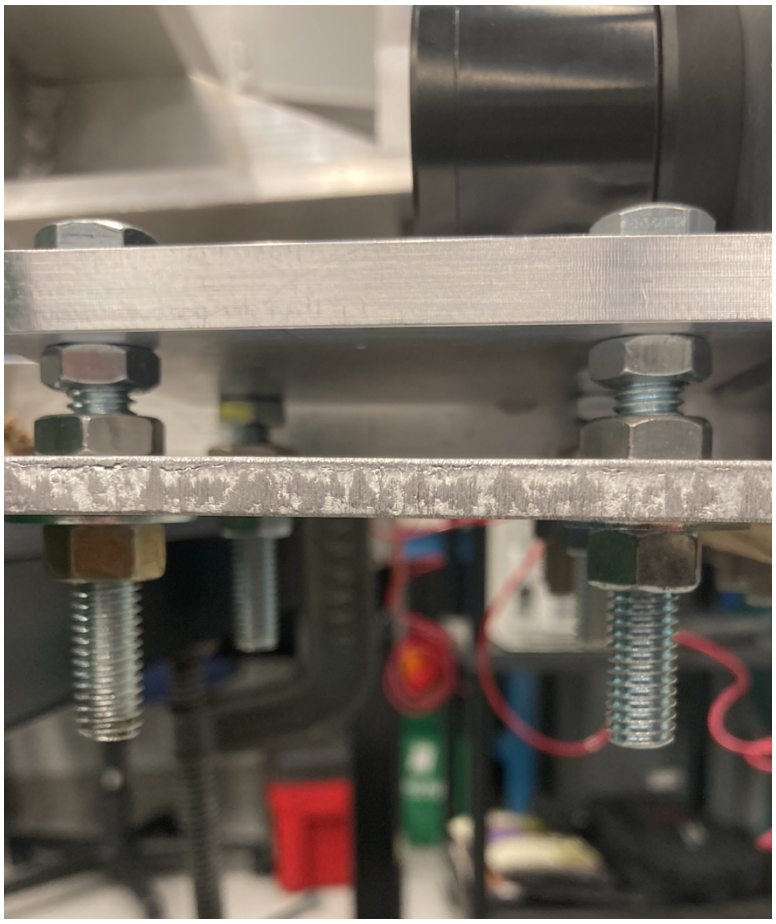

Figure 3.28. The nuts between the motor mount and platform allowed for tension adjustment of the belt.

The platform for the electronics originally was an aluminum slab that would have been welded onto the back of the base of the backbone. Instead of having the electronics farther away from the mechanism, this design was changed by bolting it to the bottom of the backbone rather than welding it to the back. Lastly, it was determined to break up the platform into two pieces, one aluminum and the other plywood, displayed in Figure 3.29. The aluminum piece would hold the motor mount while the plywood piece would hold the other electronics. The reason this was done was so the wires would rest on a non-conductive surface and it would be lighter than a metal platform (as the electronics were light and did not need a strong platform to lay on).

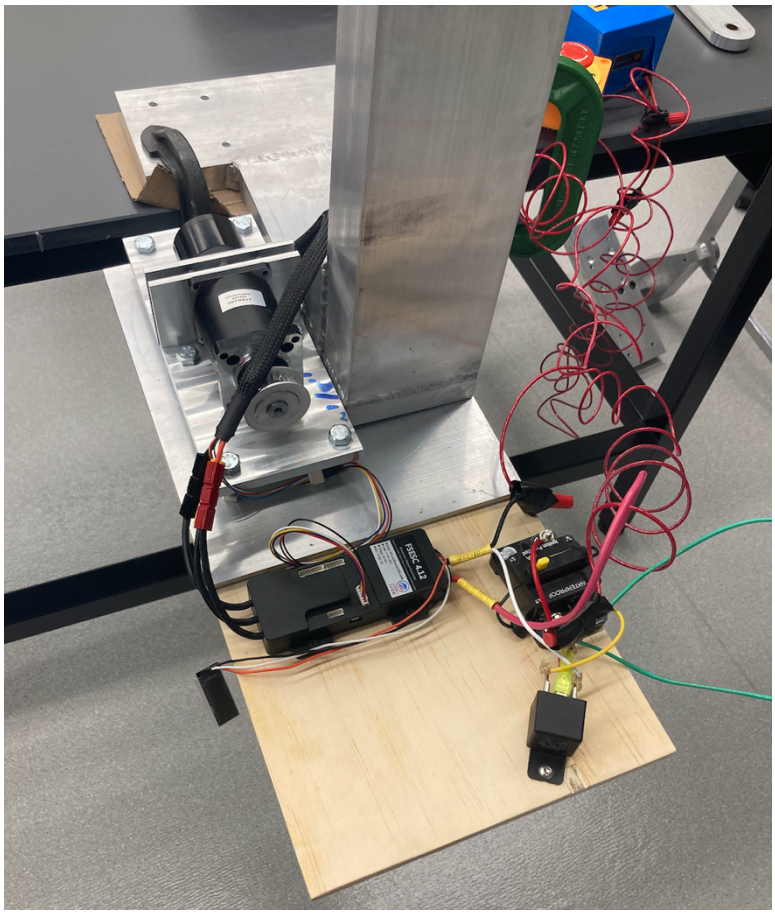

Figure 3.29. The electronics platform with all of its attached electronics and the motor mount subassembly.

3.6.2 ICARE Pedal and Foot Plate

Originally, the ICARE pedal was going to be used in this study. But the pedal has a plastic lip on the side that was not accounted for with the adapter design. Therefore, instead of modifying a pedal that is used in rehabilitating patients, an older pedal design was used. This pedal was used in previous ICARE studies when it was being developed and is shown alongside an ICARE pedal in Figure 3.30.

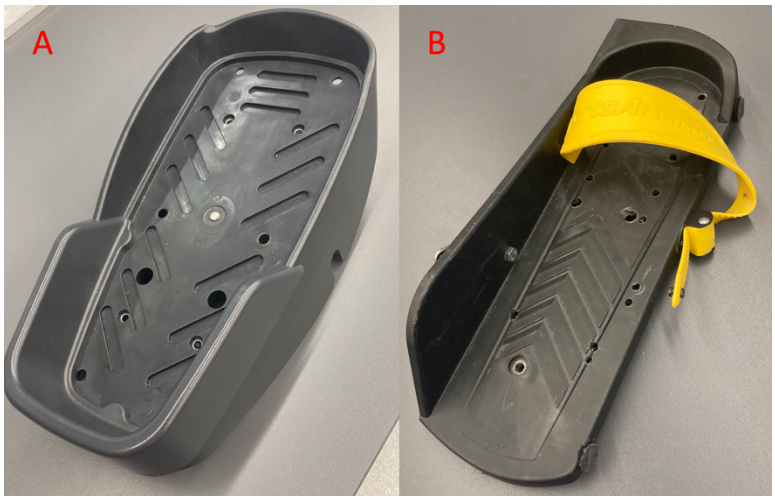

Figure 3.30. A) An ICARE pedal and B) the pedal used in testing.

There were two different foot plates on this mechanism. One foot plate was at the base of the backbone and it bolted onto the ICARE, while the other was attached to the foot plate adapter and would have the plastic pedal bolted on. The hole pattern of the ICARE pedal was copied onto the foot plates of the mechanism. While the distances between the holes was correctly spaced, the positioning of the holes relative to the front and back edges of the foot plates were wrong. In order to correct this, an ICARE pedal was placed on the foot plates and the holes were marked and then drilled.

3.7 Device Testing

Prior to testing the mechanism on the ICARE, the prototype first needed to be tested in the lab to ensure that it operated as expected. The mechanism was clamped down to the edge of a table, as seen in Figure 3.31. While the motor was activated to move the belt via the gearbox, a loud grinding noise was heard and the crank could not complete a full rotation. The experiment was immediately stopped and the motor, gearbox, and belt were disassembled from the mechanism for inspection. The set screws of the coupler (Figure 3.32) connecting the motor and gearbox had gotten loose, allowing the motor shaft to spin and grind against the inside of the coupler.

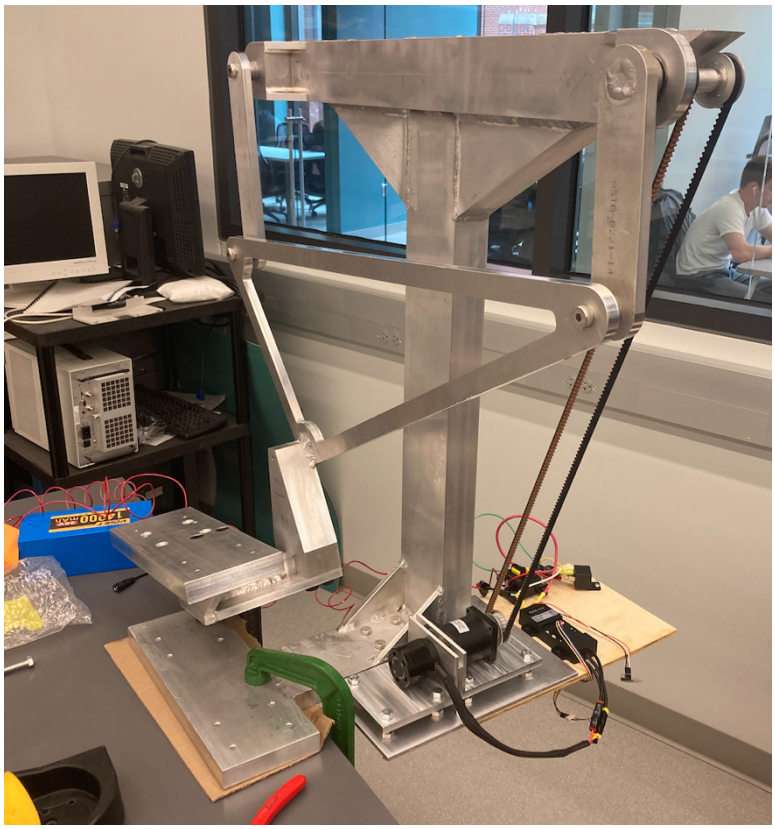

Figure 3.31. The experimental set up of the mechanism in the lab.

Figure 3.32. The coupler to the motor and gearbox, with the set screws shown.

After tightening the set screws again, another test run was performed. Just as before, a grinding noise was heard and after disassembling the motor, gearbox, and belt, the set screws had once again loosened to the point that the motor shaft was rotating within the coupler. Next, the set screws and threaded holes of the coupler were cleaned and Loctite (Connecticut, United States) was applied to them before reassembling. The set screws were given 24 hours for the Loctite to cure so that they would be less likely to loosen while the mechanism was in operation. After curing, the mechanism was again tested, but the same noise was heard with the crank not being able to fully rotate, but this time the set screws were not loose.

With the set screw issue fixed, the next possible issue that was tested was the alignment of the motor and gearbox plates. The additional nuts between the motor and gearbox plates and the platform had the advantage of adjusting the tension in the belt, but one had to make sure that all of the nuts were set to the same height. Otherwise, the alignment between the motor and gearbox would not be straight and this could wear down their internal components. The minimum distance that the motor and gearbox had to rise so that the belt could stretch between the crank and gearbox without tearing was 0.73 in. A ¾" block was instead placed below the motor and gearbox plates (Figure 3.33) to test if the alignment was causing the noise. This slight increase in the raised height did not result in such a significant loss in the belt's tension that the belt was skipping. After testing this set up, the grinding noise was still being heard and the crank was still not fully rotating.

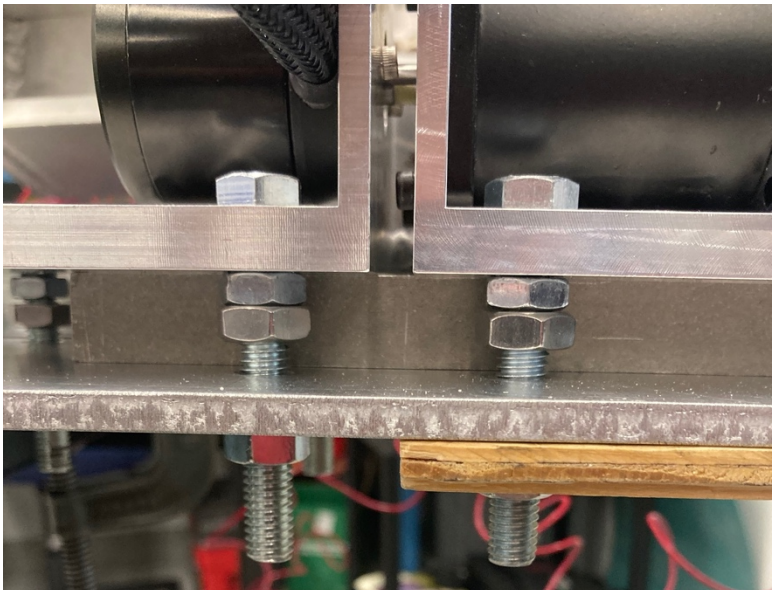

Figure 3.33. The ¾" block placed under motor and gearbox plates during an experiment.

This led the researchers to two possible theories and potential solutions. One potential issue was that the weight of the adapter, coupler, rocker, and crank was pulling on the belt, creating the tension in the belt, which was applied to the gearbox's shaft as a transverse load and caused the shaft to deflect slightly upwards. This could

have caused the internal gears to grind and for the coupler to skip teeth when it engaged with the gearbox. To fix this, a new component would have to be designed that connects to the gearbox plate and the gearbox's shaft to prevent it from experiencing the transverse load. The other possible issue was that the torque transfer in the gearbox was not performing at the same level as advertised. The solution to this problem would involve replacing the existing gearbox. At this point in the research, there was not enough time to design a new component or research and purchase a new gearbox. Therefore, this concluded the device testing, and a future student will explore solutions to the mechanism's current problems and then test the mechanism on the ICARE at Madonna.

Chapter 4 Conclusion

This thesis explored the synthesis of a mechanism to attach to and improve gait on the ICARE for patients undergoing gait rehabilitation. The synthesis input curves were created by comparing the foot centroid of the ICARE to a normal gait model in OpenSim. The main synthesis techniques that were used were three prescribed positions graphical synthesis, three prescribed points analytical synthesis, synthesis with MotionGen, atlas search method, and *fmincon()* optimization in MATLAB. With each new method, the produced mechanism became closer to being a solution to the synthesis problem.

The solution originally produced a non-cyclic coupler curve with the three prescribed points and positions methods, then it created a cyclic, oval-like solution with MotionGen, before finally creating a horizontal figure-eight shape with the atlas method and *fmincon()* optimization. The use of MATLAB to draw different mechanisms is not a novel idea, but it improved the accuracy of the graphical methods as it bypassed human error with drawing tools. Also, the optimization study proved particularly fascinating as angular weight values between 0.5 and 0.75 indicated a transitional phase in the coupler curve from a figure-eight to a comma-like shape. This proved helpful by providing a better understand of how different angular weight values performed for this synthesis problem.

The final mechanism theoretically improved the foot centroid's horizontal and vertical displacement on the ICARE, while the foot centroid's angle did not improve as significantly with the addition of the mechanism. This proved promising enough for a physical prototype to be designed and built. The physical prototype was able to be hand cranked with the moving components moving as expected. The fully assembled mechanism with electronics weighed under 60 pounds. This was a success considering a heavy mechanism could damage the ICARE, but the mechanism had to be made out of metal in order to handle the weight of a person. The mechanism may have to be moved onto or removed from the ICARE by rehabilitative staff, again emphasizing how crucial the weight was. Furthermore, the mechanism can be easily disassembled into multiple pieces and stored away, adding another benefit to its potential use in a clinical setting.

When the mechanism was tested, it produced a grinding noise and the crank would not fully rotate. These issues may have occurred due to the gearbox shaft experiencing a large enough transverse load from the belt's tension and weight of the adapter, coupler, crank, and rocker to deflect the shaft. Additionally, the gearbox may not be transmitting torque from the motor to the belt as well as advertised, potentially requiring it to be replaced. While these setbacks prevented further testing of the mechanism, these problems are relatively simple to fix and would have been solved had there been more time to do so. From the testing, the mechanism's links and welds did not fail or show signs of failure starting. The bolts and bearings at the joints likewise did not show any evidence of shearing or wear.

In summary, the existing prototype has the potential to improve the ICARE's gait, but is incomplete and cannot be tested on the ICARE. The following section outlines how these issues can be addressed in more detail and how human testing will be conducted.

Lastly, the next section will also explore how the mechanism may be redesigned for manufacturability if it progresses to that stage.

4.1 Future Work

Before human testing can be conducted, the current issues of the mechanism need to be solved. In order to prevent the gearbox's shaft from deflecting from the transverse load, a new piece can attach to the shaft and connect to the plate that the gearbox is attached to. As shown in Figure 4.1, there is a threaded hole at the end of the gearbox's shaft. An L-shaped plate could be machined with two holes on the bottom portion to line up with the hex head bolts to the left and right of the gearbox's shaft, securing it to the gearbox plate. The vertical portion of the L-shaped plate can have an indentation for a ball bearing to be press-fit, and the ball bearing will be concentric with the gearbox's shaft. A rod with a threaded end can screw into the threaded hole of the shaft after being press-fit into the ball bearing. Since the vertical portion of the L-shaped plate has an indentation for the ball bearing, there will be a wall of material behind the ball bearing to prevent the shaft from loosening out of the gearbox's shaft. While this solution will make assembling the entire mechanism more tedious, it could prevent the shaft from deflecting once everything has been assembled. If this solution is implemented and the mechanism is still not transmitting the proper amount of torque, the gearbox shall be replaced.

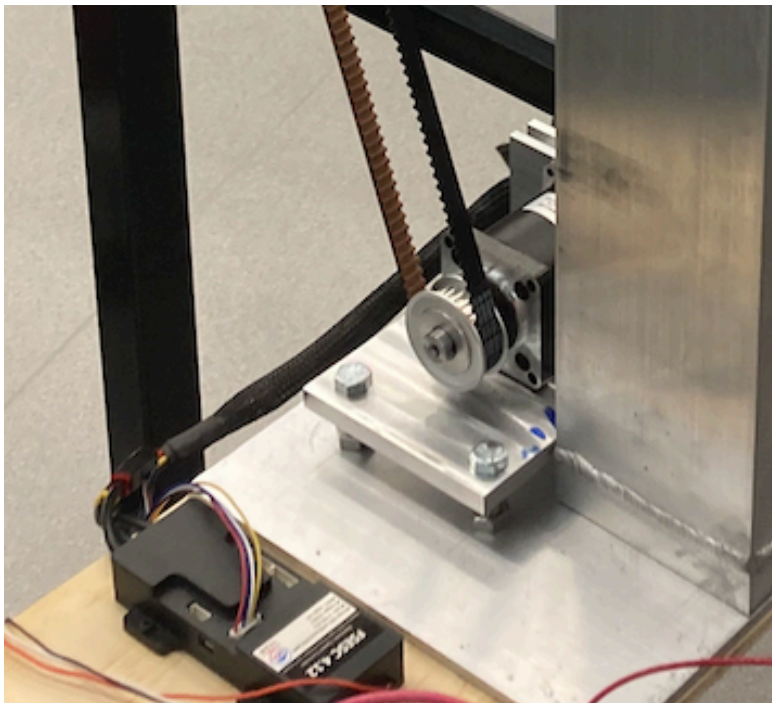

Figure 4.1. A hole is centered at the end of the gearbox's shaft.

After resolving the mechanism's problems and it has had a successful test in the lab, it will be transported for human testing at Madonna. Only the right foot's mechanism was created to gather pilot data. The plastic pedal will be removed from the

ICARE and placed on the pedal platform of the mechanism. The mechanism's base will then be bolted onto the ICARE at the location where the plastic pedal had been attached. For the left foot, a scissor lift style pedal will be used to raise the left foot to approximately the same height as the right foot. This setup will affect the kinematic chain of the legs, hips, and torso; therefore, an ICARE equipped with mechanisms on both sides may perform better or worse. The reason for only fabricating one mechanism was to have a relatively low-cost pilot comparison between a foot equipped with the mechanism and one without it.

The pilot experiment will involve having reflective markers placed on one of the research team members and having them perform three different trials while biomechanical data is recorded. The three trials will be overground walking at a self-selected pace, using the ICARE with bodyweight support and without the mechanism, and using the ICARE with both bodyweight support and the mechanism. To avoid possible mechanism failure and participant injury, the bodyweight support system of the ICARE will be utilized at a predetermined percentage of bodyweight support based on the weight of the participant. Kinematic data will be gathered with the Qualisys Motion Analysis System and Track Manager software. The sagittal plane data for both sides of the body will then be divided into gait motion cycles and averaged to create a single representative gait cycle. The data will finally be compared and analyzed for potential improvement.

If the trials show improvement, the mechanism will then be created for the left foot and a study can be performed on the benefits of having the mechanism attached to both feet. If this proves fruitful, the mechanism will be redesigned for manufacturing. One of the key challenges to overcome in this phase will be to make the mechanism sturdy enough to handle repeated use with patients who have varying weights and levels of needed bodyweight support. This was considered in the design of the prototype, but this study had the luxury of using the bodyweight support system, if necessary, as the research focused on whether the gait motion of a participant on the ICARE can even be improved with a mechanism. Generally, as an individual progresses through rehabilitation, they will lower the amount of assistance they use to continue training their muscles, therefore it is absolutely vital for the mechanism to not be reliant on the bodyweight support system.

In order to achieve this, different lightweight, but strong materials may be explored to replace aluminum 6061. The mechanism could also be moved closer to the mid-sagittal plane of the ICARE, lowering the experienced moment felt by the mechanism, but there are limited gains to be made here. The human leg tends to protrude outwardly as one goes up the leg from the foot, therefore, bringing the mechanism closer to the mid-sagittal plane runs the risk of the mechanism colliding with a person's hip. Another potential solution could be redesigning how the mechanism attaches to the ICARE. Currently, the foot plate is the only direct connection to the ICARE. Other locations can be explored that will remain stationary relative to the ground link as the ICARE is used so that the mechanism will have more attachment points and potential truss structures between attachment points to strengthen the mechanism. Redesigning the mechanism for manufacturability will most likely involve a combination

of material change and component redesign to ensure that the device will not fail under larger loads and will not damage the ICARE from being too heavy.

References

1. Buster, T., Ginoza, L., & Burnfield, J. (2006). Comparison of lower extremity sagittal plane kinematics during overground gait, treadmill walking, and elliptical training. In *Proceedings CD, American Society of Biomechanics, 30th Annual Meeting.*
2. Burnfield, J. M., Buster, T. W., Taylor, A., Keenan, S., Shu, Y., & Nelson, C. A. (2010, June). Intelligently controlled assistive rehabilitation elliptical (icare) training: an analysis of lower extremity electromyographic (EMG) demands with varying levels of motor assistance. In *RESNA Annual Conference, Las Vegas* (pp. 1-7).
3. Nelson, C. A., Burnfield, J. M., Shu, Y., Buster, T. W., Taylor, A. P., & Graham, A. (2011). Modified elliptical machine motor-drive design for assistive gait rehabilitation. *Journal of Medical Devices, 5*(2).
4. Burnfield, J. M., Shu, Y., Buster, T., & Taylor, A. (2010). Similarity of joint kinematics and muscle demands between elliptical training and walking: implications for practice. *Physical therapy, 90*(2), 289-305.
5. Burnfield, J. M., Shu, Y., Buster, T. W., Taylor, A. P., & Nelson, C. A. (2011). Impact of elliptical trainer ergonomic modifications on perceptions of safety, comfort, workout, and usability for people with physical disabilities and chronic conditions. *Physical therapy, 91*(11), 1604-1617.
6. Burnfield, J. M., Buster, T. W., Pfeifer, C. M., Irons, S. L., Cesar, G. M., & Nelson, C. A. (2019). Adapted motor-assisted elliptical for rehabilitation of children with physical disabilities. *Journal of Medical Devices, 13*(1):011006. DOI: 10.1115/1.4041588.
7. Burnfield, J. M., Cesar, G. M., Buster, T. W., Irons, S. L., & Pfeifer, C. M. (2018). Walking and Fitness Improvements in a Child with Diplegic Cerebral Palsy Following Motor-Assisted Elliptical Intervention. *Pediatric Physical Therapy, 30*(4), E1-E7. DOI: 10.1097/PEP.0000000000000541. PMID: 30277973.
8. Irons, S. L., Brusola, G. A., Buster, T. W., & Burnfield, J. M. (2015). Novel motor-assisted elliptical training intervention improves 6-minute walk test and oxygen cost for an individual with progressive Supranuclear palsy. *Cardiopulmonary Physical Therapy Journal, 26*(2), 36-41. DOI: 10.1097/CPT.0000000000000007.
9. Pusnik, Z., Nelson, C. A., Burnfield, J. M., Buster, T. W. (2021). Kinematic synthesis of gait correction for a rehabilitation machine. Accepted, *ASME 2021 International Design Engineering Technical Conferences and Computers and Information in Engineering Conference [IDETC/CIE2021]*. Accepted for Virtual Online. August 17-21, 2021.
10. Gait 2392 and 2354 Models. (2017). Retrieved January 19, 2021, from https://simtk-confluence.stanford.edu/display/OpenSim/Gait+2392+and+2354+Models
11. Mabie, H. H., & Reinholtz, C. F. (1987). *Mechanisms and dynamics of machinery*. John Wiley & Sons.
12. Erdman, A. G., & Sandor, G. N. (1997). *Mechanism design: analysis and synthesis* (3rd ed., Vol. 1). Prentice Hall.
13. Hall, A. S. (1986). *Kinematics and linkage design*. Waveland Press.
14. McCarthy, J. M. (Ed.). (2013). *21St century kinematics: the 2012 NSF Workshop*. Springer.
15. Perez, A., & McCarthy, J. M. (2005). Clifford algebra exponentials and planar linkage synthesis equations.
16. Zimmerman, R. A. (2018). Planar linkage synthesis for mixed motion, path, and function generation using poles and rotation angles. *Journal of Mechanisms and Robotics*, *10*(2), 025004.

17. Mirth, J. A. (2012, August). The application of geometric constraint programming to the design of motion generating six-bar linkages. In *International Design Engineering Technical Conferences and Computers and Information in Engineering Conference* (Vol. 45035, pp. 1503-1511). American Society of Mechanical Engineers.
18. Purwar, A. (2021). MotionGen. Retrieved May 22, 2021, from https://www.stonybrook.edu/commcms/motiongen/
19. Ge, Q. J., Zhao, P., Purwar, A., & Li, X. (2012). A novel approach to algebraic fitting of a pencil of quadrics for planar 4R motion synthesis. *Journal of computing and information science in engineering*, *12*(4).
20. Ge, Q. J., Purwar, A., Zhao, P., & Deshpande, S. (2017). A Task-Driven Approach to Unified Synthesis of Planar Four-Bar Linkages Using Algebraic Fitting of a Pencil of G-Manifolds. *Journal of Computing and Information Science in Engineering*, *17*(3).
21. Hrones, J. A., & Nelson, G. L. (1951). *Analysis of the four-bar linkage: its application to the synthesis of mechanisms*. Published jointly by the Technology Press of the Massachusetts Institute of Technology, and Wiley, New York, 231.
22. Budynas, R. G., & Nisbett, J. K. (2015). *Shigley's Mechanical Engineering Design* (10th ed.). McGraw-Hill Education.

Appendix

Appendix A1 MotionGen Results

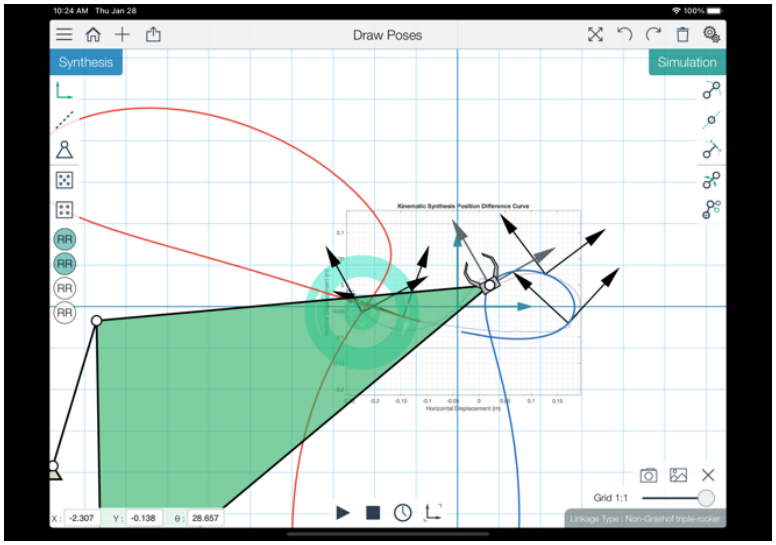

Figure A1.1. The possible coupler curves of test set 1.

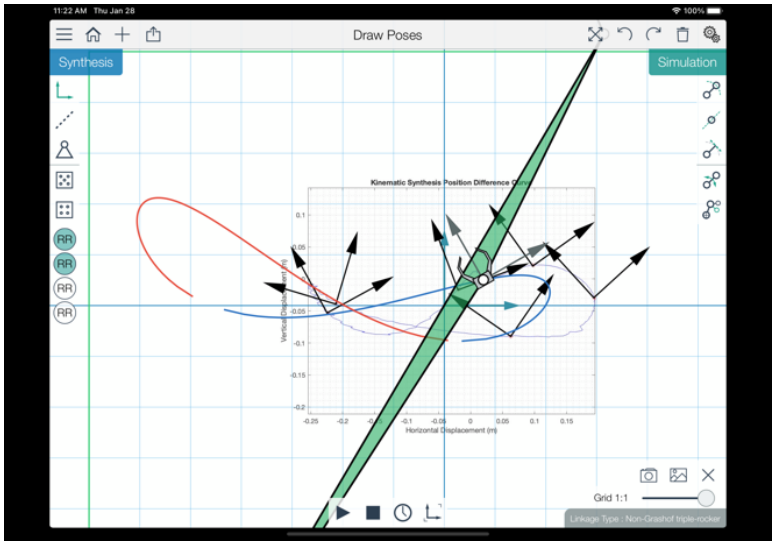

Figure A1.2. The possible coupler curves of test set 3.

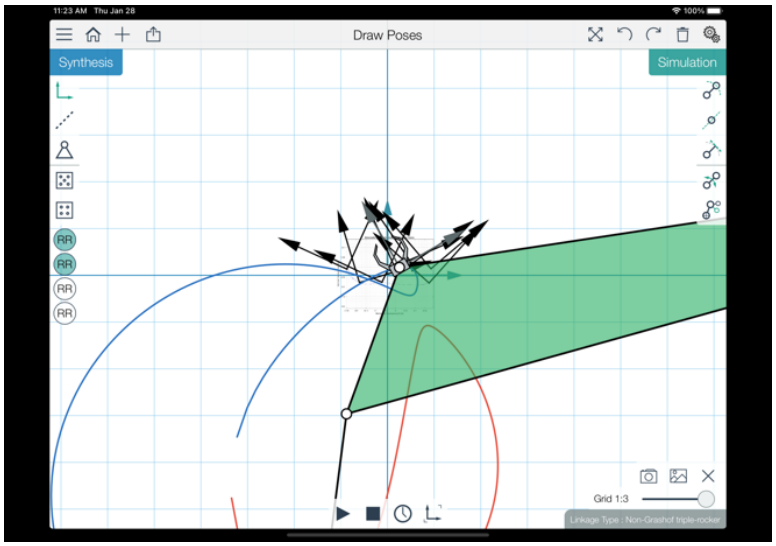

Figure A1.3. The possible coupler curves of test set 4.

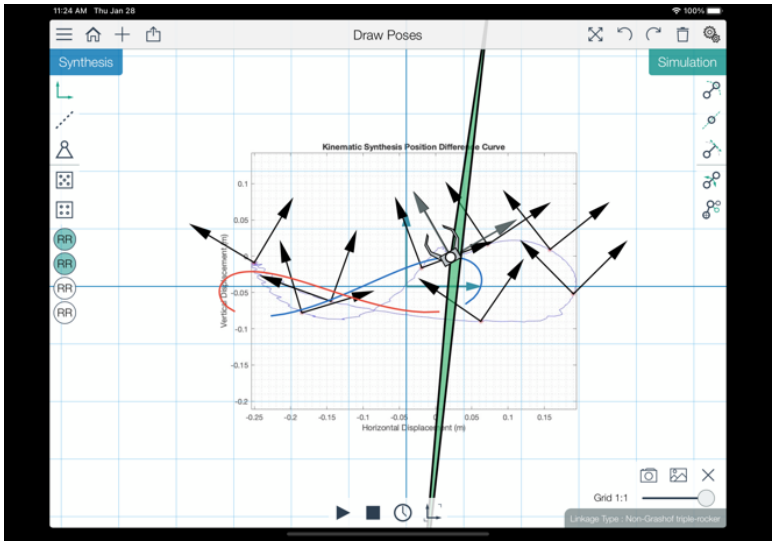

Figure A1.4. The possible coupler curves of test set 5.

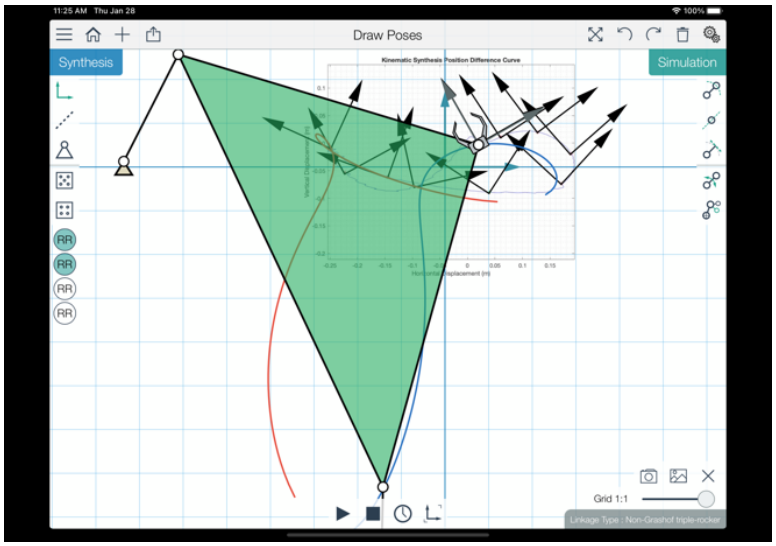

Figure A1.5. The possible coupler curves of test set 6.

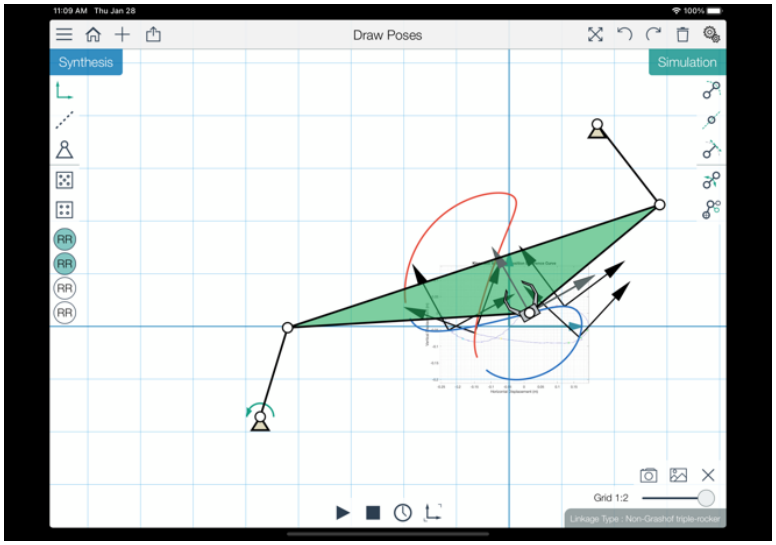

Figure A1.6. The possible coupler curves of test set 7.

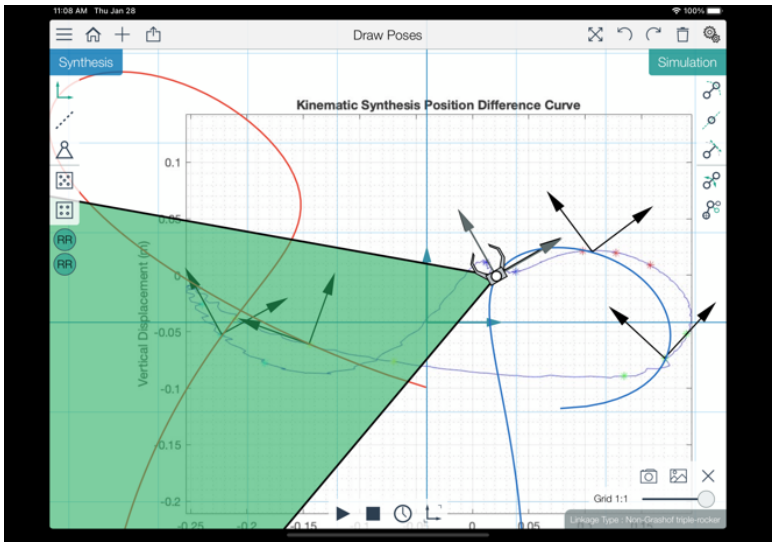

Figure A1.7. The possible coupler curves of test set 8.

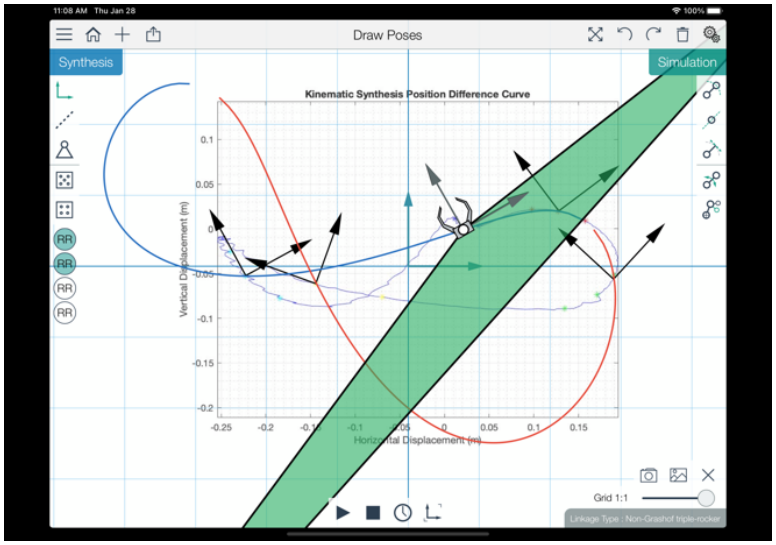

Figure A1.8. The possible coupler curves of test set 10.

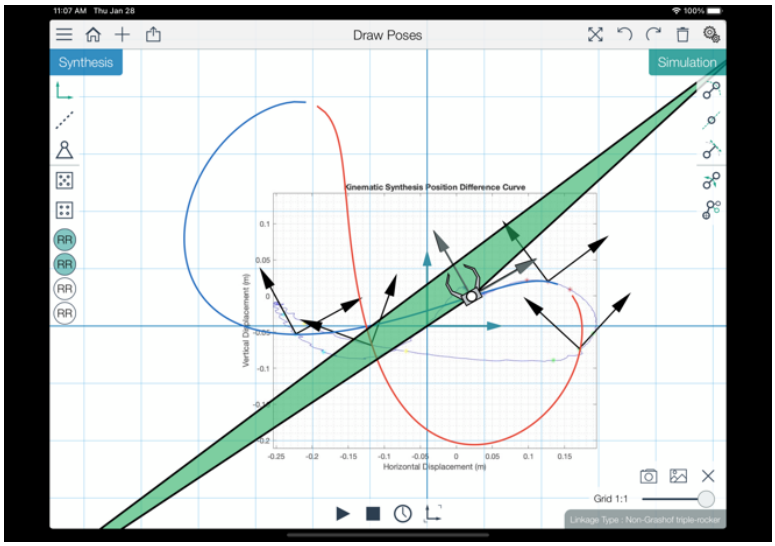

Figure A1.9. The possible coupler curves of test set 11.

Appendix A2 CAD Drawing Files

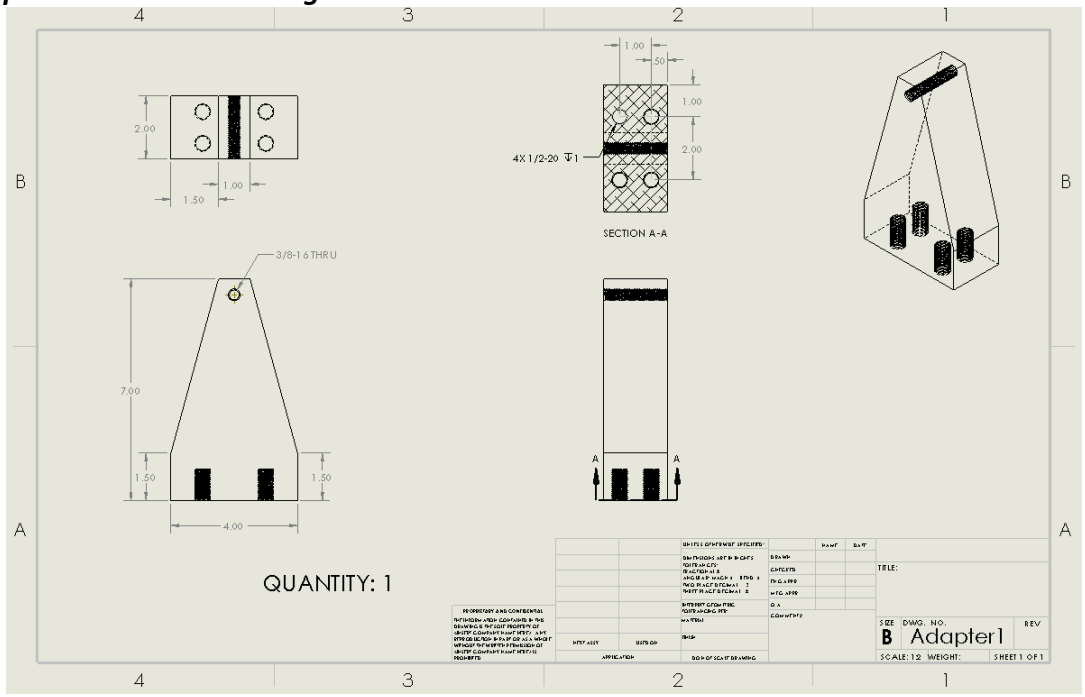

Figure A2.1. The drawing file of adapter piece 1.

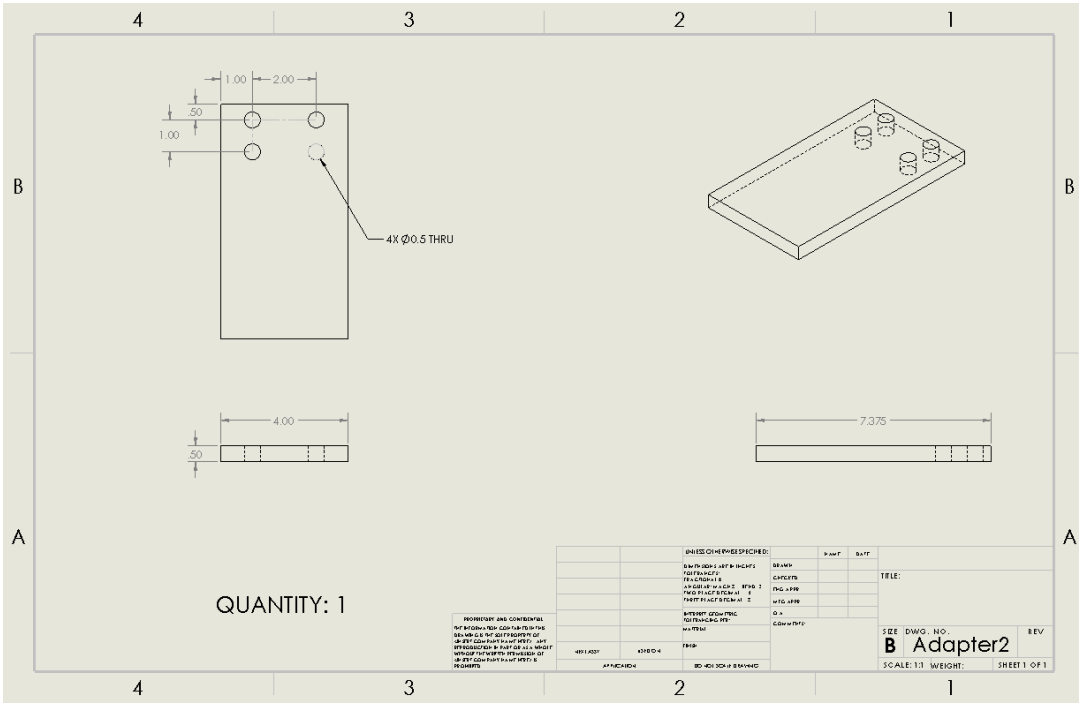

Figure A2.2. The drawing file of adapter piece 2.

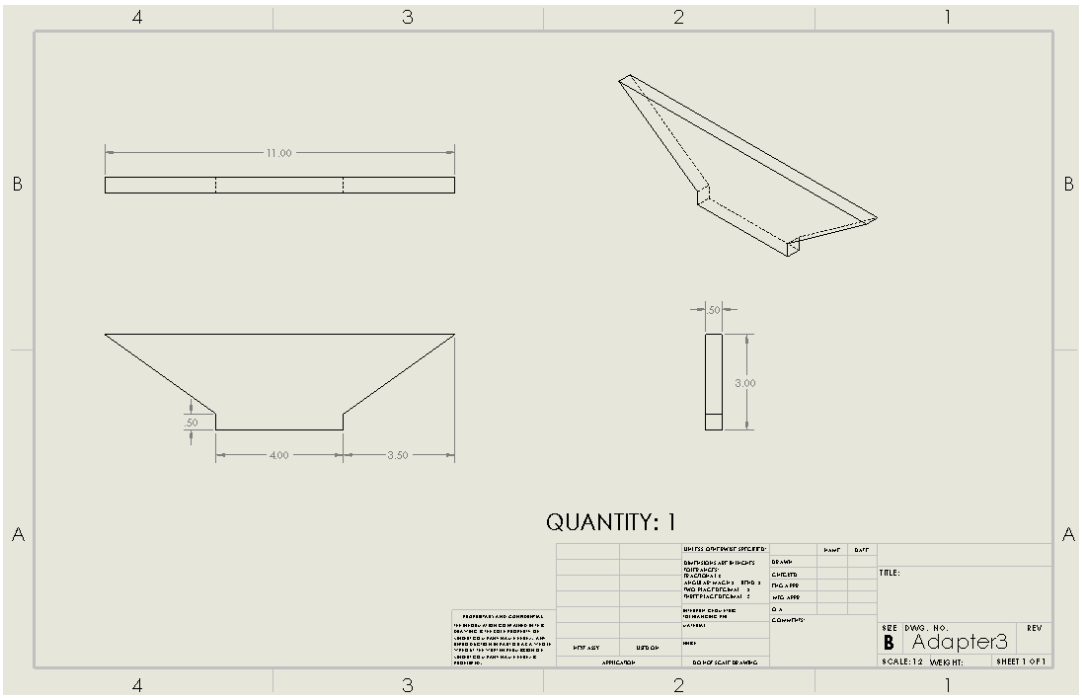

Figure A2.3. The drawing file of adapter piece 3.

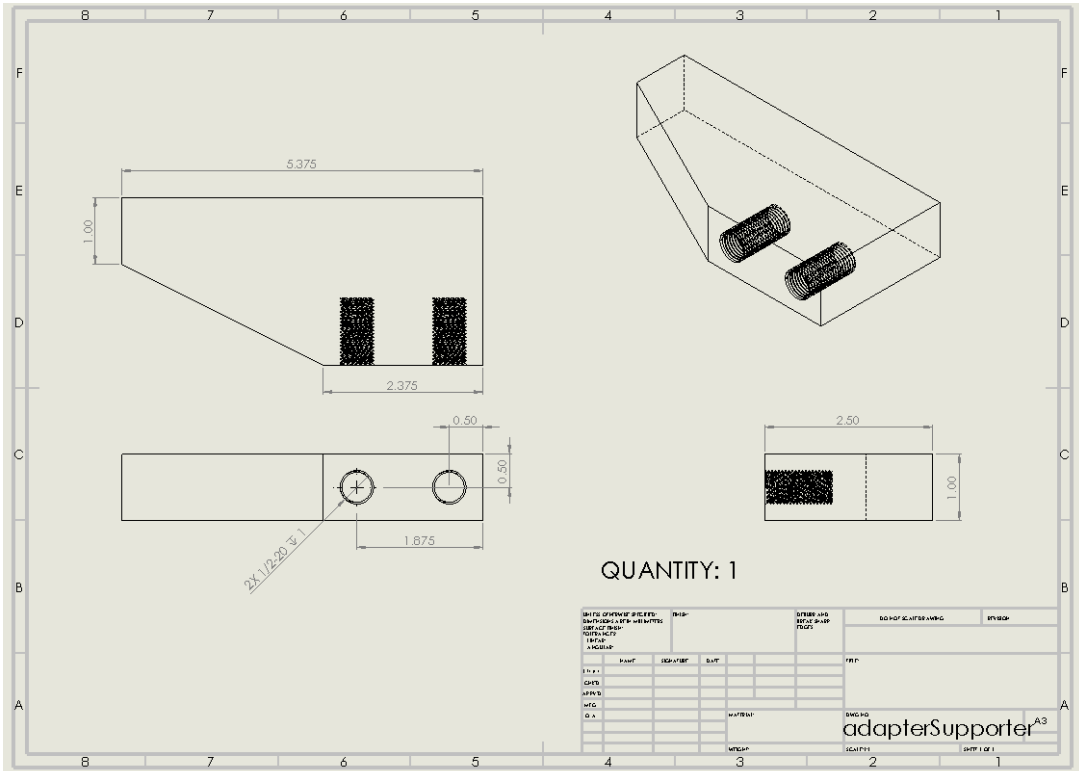

Figure A2.4. The drawing file of the vertical support of the adapter.

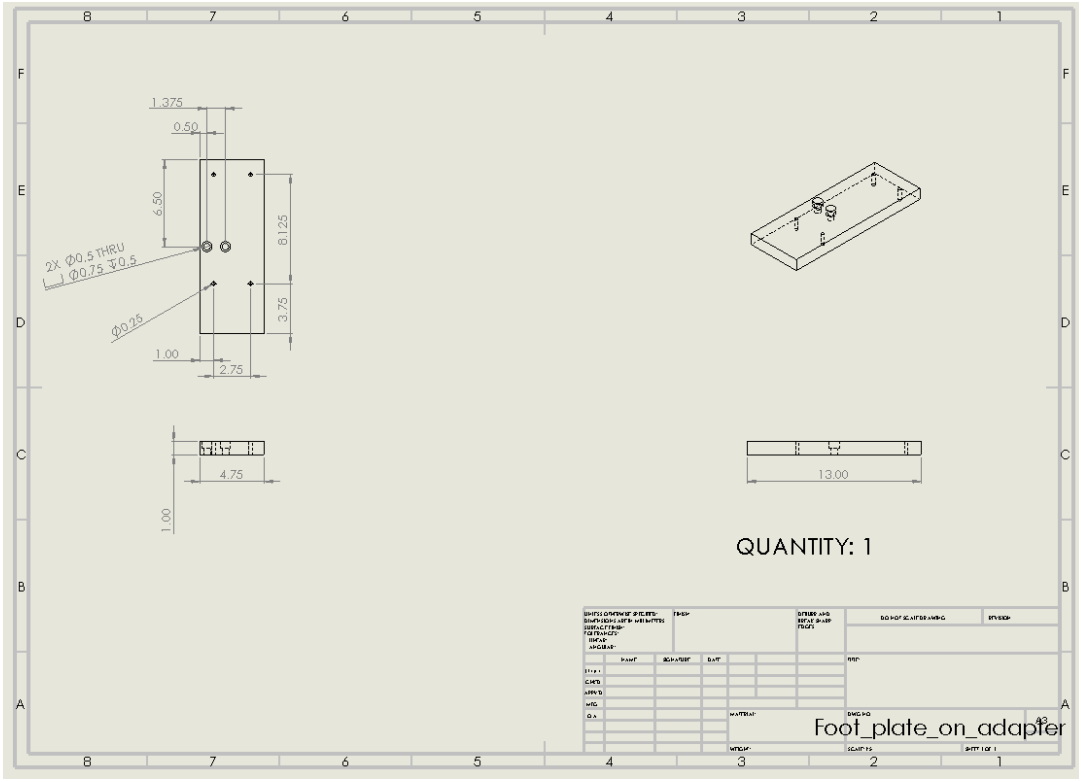

Figure A2.5. The drawing file of the adapter's foot plate.

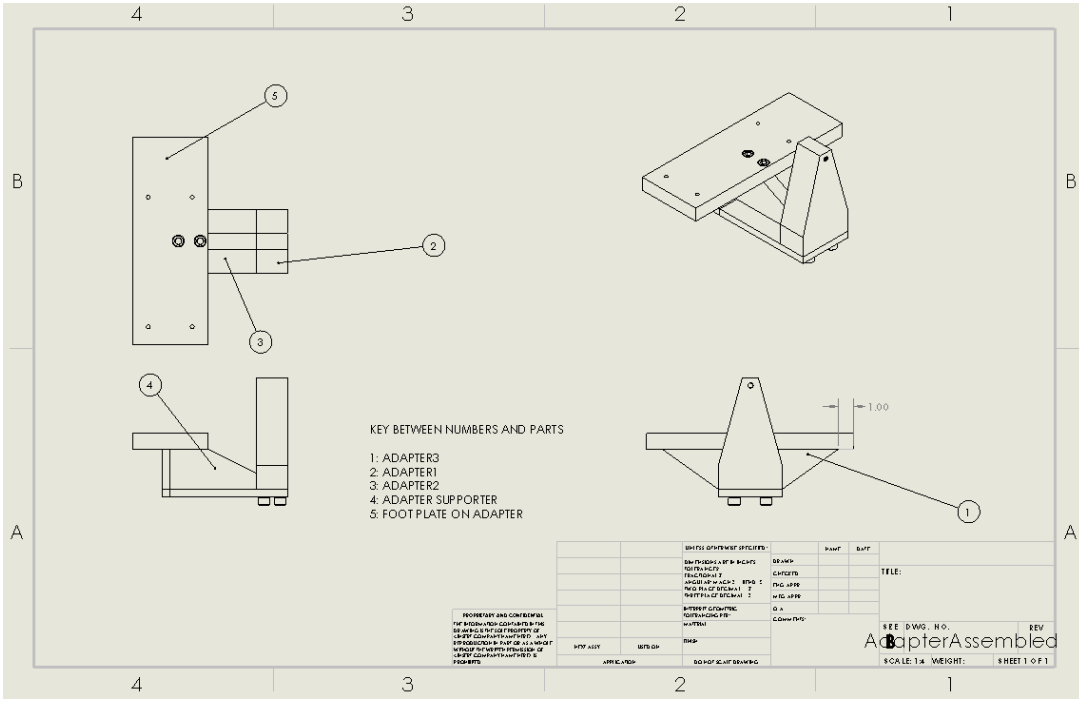

Figure A2.6. The drawing file of the adapter subassembly.

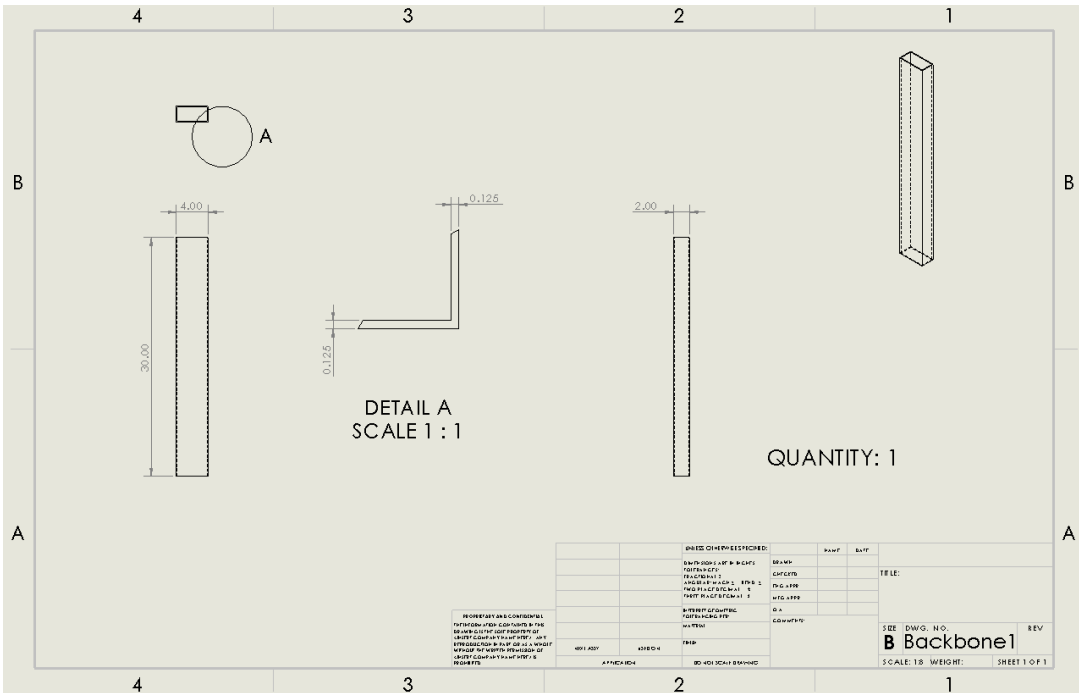

Figure A2.7. The drawing file of the vertical support of the backbone.

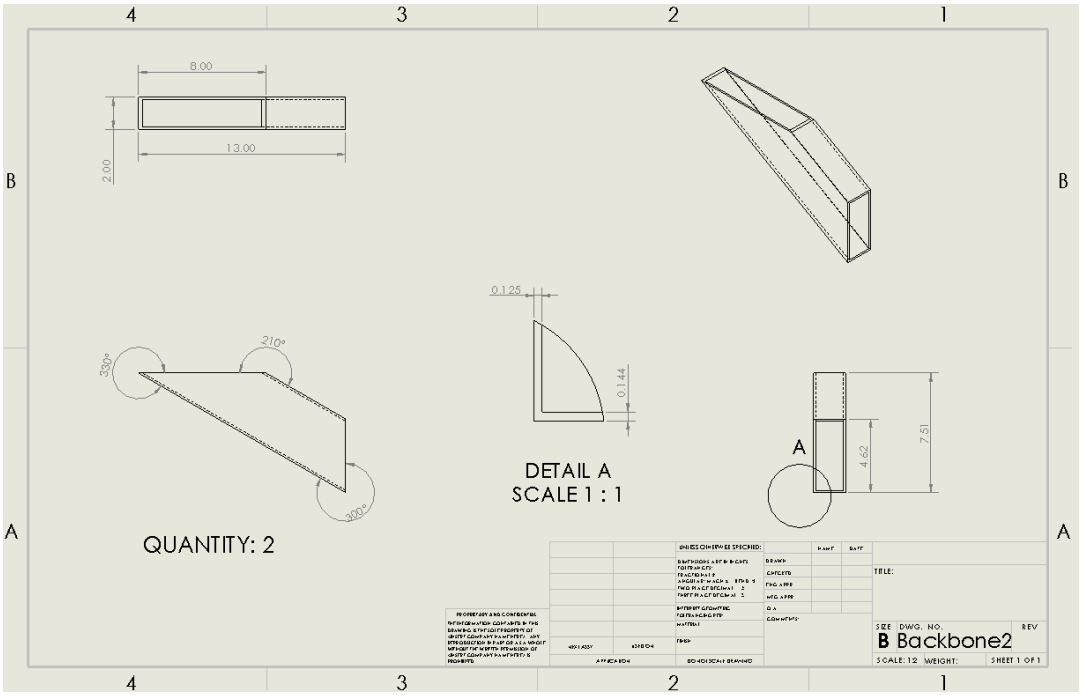

Figure A2.8. The drawing file of the arms of the backbone.

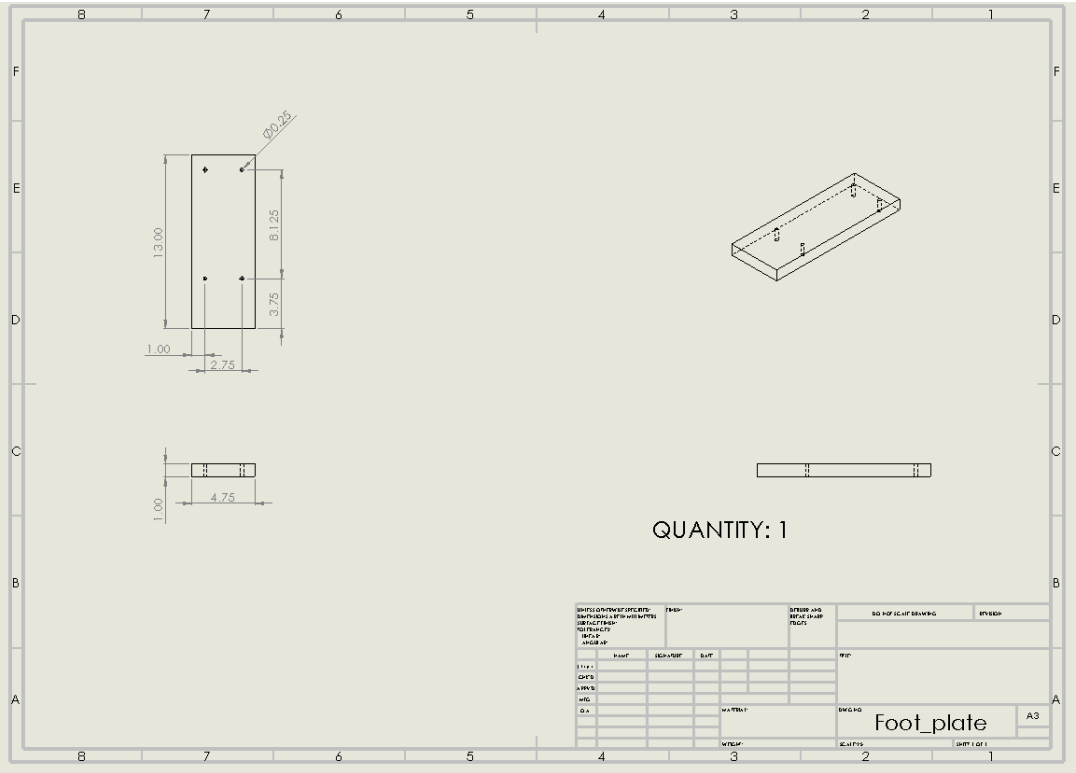

Figure A2.9. The drawing file of the foot plate.

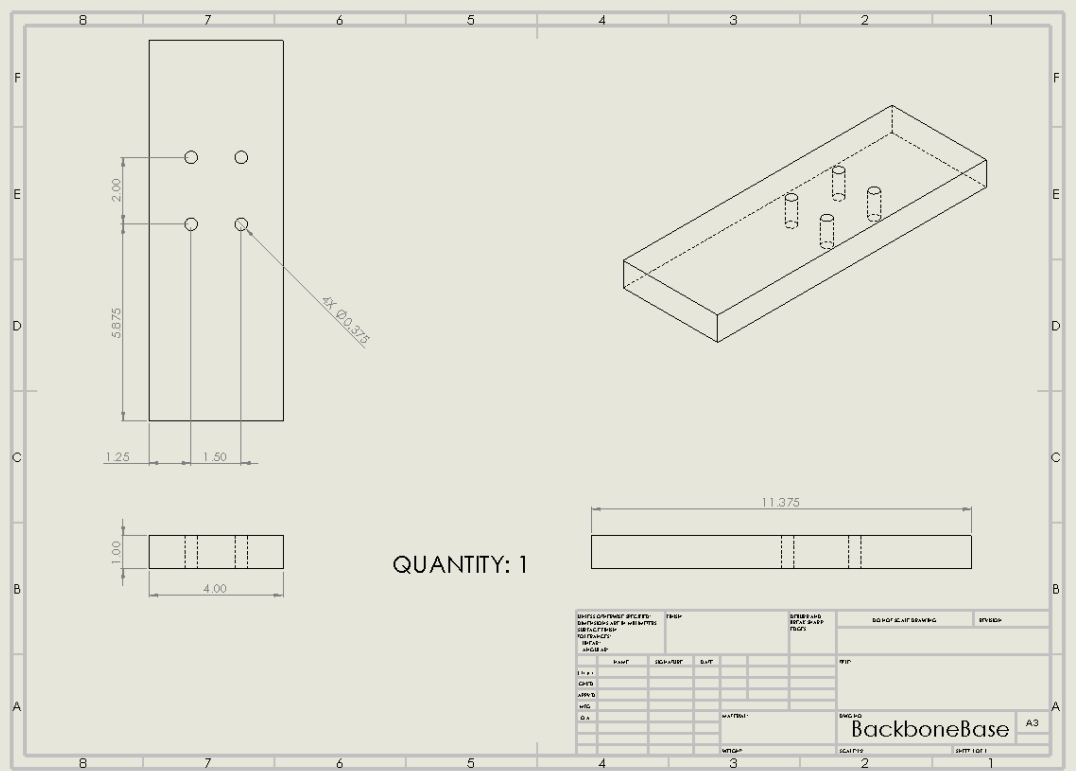

Figure A2.10. The drawing file of the base of the backbone.

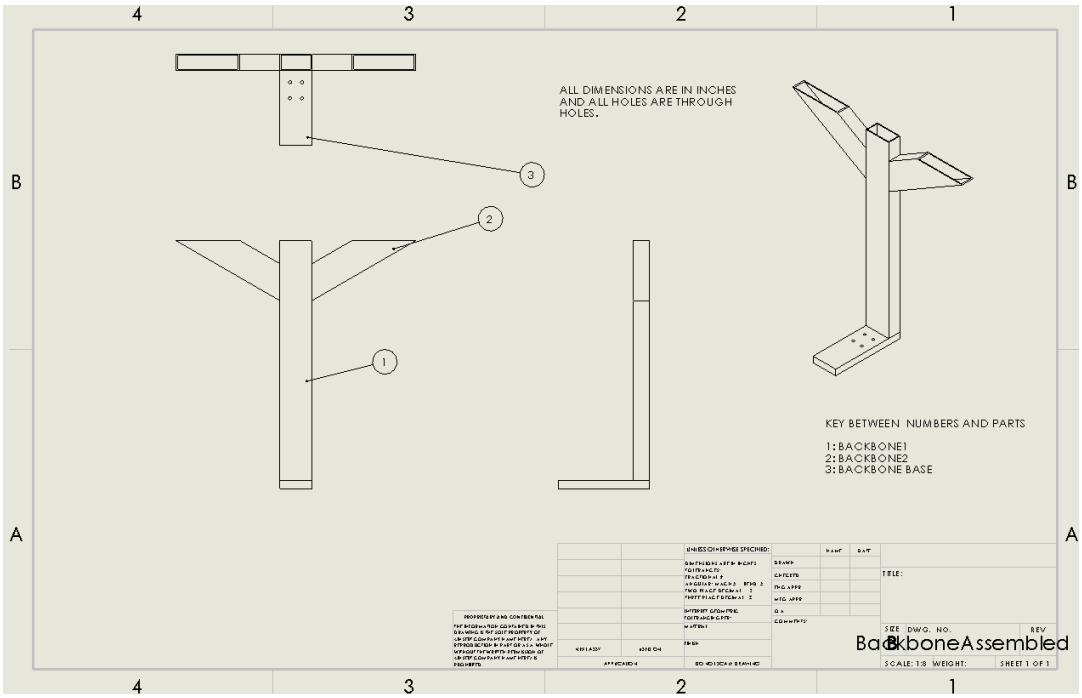

Figure A2.11. The drawing file of the backbone subassembly.

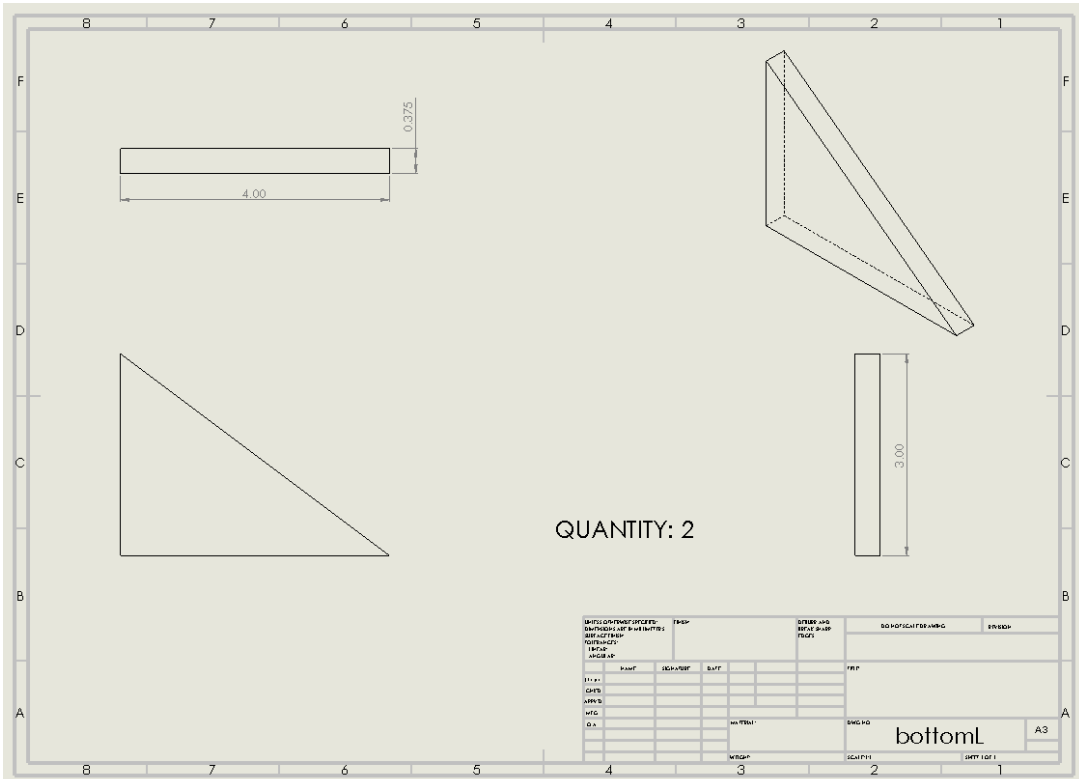

Figure A2.12. The drawing file of the bottom L-brackets.

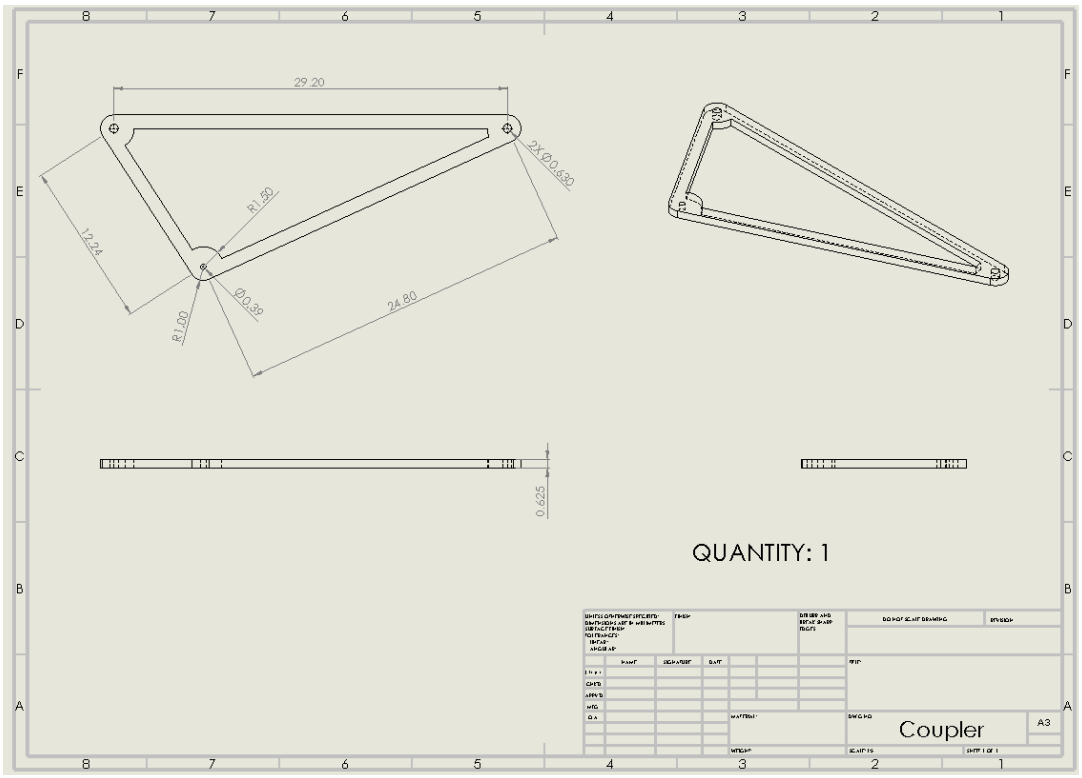

Figure A2.13. The drawing file of the coupler.

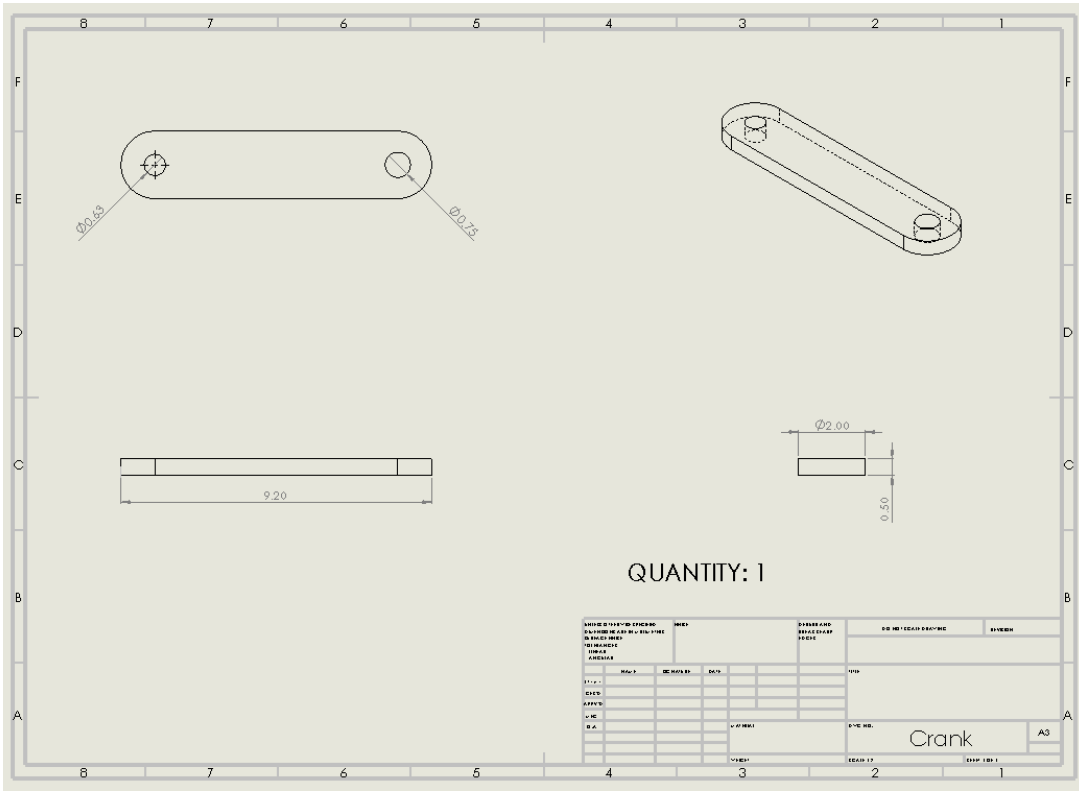

Figure A2.14. The drawing file of the crank.

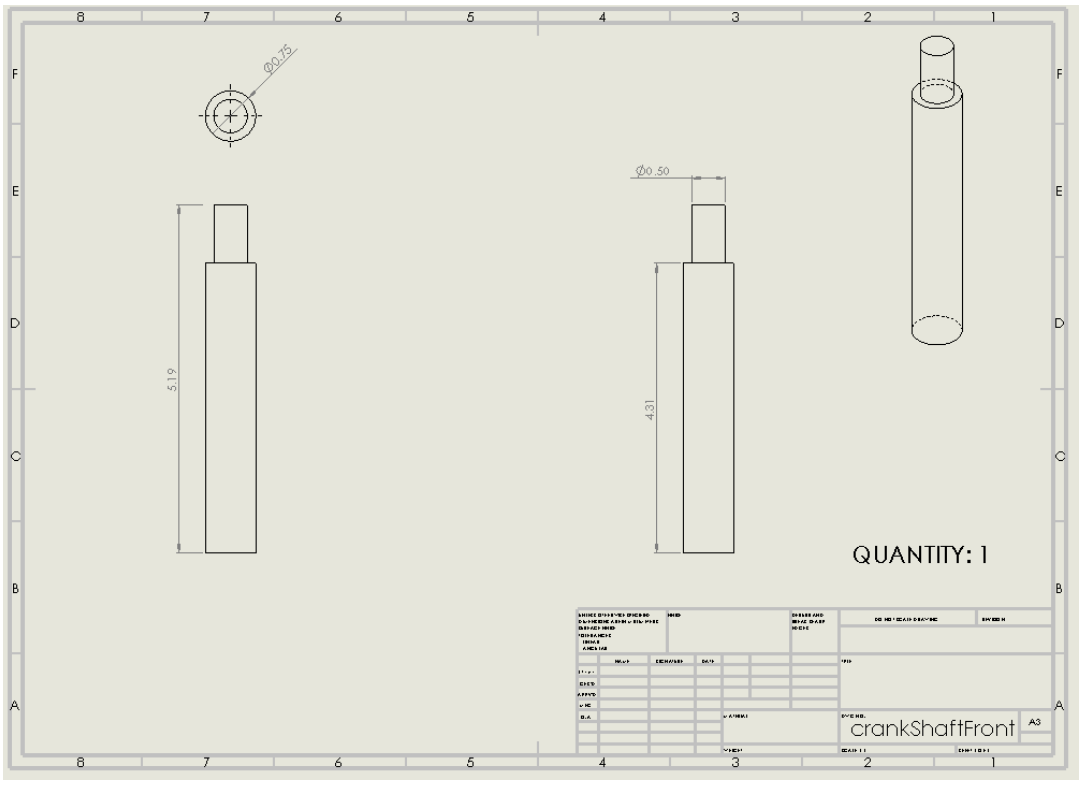

Figure A2.15. The drawing file of the crank shaft.

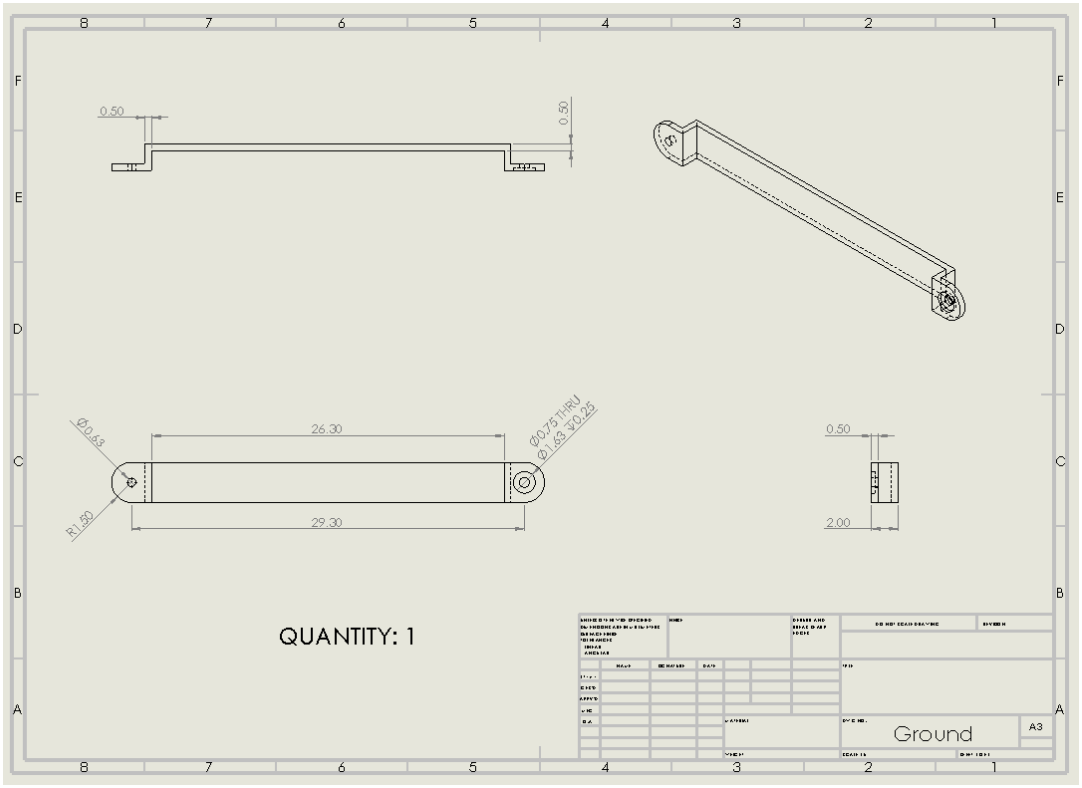

Figure A2.16. The drawing file of the ground link.

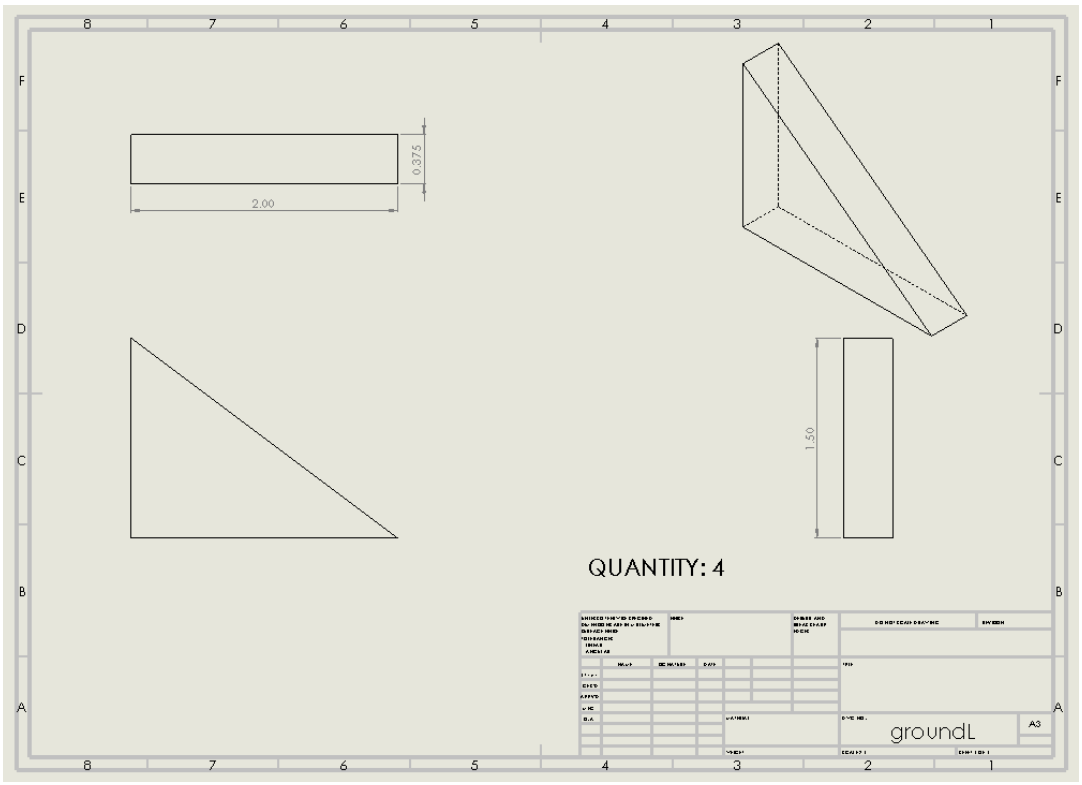

Figure A2.17. The drawing file of the ground link's L-brackets.

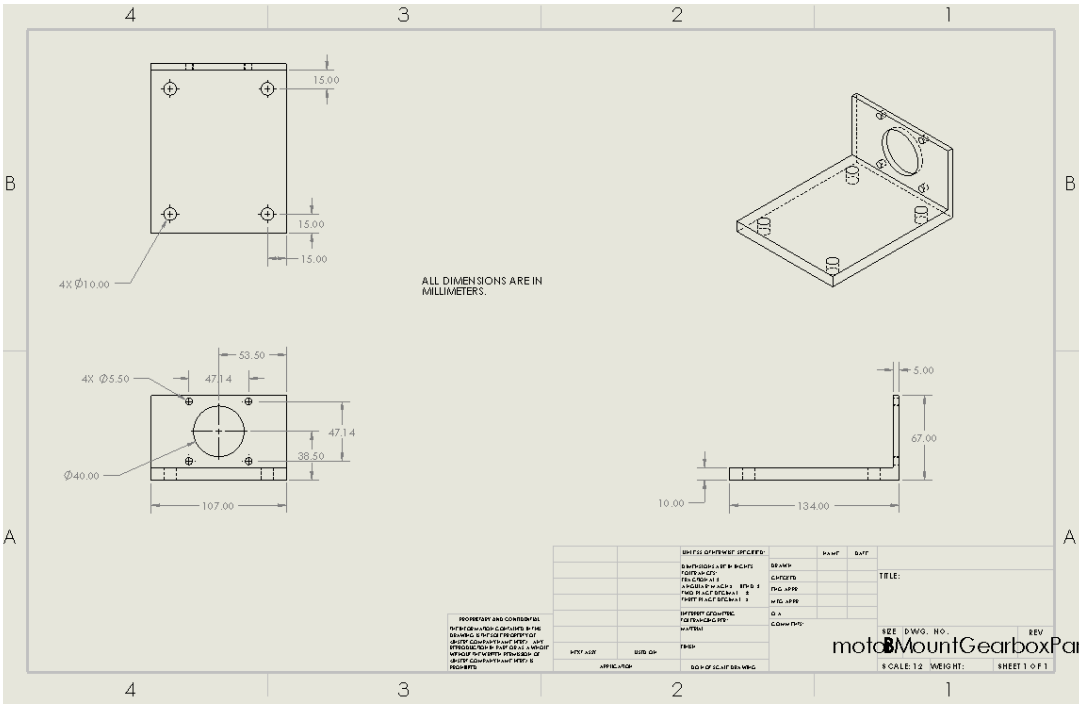

Figure A2.18. The drawing file of the gearbox's plate.

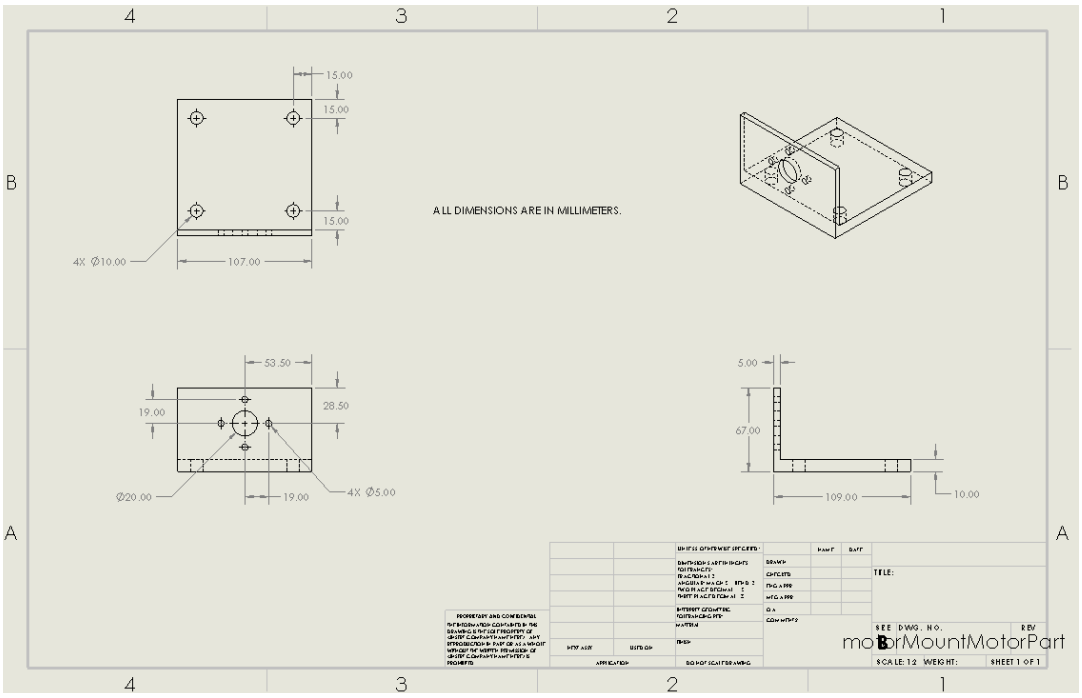

Figure A2.19. The drawing file of the motor's plate.

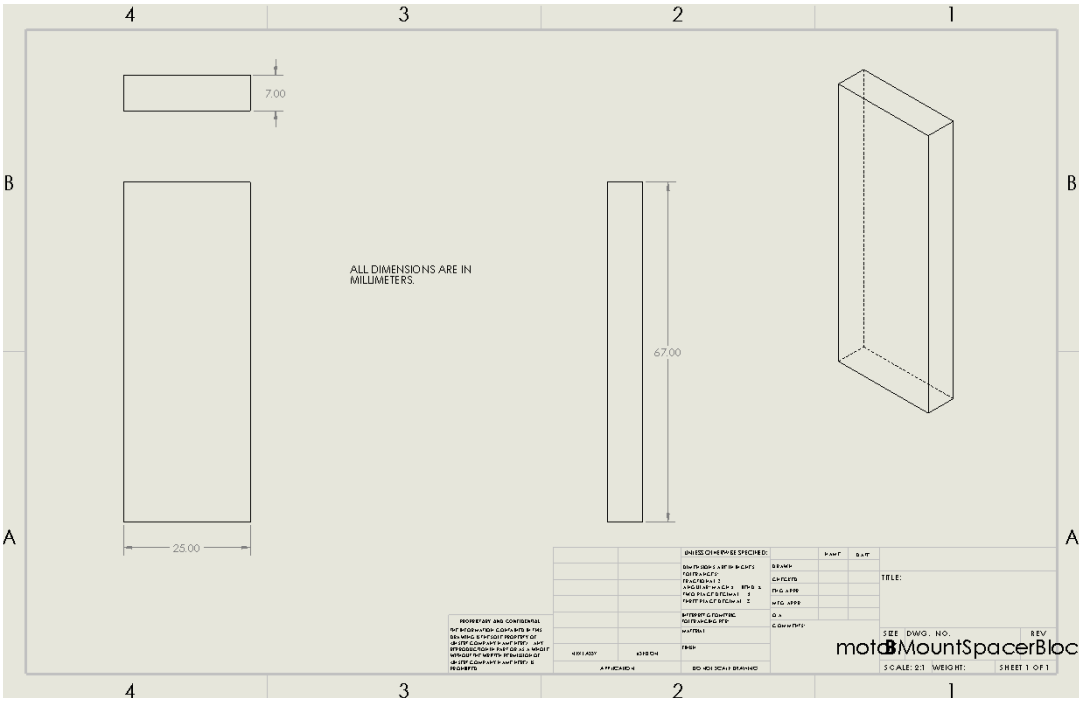

Figure A2.20. The drawing file of the spacer block for the motor mount subassembly.

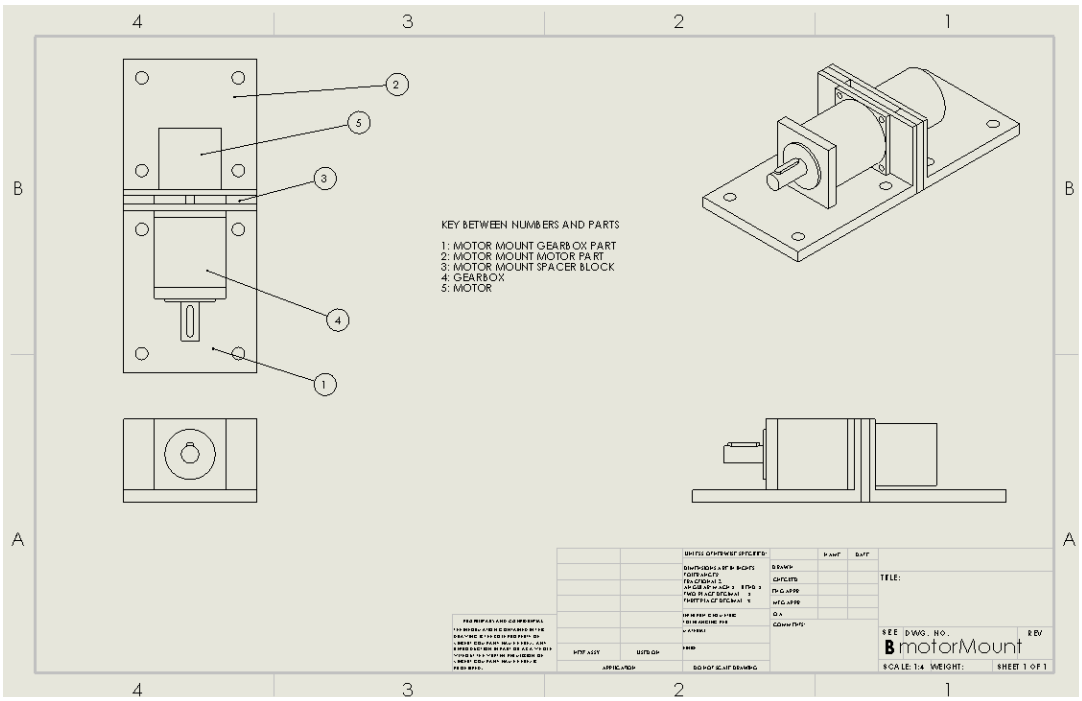

Figure A2.21. The drawing file of the motor mount subassembly.

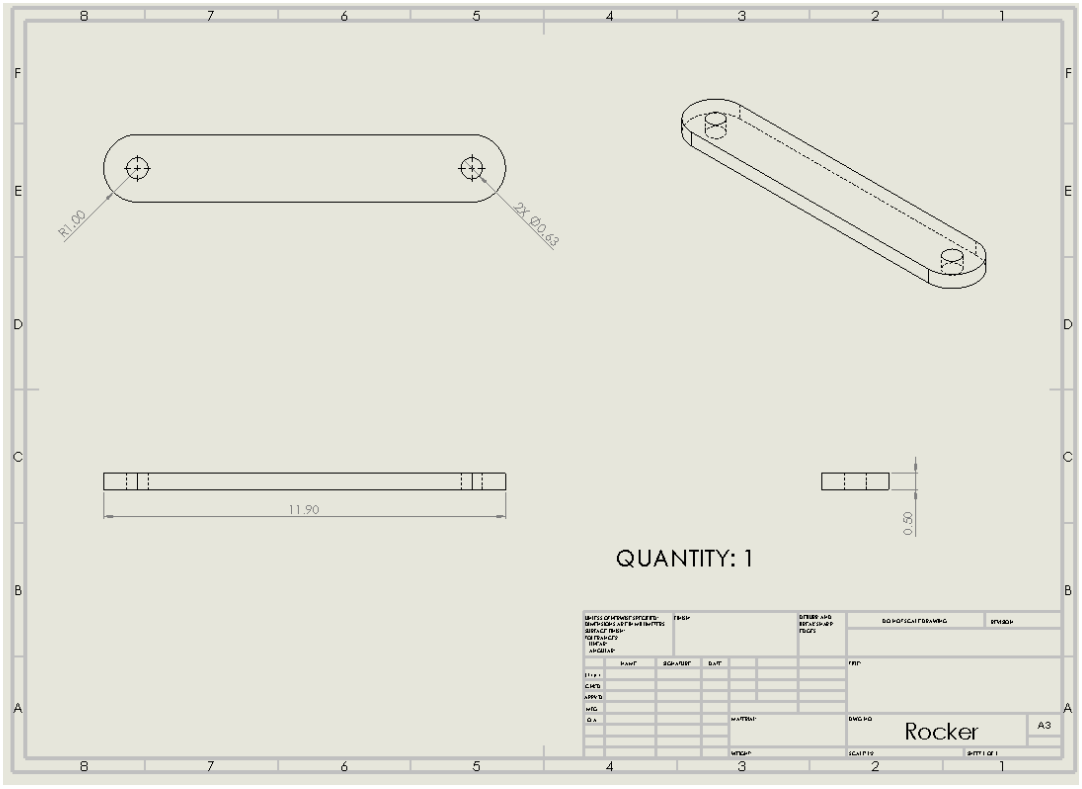

Figure A2.22. The drawing file of the rocker.

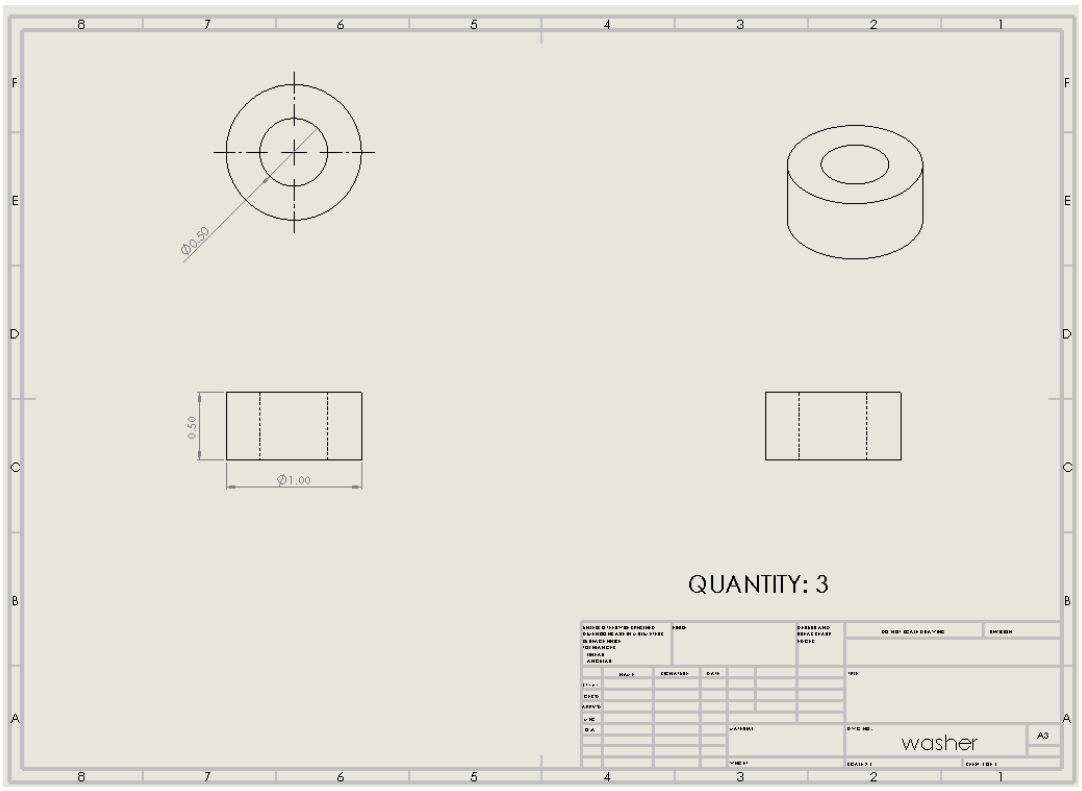

Figure A2.23. The drawing file of the custom washer.

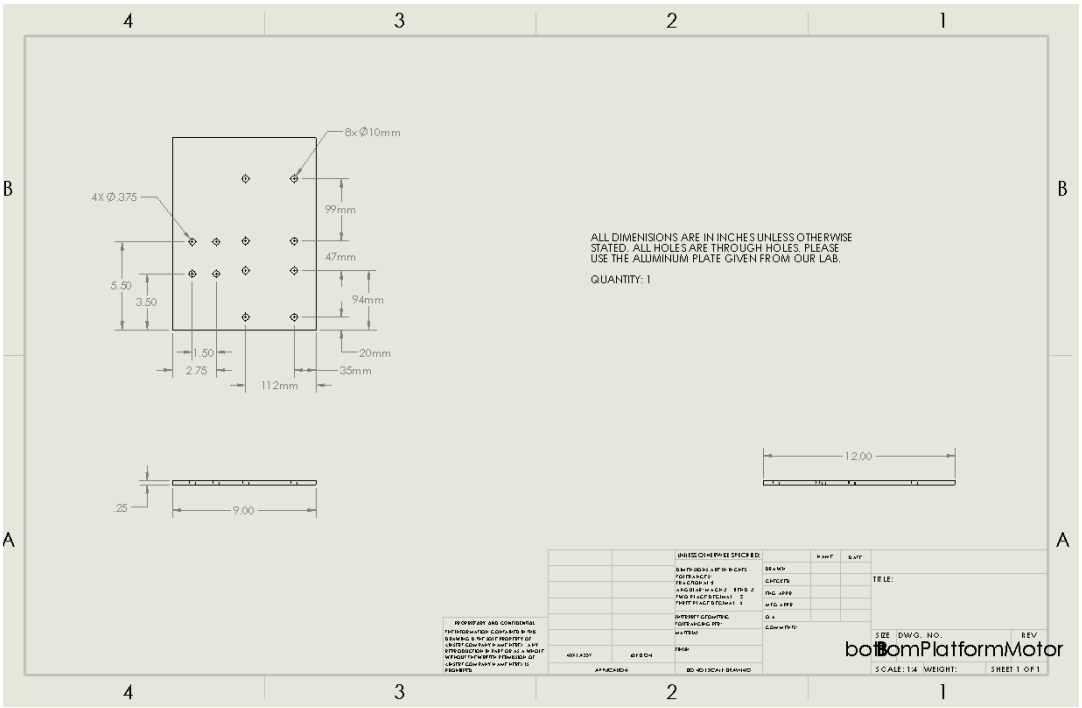

Figure A2.24. The drawing file of the aluminum plate under the motor subassembly.

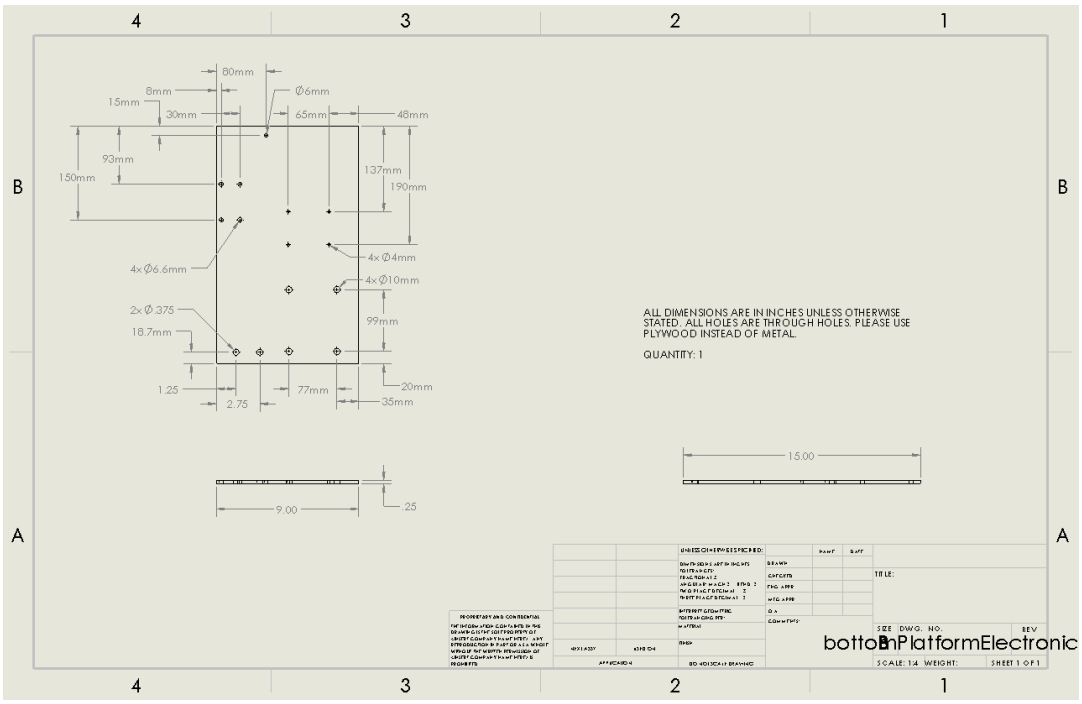

Figure A2.25. The drawing file of the wooden plate for the electronics.

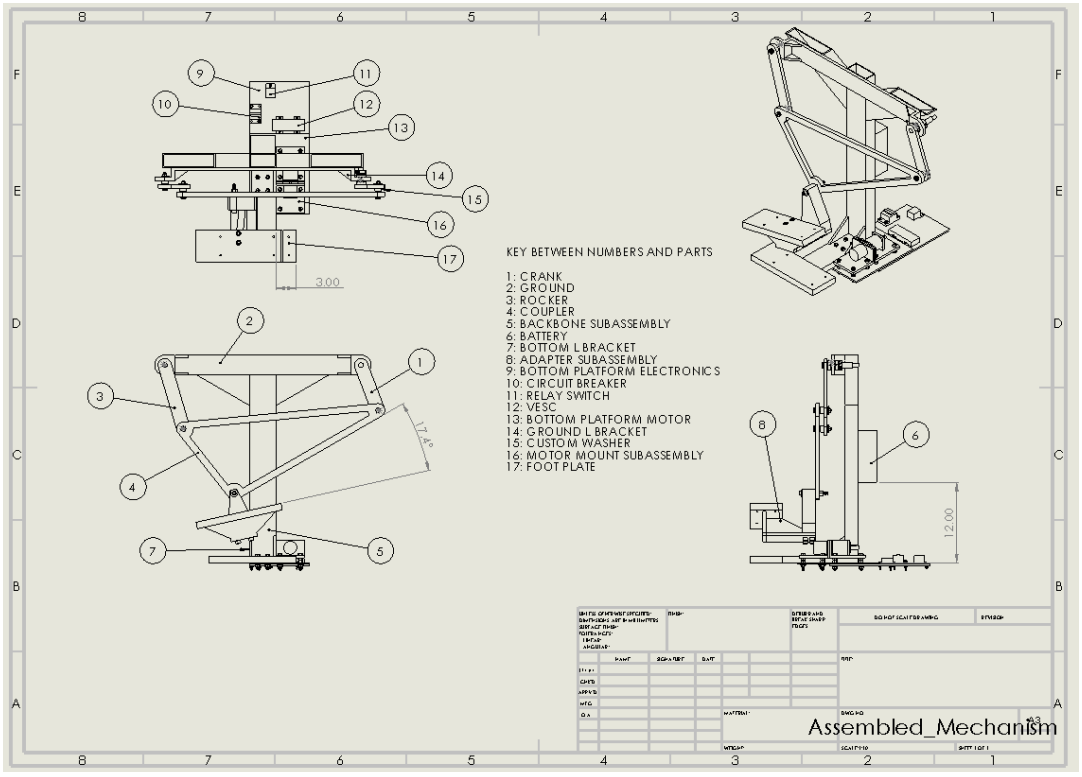

Figure A2.26. The drawing file of the assembled mechanism.

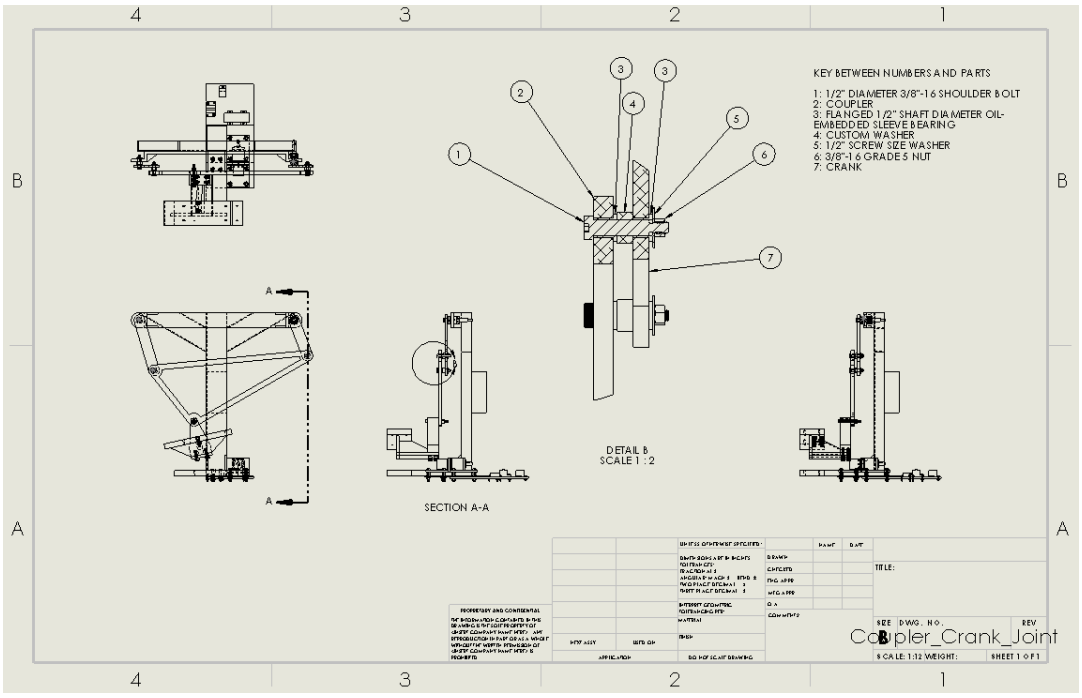

Figure A2.27. The drawing file of the coupler-crank joint.

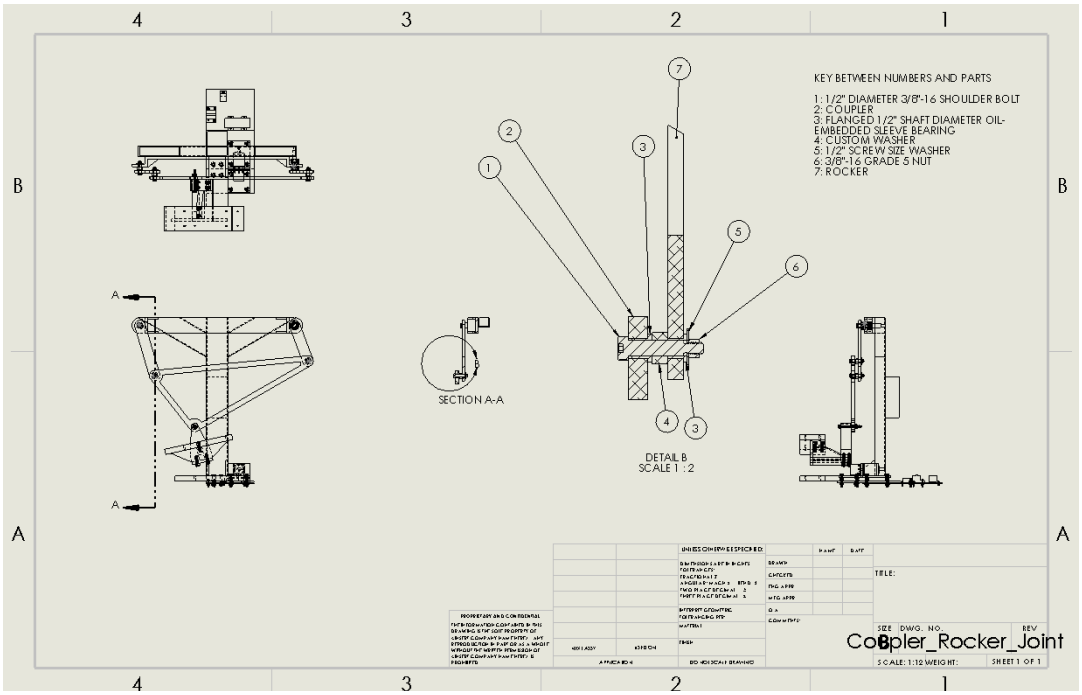

Figure A2.28. The drawing file of the coupler-rocker joint.

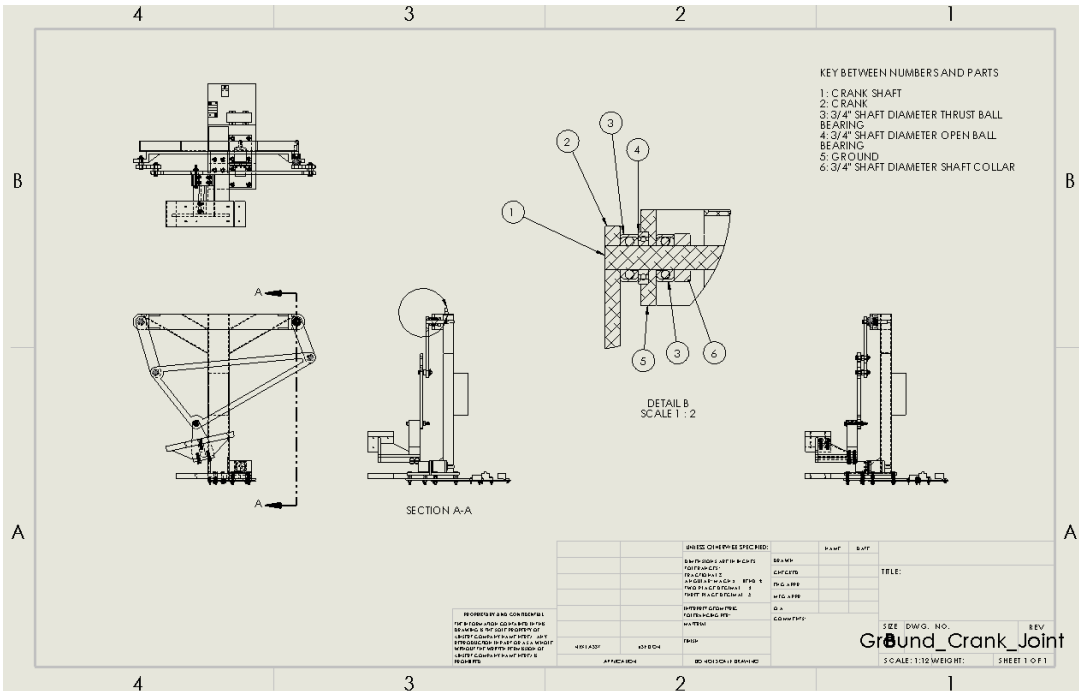

Figure A2.29. The drawing file of the ground-crank joint.

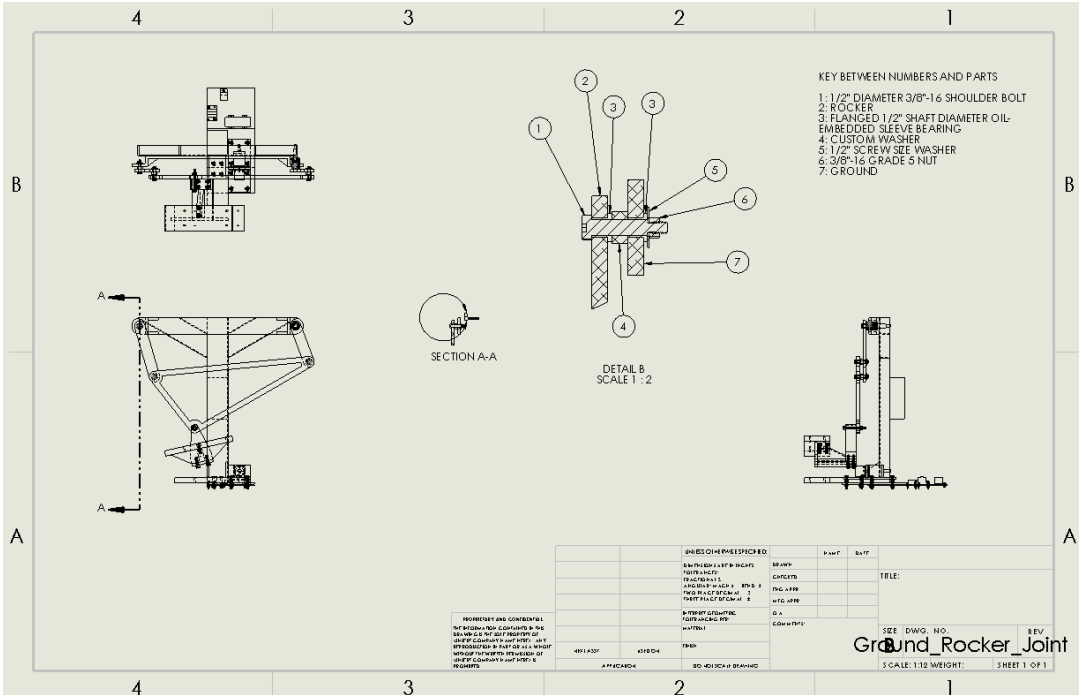

Figure A2.30. The drawing file of the ground-rocker joint.